nature portfolio

Peer Review File

Loss of *KDM6A*-mediated genomic instability and metabolic reprogramming regulates response to therapeutic perturbations in bladder cancer.

Corresponding Author: Dr Sangeeta Goswami

This file contains all reviewer reports in order by version, followed by all author rebuttals in order by version.

Version 0:

Reviewer comments:

Reviewer #1

(Remarks to the Author)
Singh et al. report a series of studies regarding potential mechanisms through which KDM6A inactivation could contribute to bladder cancer. The authors use a variety of models including established human and mouse bladder cancer cell lines and tumor tissue data. There are several partially connected components to the work but there is a certain lack of coherence to the whole thing, in my opinion, in part due to the rather superficial analysis of some of these components. The authors start by commenting on the relationship between KDM6A mutations and sensitivity to cisplatin and extrachromosomal DNA, then they go on to discuss impact of KDM6A mutations on the mismatch repair machinery and response to immunotherapy, then go on to assess the impact on the double-strand break pathway and finally go to discuss the metabolic impact on T cells and on T cell abundance and function, including the impact on histone lactylation. Loose connection and lack of depth characterize the work. Overall, the authors also fail to consider the fact that KDM6A is an early bladder cancer driver that is mainly mutated in non muscle-invasive bladder cancer while all their work is based on muscle-invasive/metastatic cancer.
Important general methodological considerations:
- the number of replicates in the experiments is not always indicated; the use of controls is not always described; the scales in the graph do not have "0" as background level.
- the correction of p-values for multiple testing is not indicated.
- statistical tests are not properly used. Student's t test can only be applied to data with a normal distribution, which is not the case in many of the comparisons.

Specific comments
1. Figure 1: to be conclusive on the association with resistance to cisplatin, robust data in more than one series should be provided. The data on final tumor weight in B should be accompanied by growth curves. The migration data does not take into consideration the effect of cell growth. The use of a single sgRNA is not appropriate. A western blot to convincingly show down-regulation of KDM6A protein expression is not shown. The impact on extrachromosomal DNA is not robustly demonstrated, the analysis is very superficial and inconclusive.
2. Effects on the MMR machinery are not convincing, as is the case for the association with response to immunotherapy. They should consider multiple independent series and perform multivariable analysis. Co-occurrence and mutual exclusivity are probably not corrected for multiple testing. The association with tumor mutational burden should be analysed if there is a real effect on MMR. The standard MMR analysis included several microsatellite sites, rather than just one. The effects are small in several of the shown comparisons. In panel H comparing one cell line to another is just inappropriate. More detais is required in the description of multiple results in Figure 2. Reduced expression of MMR proteins should be shown using western blotting, with appropriate controls.
3. The effects on the DBS break pathway are poorly analyzed. Are the differences in gene expression shown in Figure 3 related to differences in cell proliferation or cell cycle distribution? Data in panel C do not have any statistical analysis. Panels F and H in Figure 3 lack baseline comparisons.
4. Figure 4 shows very minor, and not always significant, differences in gene expression which render the conclusions less solid. The RNA-seq analysis is not properly described, nor the multiple testing applied. It is kind of surprising that the effects on cell proliferation are associated with reduced glycolysis. Panel E lacks statistics.
5. The concentrations of lactate used are very high compared to physiological levels and the effects in Figure 5-6 are often quite small. The genomic analysis is not properly controlled nor does it have sufficient explanation about replicates,

statistics, etc.

Reviewer #2

(Remarks to the Author)
This study aims to elucidate an innovative model in which loss of KDM6A regulates therapeutic response in bladder cancer through two distinct mechanisms: accumulation of extrachromosomal circular DNA (eccDNA), contributing to platinum resistance, and lactate-mediated histone lactylation, which modulates Treg function and enhances immunotherapy sensitivity. The authors integrate multi-omics analyses with comprehensive in vitro and in vivo functional assays, and the conceptual framework holds promising translational potential. However, several important issues remain to be addressed:

Major Comments
1.In Figure 1D, the figure legend states that the wound-healing assays under cisplatin treatment were performed with n = 9 biologically independent samples per group; however, the box-and-whisker plot shows approximately 12 data points for the sgScramble group and 15 for the sgKdm6a group, which is inconsistent with the stated sample size. A similar discrepancy appears in Figure 1C ("sgScramble + cisplatin" legend: n = 3 per group, yet only 2 data points are shown) and in Figure 3E, where the MFI of γ-H2AX shows 3 points for sgScramble but the percentage of γ-H2AX shows 6 points, while sgKdm6a shows 5 versus 6 points—contradicting the figure legend's claim of n = 3 for the left panel and n = 5 for the right. Such inconsistencies between declared and plotted sample sizes undermine confidence in the statistical analyses and, by extension, the study's mechanistic conclusions.
2.On line 89, the authors state, "we uncovered a previously uncharacterized role for KDM6A in tumor metabolic reprogramming. Loss of KDM6A suppressed glycolytic flux and decreased intratumoral lactate accumulation." However, Yang et al. (PMID: 36215227) have already reported that KDM6A regulates tumor glycolysis. The authors should temper their language, cite Yang et al., and discuss how their findings extend or differ from that prior work.
3.While the wound-healing assay in Figure 1 is informative, it assesses only two-dimensional migration and can be confounded by proliferation and scratch width variability. Incorporating Transwell migration and invasion assays would provide more quantitative and mechanistic insight into how KDM6A loss affects bladder cancer cell motility and invasiveness.
4.Comparing J82 (KDM6A-mutant) and RT4 (KDM6A-wildtype) cell lines offers supportive evidence, but differences in their genetic backgrounds, signaling pathways, and chromosomal alterations may also influence cisplatin sensitivity. To attribute the phenotype specifically to KDM6A, the authors should perform isogenic manipulations—for example, re-expressing KDM6A in J82 and knocking out KDM6A in RT4—and assess cisplatin response in these matched backgrounds.

Minor Comments
1.Lines 252–253: In "in J82 cells compared to RT4 cells" (Figure 4C), should this reference be to Extended Data Figure 4C?
2.All histological images lack scale bars; in Figure 3D, the white arrows are unexplained—please add scale bars and clarify the meaning of these arrows.
3.In Figure 4B, correct "Chip-seq" to "ChIP-seq."
4.The figure legend numbering for Figures 3E and 3F does not match the order shown in the panels.
5.In Figure 4F, the right-hand ECAR y-axis is labeled "mpH/min/Norm. Unit." Please clarify whether "Norm. Unit" refers to normalization by cell number or by protein content. Additionally, the points at which oligomycin and rotenone/antimycin A were added should be indicated on the graph.

Reviewer #3

(Remarks to the Author)
In this manuscript, Singh et al report that KDM6A loss in bladder cancer is associated with altered response to chemotherapy and immune checkpoint blockade treatments, by performing retrospective analysis in published data from advanced bladder cancer patients. They utilize murine cell lines and allograft tumors, as well as human cell lines, and report that KDM6A regulates key genes in several molecular pathways, including genome integrity and metabolism. The authors link the presence of oncogene copies in extrachromosomal DNA to chemotherapy resistance, and metabolic rewiring to improved immune checkpoint blockade (ICB) efficacy. Additionally KDM6A is shown to dysregulate DNA repair pathways that could also contribute to altered therapy response.
Overall, there is considerable novelty in their findings, but several mechanistic connections lack sufficient evidence. To address this issue, the authors should perform functional experiments and change the language in text so that in the revised manuscript it is clear which transcriptional effects of KDM6A loss contribute to altered therapy response and to what degree.

Major comments:
1. Overall the evidence that implicate eccDNA as a cause of chemotherapy resistance is weak (Figures 1G-J, Lines 386-387). The authors should provide experiments that show presence of oncogenes and/or chemoresistance-associated genes in eccDNA of KDM6A KO/MUT cells (e.g. by FISH). In addition, the authors should provide evidence of specific eccDNA involvement in chemoristance, e.g. by ablation of candidate genes in KDM6A MUT cells to restore chemotherapy sensitivity.
2. Comparison of only two human cell lines is not sufficient to draw conclusions about conservation of findings in human cells (Figures 1F, 2H, 3G, Extended Data Figure 4C). The authors should either use more KDM6A WT and KDM6A MUT cells (at least 3 per condition), or perform KO/KD experiments in KDM6A WT cells and/or KDM6A rescue experiments, e.g. by OE, in KDM6A MUT cells.

3. Related to Lines 171-175, Figures 2E,G and Extended Data Figures 2C-D, and Lines 212-215 3A,C, Extended Data Figures 3C-D, and Figures 4B-C and Extended Data Figure 6E: The authors should provide IGV track images (or similar) for visualization of KDM6A and H3K4me3 peaks. Also to strengthen causal relationship of KDM6A binding and Msh2 Msh6 downregulation they could show H3K27me3 ChIP-seq at these loci. Similarly, for Figure 6C, the enrichment of H3K9la and H3K18la at specific genes should be vizualized in IGV.
4. The authors provide evidence for multiple pathways that could contribute to improved ICB efficacy (Figures 2-5), yet they do not provide mechanistic evidence to assess the degree of contribution for each one. For example, overexpression of Mlh1/Msh2, Exo1/Lig3, and Ldha/HK2/Eno2 in KDM6A KO cells could lead to ICB resistance.
5. For Figures 1B and 2B, tumor growth curves should be provided.

Minor:
6. Lines 138-139 and Extended Data Figure 1B: The eccDNA study in KMD6A WT and MUT patients is incompletely described in the text, methods and the related figure. Are the levels and heterogeneity of eccDNA different between WT and MUT patients?
7. Figure 2B description is incorrect, wrong treatment is mentioned.
8. Figure 3D: how many tumors analyzed? Provide quantitation
9. Lines 230 S3E reference irrelevant
10. Lines 228-230 3E: please also provide representative images of gH2AX staining'
11. Lines 252-253 fix reference to Extended Data Figure 4C
12. Cell line suppernatant experiments in human cell lines
13. Lines 266-269: please reference the studies mentioned.

Reviewer #4

(Remarks to the Author)
This study describes a mechanistic framework by which loss-of-function mutations in the histone demethylase KDM6A modulate therapeutic responses in bladder cancer. The authors present analyses of numerous clinical cohorts and data from model systems indicating that KDM6A deficiency is associated with worse overall survival following cisplatin-based chemotherapy, but improved outcomes with immune checkpoint blockade (ICB); a noteworthy and potentially important result. Mechanistically, the authors show data that KDM6A loss promotes the accumulation of extrachromosomal circular DNA (eccDNA), contributing to cisplatin resistance. The authors show that KDM6A directly regulates DNA mismatch repair (MMR) and double-strand break repair (DSBR) genes, and that its loss impairs these pathways, resulting in genomic instability, elevated tumor mutational burden, and enhanced immunogenicity. In parallel, KDM6A deficiency suppresses intratumoral lactate production, which leads to diminished histone lactylation (H3K9la, H3K18la) in regulatory T cells (Tregs). This epigenetic alteration attenuates the expression of immunosuppressive genes, thereby enhancing effector T cell activity in the tumor microenvironment. Collectively, the authors conclude that the findings position KDM6A mutation status as a potential predictive biomarker for therapeutic stratification in bladder cancer.
Overall this paper combines epigenetic, metabolic, and the immune experiments to create a mechanistically rich study linking KDM6A loss to divergent therapeutic responses in bladder cancer. However, the limited validation of some key claims needs to be addressed to solidify its mechanistic and clinical impact. I recommend the following points be addressed prior to acceptance.

1. The association between KDM6A inactivating mutations and eccDNA is very intriguing but the mechanistic experiments rely heavily on a single murine bladder cancer cell line (MB49)+/- CRISPR-Cas9 knockout and a limited number of human cell lines. In particular the authors attempted to validate the cisplatin-resistant phenotype of KDM6A-mutant murine bladder cancer cells with the human cell lines RT4 and J82 (Fig 1F). Comparing two different human cell lines, even from the same tumor type, is prone to confounding as cell specific copy number alterations or epigenetic differences may strongly influence therapeutic response. (References "Oncogene volume 36, pages35–46 (2017); Scientific Reports volume 6, Article number: 38531 (2016)" show some of the known cell line differences.) The authors need to provide cisplatin resistance data from either a larger panel of bladder cancer cell lines with known KDM6A status or knockdown KDM6A in the T24 line to show validation in a human system comparable to the murine sgScramble and sgKdm6a cells.

2. While the study clearly demonstrates increased eccDNA in the murine sgKdm6a cells compared with sgScramble (Fig 1G), a more detailed characterization of these amplifications is needed. At the very least genome wide copy number plots of the sgScramble and sgKdm6a cells should be generated and presented. This along with sequencing the eccDNA will enable eccDNA differences to be clearly observed and specific genetic loci identified. It will significantly strengthen the association the authors are trying to show if any of the eccDNA loci correspond to some of the key oncogenes already associated with cisplatin resistance or identify new resistance genes.

3. The Chip-seq results need to be clarified. The authors present numerous "Profile Plots" of their ChIP-seq data. I cannot find an explanation in the Methods, but it seems to be a plot of the Chip-seq signal averaged across samples (e.g. Fig. 3C) and/or gene sets (e.g. Fig. 4C). This needs to be clarified for each plot; exactly what genes or gene sets and how many samples were averaged in the plot needs to be stated. Also, all the replicates for the individual gene Profile plots need to be shown in supplementary to evaluate the variability in the raw data.

Version 1:

Reviewer comments:

Reviewer #2

(Remarks to the Author)
Thank you for the careful and thorough revision. Your changes address my previous concerns and the manuscript is now acceptable for publication.

Reviewer #3

(Remarks to the Author)
The authors addressed the majority of my comments adequately. The only exception is major comment 3: the authors presented genome viewer plots that are (a) low quality since the range is too small to be discerned, and (b) too zoomed in, meaning they show a very narrow view of the gene locus that does not allow proper evaluation of peak signal compared to background.

Version 2:

Reviewer comments:

Reviewer #3

(Remarks to the Author)
The authors addressed the requests properly. I would note that the zoomed out genomic visualization of ChIP-seq reveals that the peaks evaluated are quite small and their significance is questionable. Since this is clearly shown in the main figure, the manuscript is acceptable for publication. The authors might want to be more reserved in their claims concerning changes in H3K4me3.

REVIEWER COMMENTS

Reviewer #1 (Remarks to the Author): with expertise in bladder cancer

Singh et al. report a series of studies regarding potential mechanisms through which KDM6A inactivation could contribute to bladder cancer. The authors use a variety of models including established human and mouse bladder cancer cell lines and tumor tissue data. There are several partially connected components to the work but there is a certain lack of coherence to the whole thing, in my opinion, in part due to the rather superficial analysis of some of these components. The authors start by commenting on the relationship between KDM6A mutations and sensitivity to cisplatin and extrachromosomal DNA, then they go on to discuss impact of KDM6A mutations on the mismatch repair machinery and response to immunotherapy, then go on to assess the impact on the double-strand break pathway and finally go to discuss the metabolic impact on T cells and on T cell abundance and function, including the impact on histone lactylation. Loose connection and lack of depth characterize the work. Overall, the authors also fail to consider the fact that KDM6A is an early bladder cancer driver that is mainly mutated in non muscle-invasive bladder cancer while all their work is based on muscle-invasive/metastatic cancer.
Important general methodological considerations:
- the number of replicates in the experiments is not always indicated; the use of controls is not always described; the scales in the graph do not have "0" as background level.
- the correction of p-values for multiple testing is not indicated.
- statistical tests are not properly used. Student's t test can only be applied to data with a normal distribution, which is not the case in many of the comparisons.

We thank the Reviewer for the assessment of our manuscript. While *KDM6A* mutation is more common in non-muscle-invasive bladder cancer, we would like to highlight that around 26% of patients with muscle invasive bladder cancer harbor mutations in *KDM6A*[1].

Specific comments
1. Figure 1: to be conclusive on the association with resistance to cisplatin, robust data in more than one series should be provided. The data on final tumor weight in B should be accompanied by growth curves. The migration data does not take into consideration the effect of cell growth. The use of a single sgRNA is not appropriate. A western blot to convincingly show down-regulation of KDM6A protein expression is not shown. The impact on extrachromosomal DNA is not robustly demonstrated, the analysis is very superficial and inconclusive.

Author's Response: We thank the Reviewer for the comments.

- To address the Reviewer's concerns and to strengthen our conclusions, we have provided additional data to demonstrate the association of *KDM6A* mutation with cisplatin resistance. We performed experiments with an expanded panel of both murine and human bladder cancer cell lines. We generated independent CRISPR-Cas9 *Kdm6a* knockout clones using multiple sgRNAs in MB49 cells. Additionally, we used two human bladder cancer cell lines RT4 and ScaBER[2] to generate *KDM6A* knockout cells K2 and B7 respectively. Western blotting confirms effective loss of KDM6A protein (Figure **1a** and Figure **2a** in the point-by-point response letter and Extended Data Fig. **1A, B** in revised manuscript). Consistent with our previous findings, assays of cisplatin cytotoxicity, spheroid formation, transwell invasion and wound healing assay uniformly demonstrated enhanced cisplatin resistance in sgKdm6a clones as well as in K2 and B7 cells compared with control clones in both murine and human cell lines (Figure **1b-e** and Figure **2b-f** in the point-by-point response letter and Fig. **1C-G** and Extended Data Fig. **1D-K** in revised manuscript).

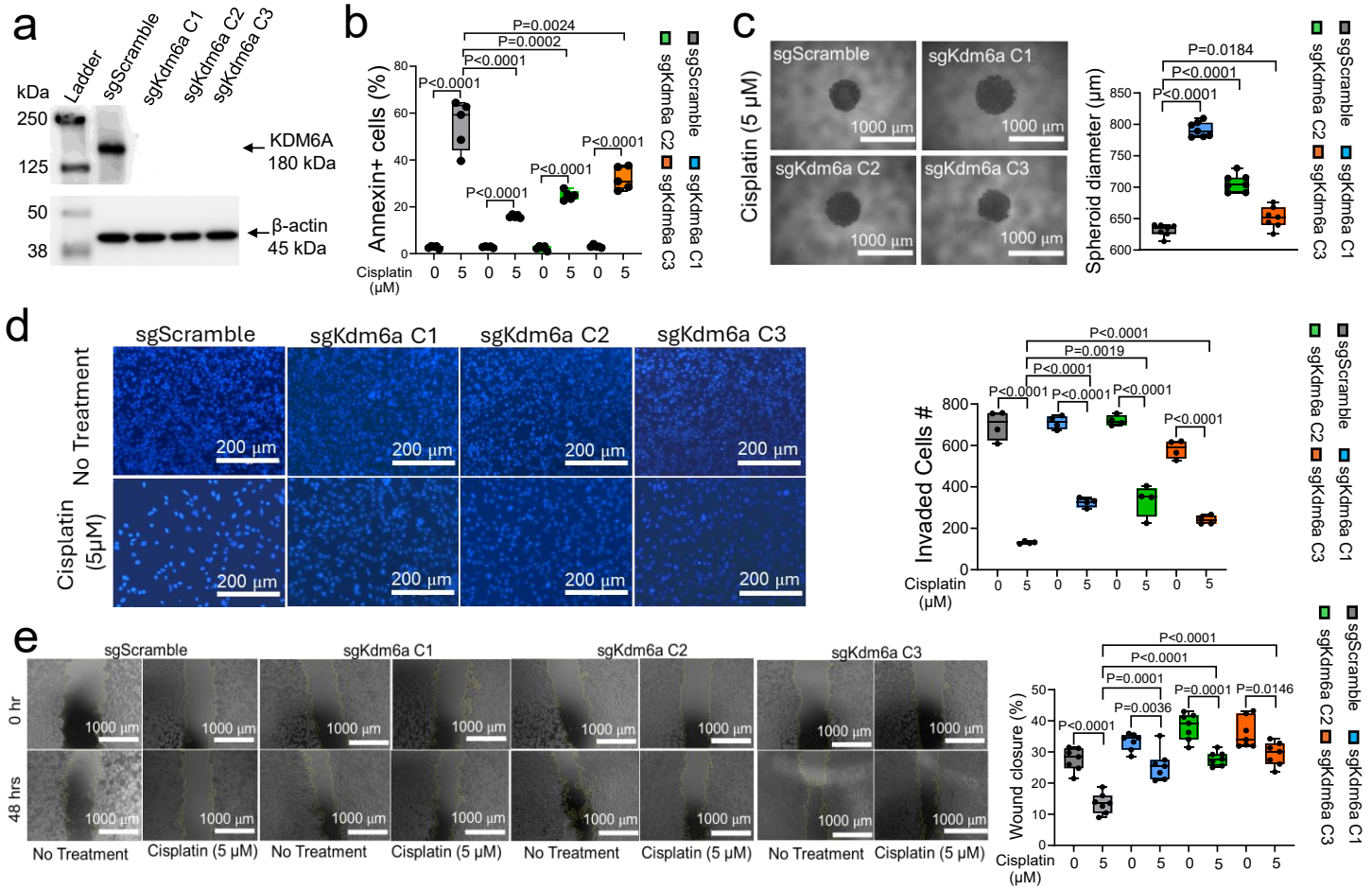

Figure 1: a: Representative western blot image indicating the expression of KDM6A (180 kDa) and β-ACTIN (45 kDa) in sgScramble and sgKdm6a Clones C1, C2 and C3 cell lines. Data is representative of two independent experiments. **b:** Box-and-whisker plot demonstrating percentage of Annexin positive cells of sgScramble and sgKdm6a cell lines treated with or without 5 μM cisplatin for 48 hours. (n=5 biologically independent samples per group). Two-tailed Student's t-test was performed. **c:** Representative images (Left) and box-and-whisker plot (Right) showing the diameter of sgScramble and sgKdm6a spheroids treated with 5 μM cisplatin for 48 hours. (n=7 biologically independent samples per group). Two-tailed Student's t-test was performed. For the representative images, data is indicative of two independent experiments. Scale bar is included. **d:** Representative images (Left) and box-and-whisker plot (Right) demonstrating the invaded cell number in Transwell assay for sgScamble and sgKdm6a clones treated with or without 5 μM cisplatin for 48 hours. (n=4 independent visual fields). Two-tailed Student's t-test was performed. For the representative images, data is indicative of two independent experiments. Scale bar is included. **e:** Representative images (Left) and box-and-whisker plot (Right) depicting the percentage of wound closure of sgScramble and sgKdm6a clones treated with or without 5 μM cisplatin for 48 hours. (n=7 biologically independent samples per group). Two-tailed Student's t-test was performed. For the representative images, data is indicative of two independent experiments. Scale bar is included. For all the box-and-whisker plots, the center line marks the median, the edges of the box represent the interquartile (25th–75th) percentile and the whiskers represent minimum-maximum values.

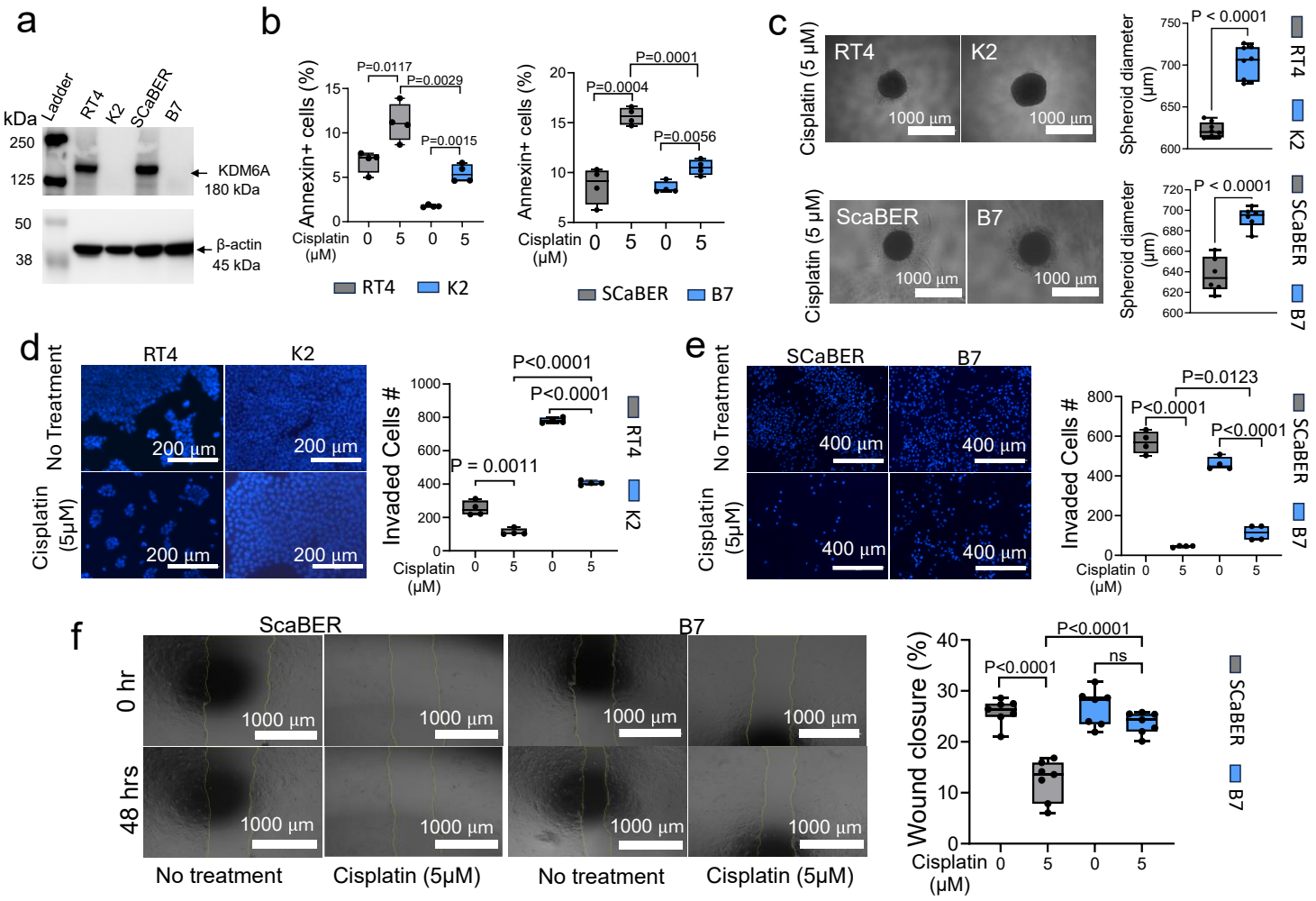

Figure 2: a: Representative western blot image indicating the expression of KDM6A (180 kDa) and β-ACTIN (45 kDa) in RT4, K2, ScaBER and B7 cell lines. Data is representative of two independent experiments. **b:** Box-and-whisker plots demonstrating percentage of Annexin positive cells of RT4 and K2 (Left) and ScaBER and B7 (Right) cell lines treated with or without 5 μM cisplatin for 48 hours. (n=4 biologically independent samples per group). Two-tailed Student's t-test was performed. **c:** Representative images (Left) and box-and-whisker plot (Right) comparing the diameter of RT4 and K2 (Top) and ScaBER and B7(Bottom) spheroids treated with 5 μM cisplatin for 48 hours. (n=8 (Top) and n=6 (Bottom) biologically independent samples per group). Two-tailed Student's t-test was performed. For the representative images, data is indicative of two independent experiments. Scale bar is included. **d-e:** Representative images (Left) and box-and-whisker plot (Right) showing the number of invaded cells in Transwell assay for RT4 and K2 (**d**) and ScaBER and B7 (**e**) cell lines treated with or without 5 μM cisplatin for 48 hours. (n=4 independent visual fields). Two-tailed Student's t-test was performed. For the representative images, data is indicative of two independent experiments. Scale bar is included. **f:** Representative images (Left) and box-and-whisker plot (Right) depicting the percentage of wound closure of ScaBER and B7 cells treated with or without 5 μM cisplatin for 48 hours. (n=7 biologically independent samples per group) Two-tailed Student's t-test was performed. For the representative images, data is indicative of two independent experiments. Scale bar is included. For all the box-and-whisker plots, the center line marks the median, the edges of the box represent the interquartile (25th–75th) percentile and the whiskers represent minimum-maximum values.

- To address the Reviewer's comment on growth curves accompanying the final tumor weight in Fig. **1B**, we have now provided both tumor growth curve and endpoint weights. (Figure **3** in the point-by-point response letter and Fig. **1B** and Extended Data Fig.**1C** in revised manuscript). Consistent with the tumor weight, growth curves also

demonstrated that cisplatin-based chemotherapy showed greater benefit in mice with sgScramble tumors compared to those with sgKdm6a tumors, highlighting cisplatin resistance following Kdm6a loss.

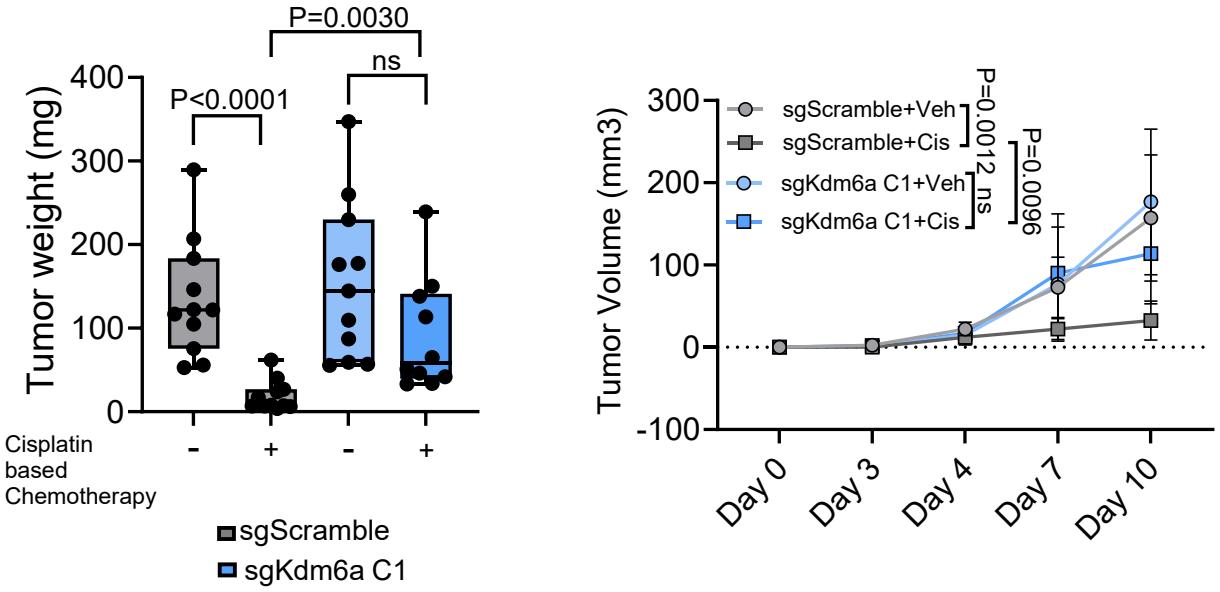

Figure 3: Box-and-whisker plot illustrating the tumor weights (Left) and corresponding tumor growth curves indicating the tumor volumes (Right) of sgScramble and sgKdm6a C1 tumors from mice treated with and without cisplatin-based chemotherapy. (n=10-11 mice per group). Two-tailed Student's t-test (Left) and Two-way ANOVA (Right) was performed. For the box-and-whisker plot, the center line marks the median, the edges of the box represent the interquartile (25th–75th) percentile and the whiskers represent minimum-maximum values.

- To address the concern regarding cell proliferation in migration assays, we performed wound-healing and transwell experiments under low-serum conditions, thereby minimizing confounding growth effects (Figure **4a, b** in the point-by-point response letter and Fig.**1D** and Extended data Fig.**1F, H** in revised manuscript). This has been clarified in the Methods. Additionally, we have performed CFSE based labelling and flowcytometry assay using these cell lines which demonstrated that the proliferation rates for both sgKdm6a and sgScramble cells were similar over the treatment period (Figure **4c** in the point-by-point response letter and Extended data Fig.**1L** in revised manuscript).

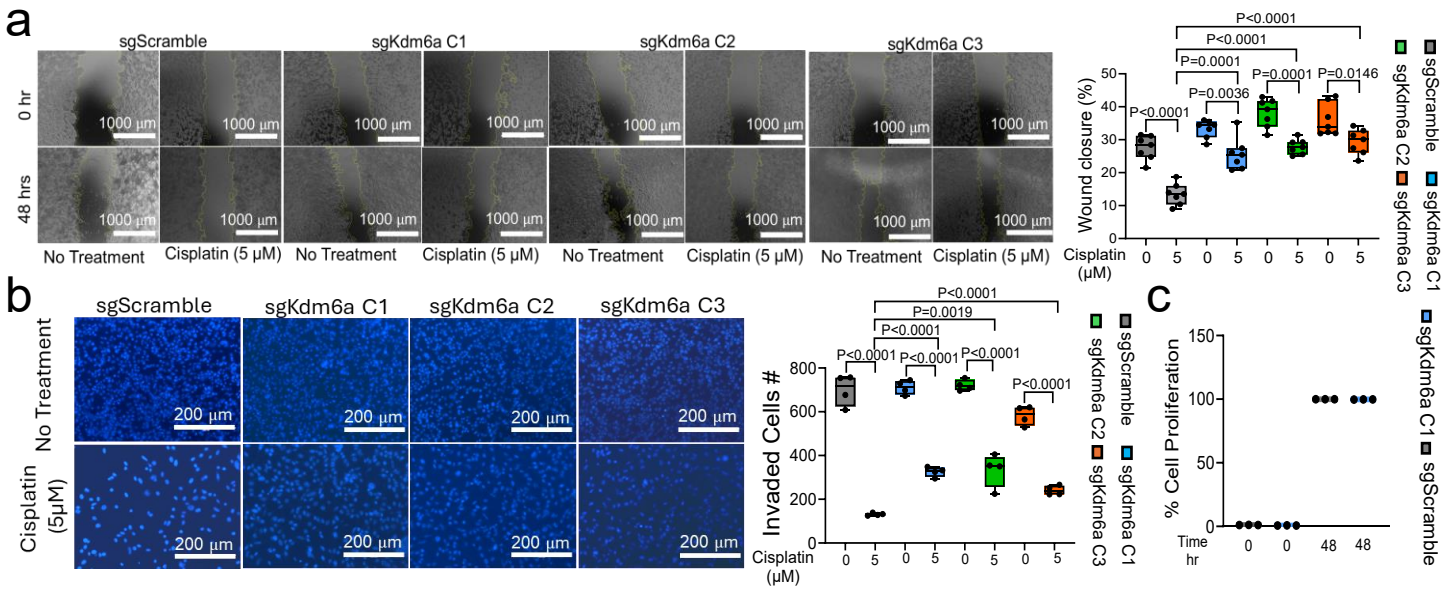

Figure 4: a: Representative images (Left) and box-and-whisker plot (Right) depicting the percentage of wound closure of sgScramble and sgKdm6a clones treated with or without 5 μM cisplatin for 48 hours. (n=7 biologically independent samples per group). Two-tailed Student's T-test was performed. For the representative images, data is indicative of two independent experiments. Scale bar is included. **b:** Representative images (Left) and box-and-whisker plot (Right) demonstrating the invaded cell number in Transwell assay for sgScamble and sgKdm6a clones treated with or without 5 μM cisplatin for 48 hours. (n=4 independent visual fields). Two-tailed Student's t-test was performed. For the representative images, data is indicative of two independent experiments. Scale bar is included. **c:** Box-and-whisker-plot displaying percentage of cell proliferation in sgScramble and sgKdm6a C1 cells at 0 and 48 hour timepoints. (n=3 biologically independent samples per group). Data representative of two independent experiments. For all the box-and-whisker plots, the center line marks the median, the edges of the box represent the interquartile (25th–75th) percentile and the whiskers represent minimum-maximum values.

- To address the Reviewer's concern regarding the impact on extrachromosomal DNA in cisplatin resistance, we performed whole genome sequencing (WGS) on human bladder cancer cell lines RT4 and K2 (KDM6A-KO RT4 cells). Our WGS analysis demonstrated the following:

  The genome-wide copy number heatmap of RT4 and K2 cells showed increased copy number gains in various genomic regions specifically in chromosomes 2, 3, and 7, indicating increased amplifications in these regions upon KDM6A loss. (Figure **5** in the point-by-point response letter and Fig.**1H** in revised manuscript).

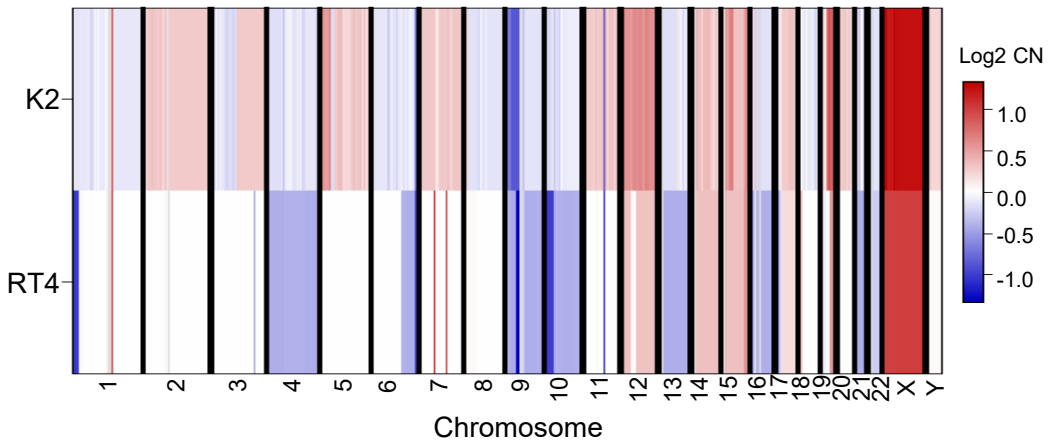

Figure 5: The heatmap showing genome-wide copy-number changes in K2 and RT4 bladder cancer cell lines. The red tones denote copy number gains or amplifications, and blue tones represent copy number losses or deletions.

Analysis of the circular-amplicons using Circle-map showed multiple circular amplicons carrying critical genes implicated in promoting cisplatin resistance including *TP63*[3, 4, 5], , *CLDN4*[6, 7], *GLI2*[8, 9, 10, 11], *LUC7L3*[12, 13], *ERCC4*[14, 15]and *SHCBP1*[16, 17, 18] in KDM6A KO cells (K2 cells) (Figure **6** in the point-by-point response letter and Fig **1I** and Extended data Fig. **2E** in revised manuscript). We used the standard thresholds of split reads greater than 2 and circle score higher than 50 to ensure the reliability of observations which has been described in the Methods section of the revised manuscript.

As the genome wide copy number heatmap showed increased amplifications in chromosomes 2, 3, and 7, we evaluated copy numbers for the eccDNA gene loci. Coverage plot of the genes showed increased copy numbers in K2 cells than RT4 cells. (Figure **7** in the point-by-point response letter and Fig **1I** and Extended data Fig. **2F** in revised manuscript).

To summarize, these results show KDM6A loss mediated formation of eccDNA as a vehicle for multiple critical genes that drive cisplatin resistance in bladder cancer cells.

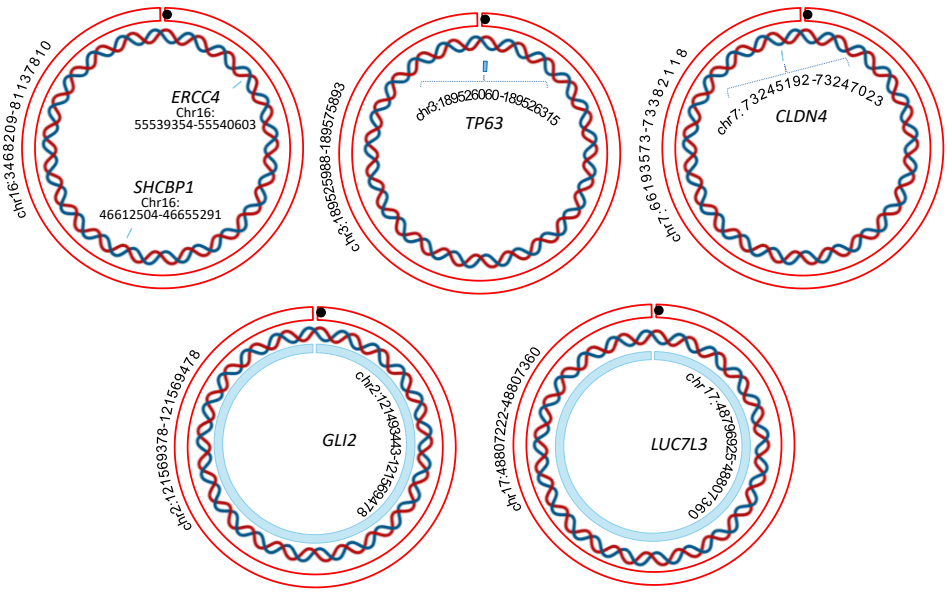

Figure 6: Circos plots displaying indicated eccDNA amplicons identified in K2 cells. The outer red ring represents whole amplicon, the black dot marks the start coordinate of indicated amplicon, and the inner blue region denotes the regions mapped to indicated genes within the respective amplicon.

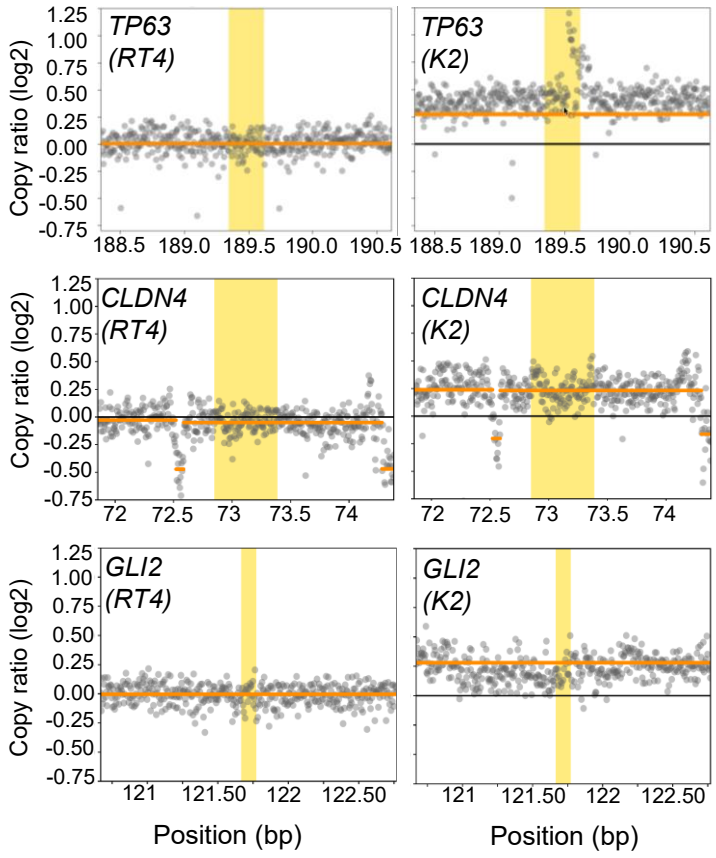

Figure 7: The scatter plots showing the copy number amplifications for indicated genes at their eccDNA loci in RT4 and K2 cells. The gray dots represent probes across the region labeled on x-axis, while y-axis represents the copy ratio (log2) at that genomic position for the gray dots. The orange horizontal line is the segmentation line indicating true copy number state for the segment, and the yellow vertical bars mark the regions for *TP63, CLDN4* and *GLI2* within the amplicon.

2. Effects on the MMR machinery are not convincing, as is the case for the association with response to immunotherapy. They should consider multiple independent series and perform multivariable analysis. Co-occurrence and mutual exclusivity are probably not corrected for multiple testing. The association with tumor mutational burden should be analysed if there is a real effect on MMR. The standard MMR analysis included several microsatellite sites, rather than just one. The effects are small in several of the comparisons shown. In panel H comparing one cell line to another is just inappropriate. More details is required in the description of multiple results in Figure 2. Reduced expression of MMR proteins should be shown using western blotting, with appropriate controls.

Author's Response: We thank the Reviewer for these important comments.

- The MSI-High phenotype is primarily driven by attenuation of expression of genes associated with MMR machinery secondary to mutations in the DNA MMR system, which in turn leads to a higher tumor mutation burden (TMB). Our prior analysis demonstrated a higher TMB in patients harboring *KDM6A* mutation across two independent datasets (IMvigor210[19] and TCGA-BLCA[1]) (Figure **8a** in the point-by-point response letter and Fig. **2C** in the revised manuscript). Based on the Reviewer's suggestion, we reanalyzed all co-occurrence and mutual exclusivity analyses, correcting for multiple testing using the Benjamini–Hochberg FDR[20] (Figure **8b** in the point-by-point response letter and Fig. **2D** in the revised manuscript). This confirmed no significant correlation between cooccurrence of *KDM6A* mutations and mutations in MMR machinery genes.

- To directly link KDM6A loss with MMR machinery disruption, we analyzed RNA sequencing data from two sgKdm6a cell clones following KDM6A knockout (Figure **8c** in the point-by-point response letter and, Fig. **2G** and Extended Data Fig. **3J** in the revised manuscript). We noted a significant attenuation of the MMR pathway, evidenced by a reduction in the expression of multiple MMR pathway genes. To establish a mechanistic link between KDM6A loss and MMR pathway disruption, ChIP seq analysis was performed. We found that the loss of KDM6A led to reduced KDM6A binding, enrichment of H3K27me3 repressor marks and a concomitant reduction in the enrichment of H3K4me3 activation marks at the promoters of key MMR genes, including *MSH2* and *MSH6* (Figure **8d** in the point-by-point response letter and Fig. **2F** and Extended Data Fig. **3G** in the revised manuscript).

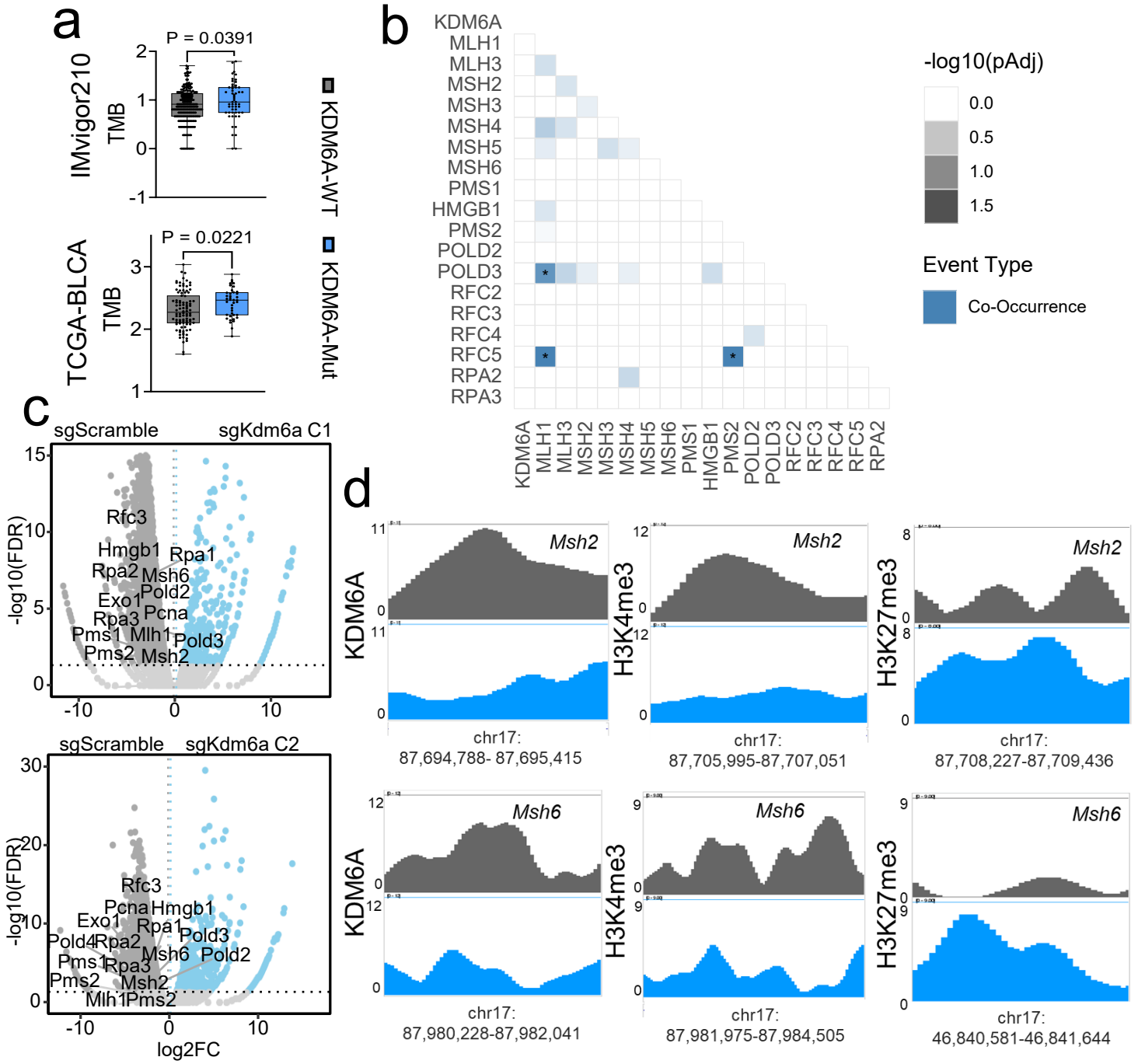

Figure 8: a: Box-and-whisker plots representing TMB in KDM6A-WT and KDM6A-Mut patients with advanced bladder cancer, from two patient cohorts. (IMVigor210, n=293 patients; TCGA BLCA, n=136 patients). Two-sided Wilcoxon test was performed. **b:** Somatic interaction plot depicting co-occurrence in patients from the TCGA bladder cancer cohort (n=412 patients). Two-tailed Pair wise Fisher's exact test was performed and derived p-values were adjusted with Benjamini–Hochberg method (-log10(pAdj)). **c:** Volcano plot representing differential expression of the indicated genes involved in MMR pathway between sgScramble and sgKdm6a C1 (Top) and sgScramble and sgKdm6a C2 (Bottom) cell lines from RNA-seq. Volcano plots show the log2 ratio of fold change (log2FC) plotted against the Absolute Confidence, -log10 adjusted p-value (-log10(FDR)). The p-values were calculated with two tailed exact test under a negative binomial distribution using EdgeR and adjusted with Benjamini–Hochberg method. **d:** Genome browser plots representing KDM6A (Left), H3K4me3 (Middle) and H3K27me3 (Right) peaks for indicated gene loci in sgKdm6a and sgScramble C1 cells. For all the box-and-whisker plots, the center line marks the median, the edges of the box represent the interquartile (25th–75th) percentile and the whiskers represent minimum-maximum values.

- Extending our previous findings, we performed CRISPR-Cas9 mediated knockout of KDM6A in two additional human bladder cancer cell lines, RT4 and ScaBER. The knockout cells for the RT4 and ScaBER cell lines are designated as K2 and B7 respectively. We validated the downregulation of KDM6A using western blot (Figure **9a** in the point-by-point response letter and Extended Data Fig. **1B** in the revised manuscript). Subsequent qRT-

PCR analysis demonstrated a significant reduction in key MMR machinery genes like *MSH2* and *MSH6* (Figure **9b** in the point-by-point response letter and, Fig. **2I** and Extended Data Fig. **4A** in the revised manuscript). Additionally, to validate our previous mechanistic studies in murine cell lines, we performed ChIP-qPCR analysis which confirmed the direct binding of KDM6A to MMR pathway genes in RT4 cells. Reduction in KDM6A binding to *MSH6* and *MLH1* alongside a reduction in H3K4me3 enrichment at *MSH6*, *MLH1* and *MSH2* gene promoters supported a direct role for KDM6A in maintaining the epigenetic landscape of these critical repair genes (Figure **9c, d** in the point-by-point response letter and Extended Data Fig. **4D, E** in the revised manuscript).

These data suggest that the attenuation of MMR-associated gene expression results from direct transcriptional regulation by KDM6A rather than from co-occurring mutations in canonical MMR genes, underscoring the role of KDM6A as an upstream epigenetic regulator of genomic stability.

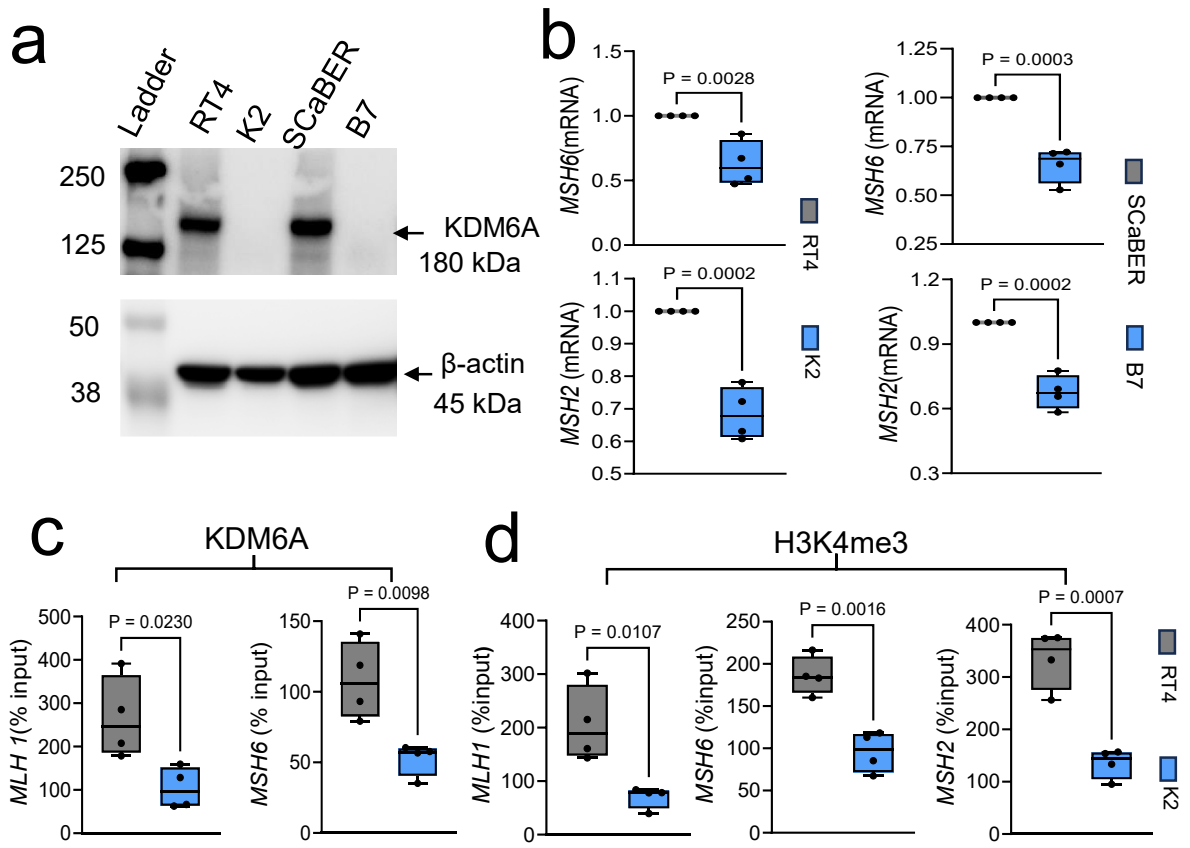

Figure 9: a: Representative western blot image indicating the expression of KDM6A (180 kDa) and β-ACTIN (45 kDa) in RT4, K2, ScaBER and B7 cell lines. Data is representative of two independent experiments. **b:** Box-and-whisker plots demonstrating relative expression of *MSH6* and *MSH2* genes in RT4 and K2 (Left) and ScaBER and B7 (Right) cell lines. (n=4 biologically independent samples per group). Two-tailed Student's t-test was performed. **c-d:** Box-and-whisker plot showing the ChIP-qPCR analysis of KDM6A (**c**) and H3K4me3 (**d**) gene enrichment at the indicated gene promoters in RT4 and K2 cell lines. (n=4 biologically independent samples per group). Two-tailed Student's t-test was performed. For all the box-and-whisker plots, the center line marks the median, the edges of the box represent the interquartile (25th–75th) percentile and the whiskers represent minimum-maximum values.

- To address the Reviewer's comment that standard MMR analysis should assess multiple microsatellite loci rather than a single site, we performed Fluorescent Fragment Length Analysis (FFLA) to evaluate microsatellite instability (MSI) across murine and human bladder cancer models. Specifically, we analyzed murine sgScramble (N=7) and sgKdm6a (N=7) tumors using markers mBAT64, mBAT24, mBAT37, and mBAT59, and human bladder cancer cell lines RT4 (wild-type KDM6A) and K2 (KDM6A knockout) using NR27, NR21, NR24, BAT25, and BAT26. Among these markers, we observed reproducible modal peak shifts associated with KDM6A loss. The mBAT64 locus showed 5-nucleotide leftward shift in sgKdm6a murine tumors compared with sgScramble controls, while the NR21 locus in K2 human cells exhibited a corresponding 5-nucleotide rightward shift. Although these changes were limited to specific loci, they are consistent with microsatellite instability and

support impaired MMR fidelity following KDM6A loss (Figure **10a, b** in the point-by-point response letter and Fig. **2J** and Extended Data Fig. **4F-H** in the revised manuscript).

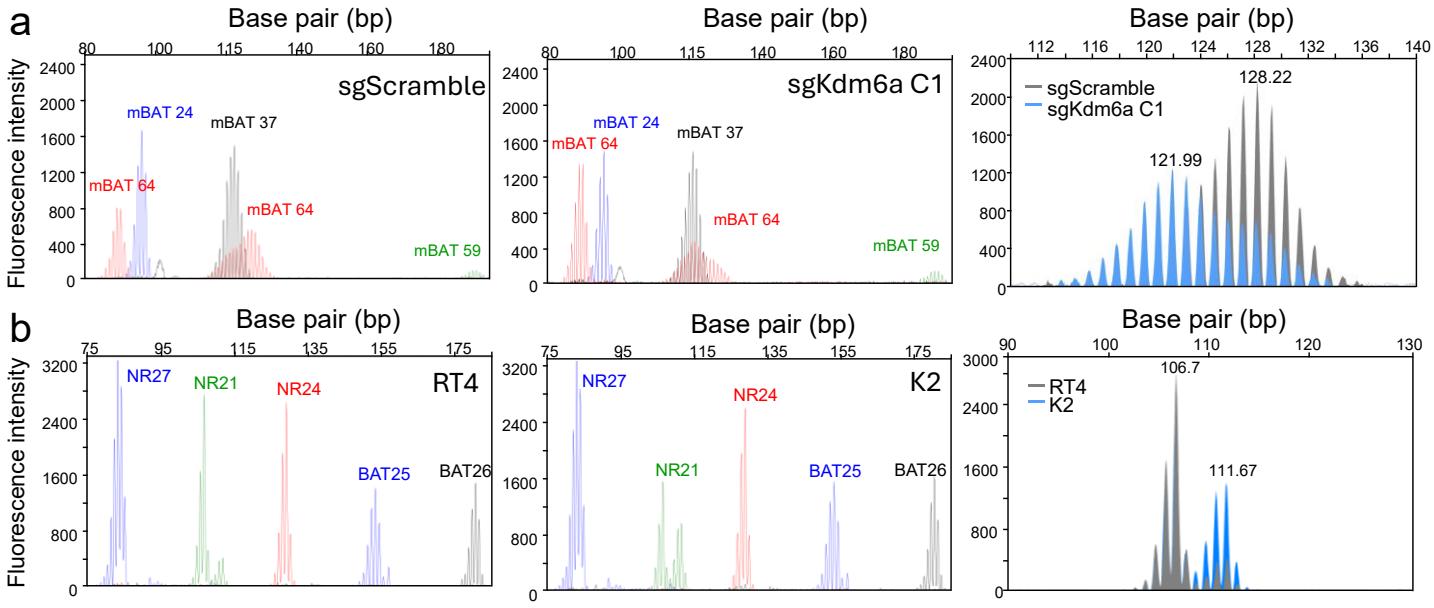

Figure 10: a: Representative electropherograms derived from Fragment Fluorescent Length Analysis (FFLA) of all indicated murine microsatellite markers (Left, Middle) and overlayed mBAT64 marker (Right) in sgScramble and sgKdm6a C1 tumors. **b:** Representative electropherogram derived from FFLA analysis of all indicated human microsatellite markers (Left, Middle) and overlayed NR21 marker (Right) from RT4 and K2 cells. Data is representative of two independent experiments.

- To address the Reviewer's concern regarding the comparison of one cell line to another, we have expanded our analysis by generating CRISPR-Cas9 mediated KDM6A knockout cell lines K2 and B7 in two additional human bladder cancer cell lines, RT4 and ScaBER respectively. We validated the loss of KDM6A using western blot (Figure **9a** in the point-by-point response letter and Extended Data Fig. **1B** in the manuscript). Consistent to our murine RNA-seq data with the sgScramble and sgKdm6a clones, we observed a significant reduction in expression of key MMR machinery genes like, *MSH2* and *MSH6* (Figure **9b** in the point-by-point response letter and Fig. **2I** and Extended Data Fig. **4A** in the revised manuscript). Further ChIP-qPCR data in RT4 and K2 cell lines demonstrated reduced KDM6A binding at MLH1 and MSH6 genes alongside reduced H3K4me3 enrichment at MLH1, MSH6 and MSH2 corroborating our previous mechanistic studies. (Figure **9c, d** in the point-by-point response letter and Extended Data Fig. **4D, E** in the revised manuscript)

- To address the Reviewer's concern regarding reduced expression of MMR proteins, we used flow cytometry to assess the protein expression levels of MSH2 and MSH6 in these cells (Figure **11a, b** in the point-by-point response letter and Extended Data Fig. **4B, C** in the manuscript). Consistent with our gene expression data, we observed a decrease in protein expression in both human cells in absence of KDM6A expression. We selected flow cytometry as it provides precise and quantitative measurement of protein expression over western blot which offers semi quantitative analysis.

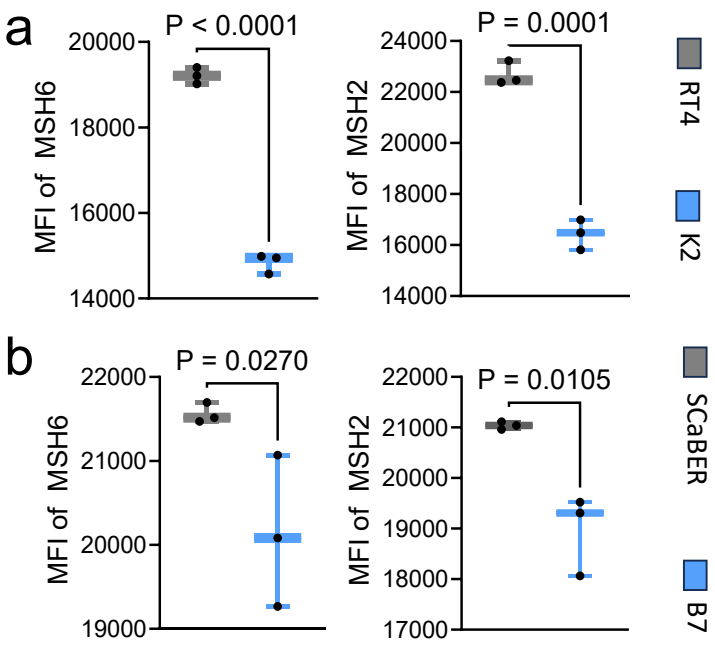

Figure 11: a-b: Box-and-whisker plots demonstrating MFI of MSH6 (Left) and MSH2 (Right) in RT4 and K2 (**a**) and ScaBER and B7 (**b**) cell lines. (n=3 biologically independent samples per group). Two-tailed Student's t-test was performed. For all the box-and-whisker plots, the center line marks the median, the edges of the box represent the interquartile (25th–75th) percentile and the whiskers represent minimum-maximum values.

3. The effects on the DBS break pathway are poorly analyzed. Are the differences in gene expression shown in Figure 3 related to differences in cell proliferation or cell cycle distribution? Data in panel C do not have any statistical analysis. Panels F and H in Figure 3 lack baseline comparisons.

Author's Response: We thank the Reviewer for these thoughtful comments.

- Our murine RNA-seq data demonstrated reduced expression of DSBR pathway genes such as *Exo1, Lig3* and *Baz1b* in sgKdm6a cells as compared to sgScramble cells (Figure **12a** in the point-by-point response letter and Fig. **3C** and Extended data Fig. **5H** in the revised manuscript). Additionally, our ChIP seq analysis demonstrated reduction in KDM6A binding at the promoter of genes associated with DSBR pathway in sgKdm6a cells with a reduction in enrichment of H3K4me3 at these gene promoters (Fig. **3A** in the revised manuscript). To address the Reviewer's concern regarding the impact on DSBR pathway, we expanded the analysis to further validate our data, incorporating an alternative sgKdm6a clone (sgKdm6a C2) and two human bladder cancer cell lines (RT4 and ScaBER).

- Consistent with our prior findings, analysis of the additional murine sgKdm6a clone C2 revealed reduced expression of genes such as *Exo1*, *Lig3*, and *Baz1b*, accompanied by diminished KDM6A binding and attenuated H3K4me3 enrichment at their promoter regions (Figure **12a, b** in the point-by-point response letter and Extended data Fig. **5D, H** in revised manuscript). Similarly, with the loss of KDM6A in K2 and B7 cell lines, significant decrease in the expression of gene like *BAZ1B*, *EXO1* and *LIG3* were observed (Figure **12c, d** in the point-by-point response letter and Extended Data Fig. **5I, J** in the revised manuscript). ChIP-qPCR analysis further showed decreased KDM6A occupancy and H3K4me3 enrichment at these loci in K2 cells with KDM6A loss, consistent with our murine data (Figure **12e, f** in the point-by-point response letter and Extended Data Fig. **5K, L** in the revised manuscript).

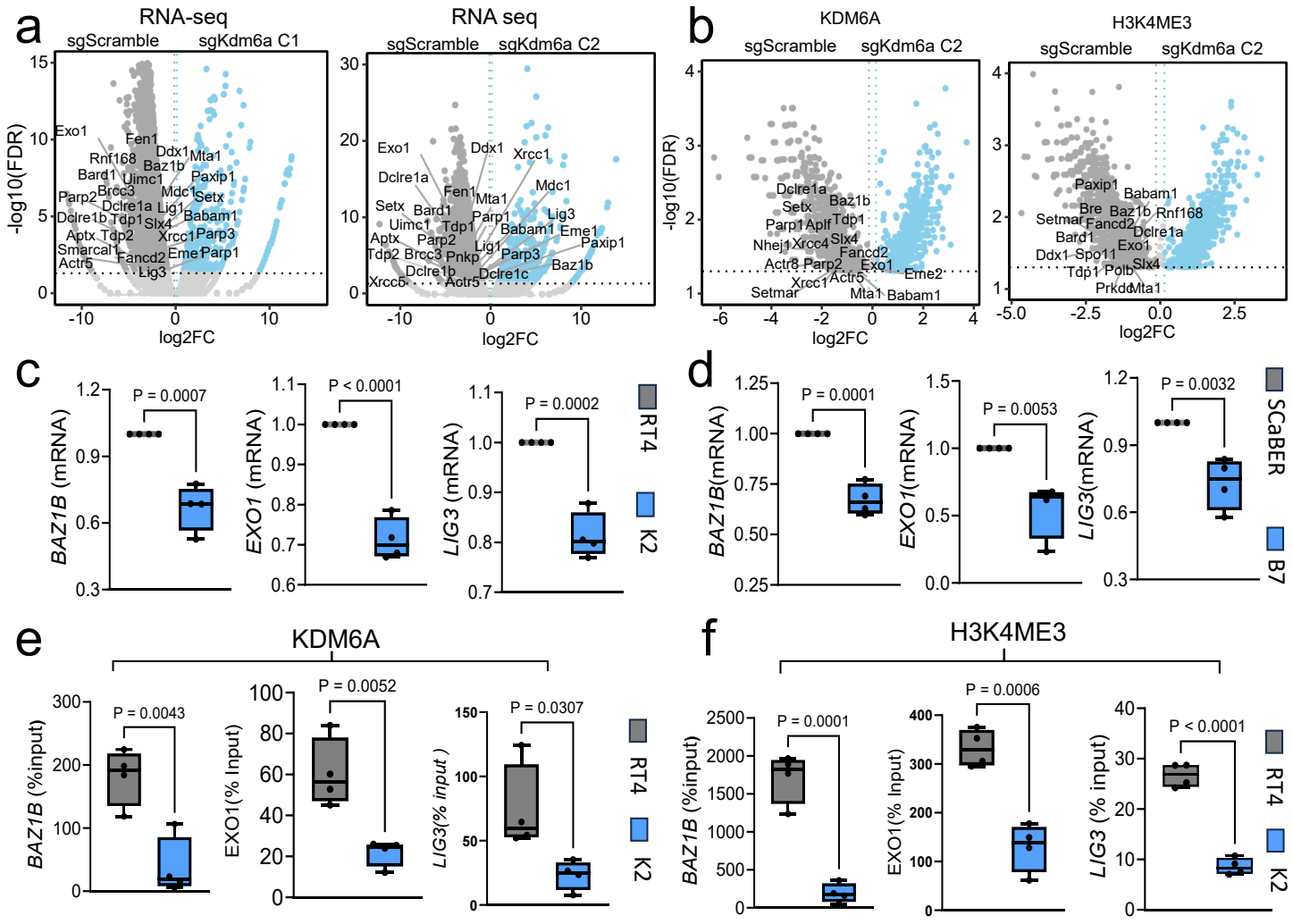

Figure 12: a: Volcano plots representing differential expression of the indicated genes involved in DSBR pathway between sgScramble and sgKdm6a C1 (Left) and sgScramble and sgKdm6a C2 (Right) cell lines from RNA-seq. Volcano plots show the log2 ratio of fold change (log2FC) plotted against the Absolute Confidence, -log10 adjusted p-value (-log10(FDR)). The p-values were calculated with two tailed exact test under a negative binomial distribution using EdgeR and adjusted with Benjamini–Hochberg method. **b:** Volcano plots demonstrating the differential enrichment of KDM6A (Left Panel) and H3K4me3 (Right Panel) marks in the indicated genes involved in DSBR pathway between sgScramble and sgKdm6a C2 cell lines, from ChIP-seq. Volcano plots show the log2 ratio of fold change (log2FC) plotted against the Absolute Confidence, -log10 adjusted p-value (-log10(FDR)). The p-values represent two-tailed probability distribution based on Bayesian model calculated using MAnorm **c-d:** Box-and-whisker plots demonstrating relative expression of *BAZ1B, EXO1* and *LIG3* genes in RT4 and K2 cell lines (**c**) and ScaBER and B7 cell lines (**d**) (n=4 biologically independent samples per group). Two-tailed Student's t-test was performed. **e-f:** Box and whisker plots showing the ChIP-qPCR analysis of KDM6A (**e**) and H3K4me3 (**f**) enrichment at the *BAZ1B, EXO1* and *LIG3* gene promoters in RT4 and K2 cell lines. (n=4 biologically independent samples per group). Two-tailed Student's t-test was performed. For all the box-and-whisker plots, the center line marks the median, the edges of the box represent the interquartile (25th–75th) percentile and the whiskers represent minimum-maximum values.

- To address the Reviewer's concern regarding potential confounding by cell proliferation or cell cycle distribution, we performed flow cytometry-based cell proliferation and cell cycle analysis using cell permeable labeling dyes. We observed no significant differences between the control and KDM6A knockout cells (Figure **13a-c** in the point-by-point response letter and Extended Data Fig. **1L, 5M** in the revised manuscript). This suggests that the reduction in the expression of genes associated with DSBR pathway is not secondary to altered proliferation or cell cycle phase distribution in murine and human bladder cancer cell lines.

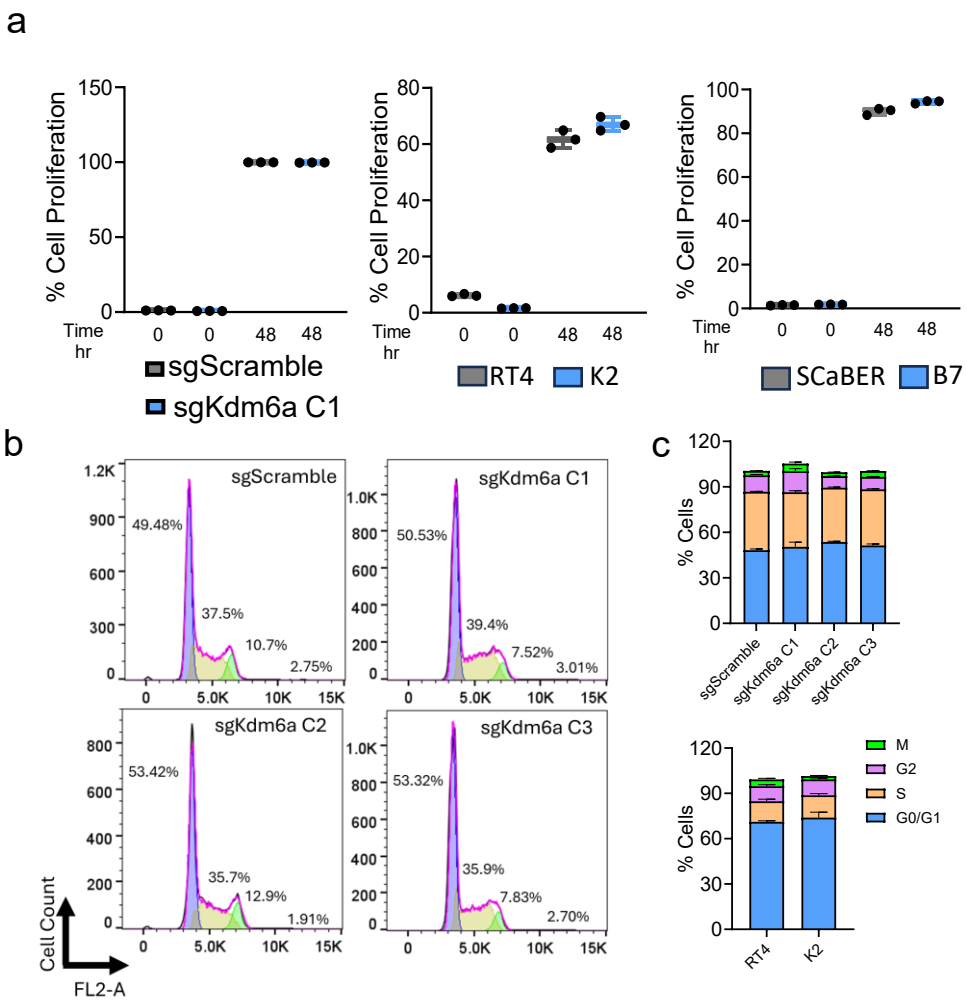

Figure 13: a: Box-and-whisker plots demonstrating percentage of cell proliferation in indicated cell lines at 0 and 48 hour timepoints. (n=3 biologically independent samples per group). Data is representative of two independent experiments. **b-c:** Representative histogram plots illustrating the cell cycle progression percentages in sgScramble, sgKdm6a C1, C2 and C3 cell lines (**b**). Stacked bar plots (**c**) depicting the percentage of cell cycle distribution in sgScramble and sgKdm6a clones (Top) and RT4 and K2 cells (Bottom). (n=3 biologically independent samples per group). Data representative of two independent experiments. For all the box-and-whisker plots, the center line marks the median, the edges of the box represent the interquartile (25th–75th) percentile and the whiskers represent minimum-maximum values.

- To address the Reviewer's comment regarding Extended data Fig. **5F** in the revised manuscript, we would like to clarify that the profile plots represent chromatin signals, whereas the accompanying bar plots show RNA expression levels (counts per million) for genes identified in the differential ChIP-seq and RNA-seq analyses of sgScramble and sgKdm6a C1 cells (Fig. **3A, C** in the revised manuscript). For the profile plots, we extracted peak regions from the differential ChIP-seq analysis of the respective genes and calculated binding scores, which were visualized over a ±1 kb region surrounding the TSS to compare signal intensity between sgKdm6a and sgScramble. To further strengthen these findings, we repeated the analysis in an independent sgKdm6a clone (sgKdm6a C2). Consistent with our previous data, we observed a decrease in expression of genes associated with DSBR pathway along with decreased binding of KDM6A and corresponding reduction in H3K4me3 enrichment in these gene promoter indicating role of KDM6A in regulating DSBR (Figure **12b** in the point-by-point response letter and Extended data Fig. **5D** in the revised manuscript).

- To address the Reviewer's comment regarding the baseline comparisons in Fig. **3E** and **3G** in the revised manuscript, we have included baseline γ-H2AX foci measurements (without Etoposide treatment), from confocal microscopy, which showed a higher abundance of γ-H2AX foci in sgKdm6a C1 cells as compared to sgScramble cells (Figure **14a** in the point-by-point response letter and Fig. **3E** in the revised manuscript). We would also like to clarify that the COMET assay presented in Fig. **3G** in the revised manuscript was performed without the addition of DNA damage inducer (Etoposide). Consistent results were observed in the RT4 and K2

cell lines, where γ-H2AX foci and COMET assay parameters (tail DNA percentage, Olive Tail moment, and tail moment) were all significantly increased upon KDM6A loss in K2 cells (Figure **14b, c** in the point-by-point response letter and Fig. **3H, I** in the revised manuscript).

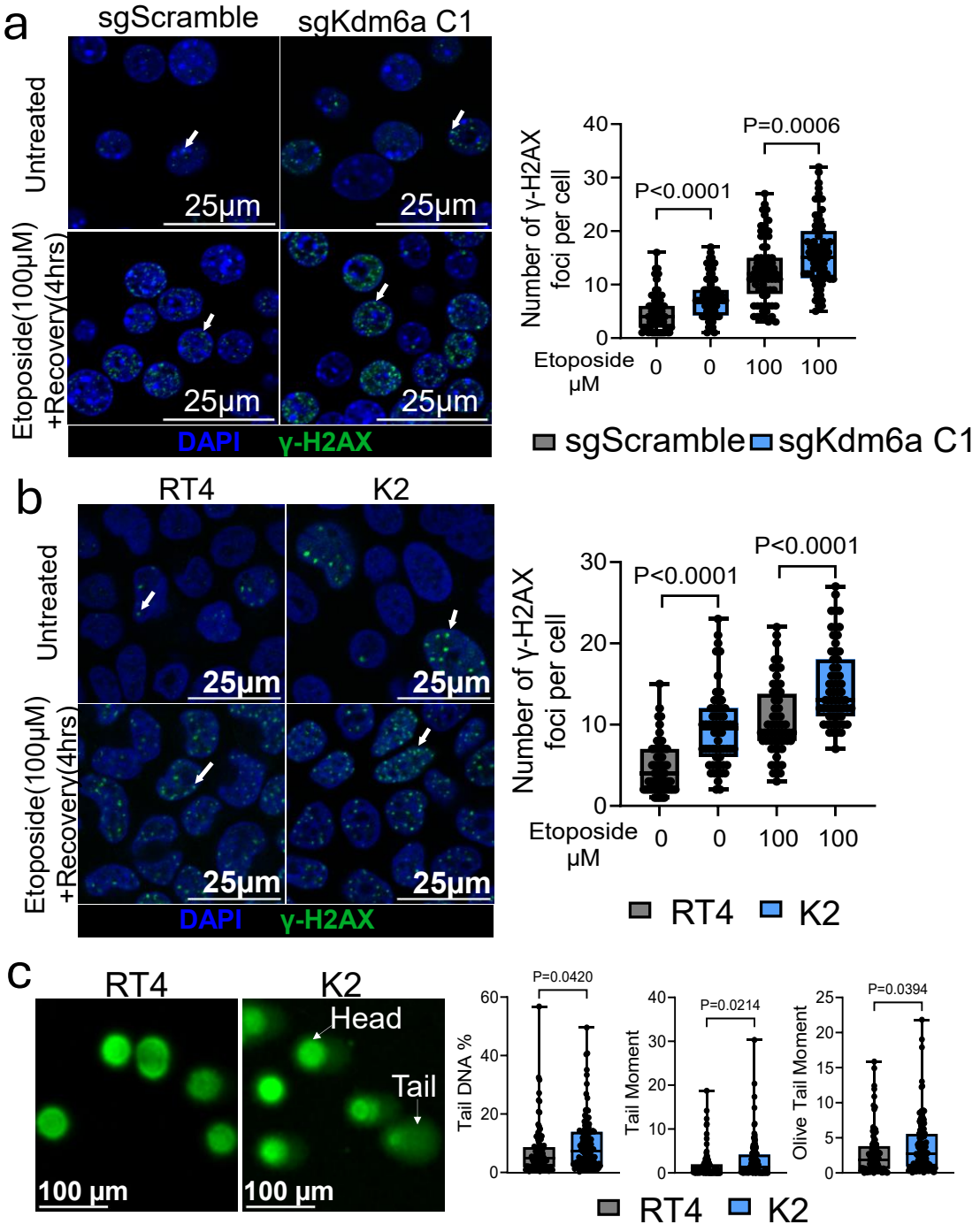

Figure 14: a-b: Representative microscopy images (Left) showing untreated cells and cells treated with 100 μM Etoposide followed by 4 hours of recovery depicting γ-H2AX foci formation (green-FITC) and nuclei (blue-DAPI) in sgScramble and sgKdm6a C1 (**a**) and RT4 and K2 (**b**) cells. The white arrows indicate γ-H2AX foci. Data is representative of two independent experiments. Scale bar is included. Corresponding box-and-whisker plots (Right) depicting number of gamma-H2AX foci per cell in sgScramble and sgKdm6a C1 cell lines(**a**) and RT4 and K2 cells (**b**) with no treatment or Etoposide treatment with 4 hours of recovery. Two-tailed Student's t-test was performed. (n=72 cells (**a**) and 60 cells (**b**) per group). **c.** Representative images (Left) displaying comet-like appearance of DNA (vista green) upon single cell alkaline electrophoresis of RT4 and K2 cells. White arrows points to comet head and comet tail. Data is indicative of two independent experiments. Scale bar is included. Box-and-whisker plots (Right) representing the Tail DNA %, Tail Moment and Olive Moment of the corresponding comet formed in RT4 and K2 cells. (n=106 RT4 cells and 131 K2 cells). Two-tailed Student's t-test was performed. For all the box-and-whisker plots, the center line marks the median, the edges of the box represent the interquartile (25th–75th) percentile and the whiskers represent minimum-maximum values.

Overall, we would like to highlight that among the genes downregulated following *KDM6A* loss, *EXO1* and *LIG3* functions at the interface of the MMR and DSBR pathways. *EXO1*[21, 22, 23, 24] orchestrates the excision step of mismatch repair and contributes to DNA end resection during homologous recombination, whereas *LIG3*[25] mediates repair-gap ligation and supports alternative end-joining under replicative stress. Downregulation of these genes, alongside reduction in the expression of other MMR associated genes, compromises mismatch repair pathway and elements of DSBR pathway, collectively promoting genomic instability. Notably, the repair deficiency arising from KDM6A loss is mechanistically distinct from classical MSI-high or DSBR-defective tumors, as it stems from epigenetic transcriptional repression rather than direct mutational inactivation of canonical repair genes, defining a unique, chromatin-driven form of genomic instability. We have included this in the Discussion section in the revised manuscript.

4. Figure 4 shows very minor, and not always significant, differences in gene expression which render the conclusions less solid. The RNA-seq analysis is not properly described, nor the multiple testing applied. It is kind of surprising that the effects on cell proliferation are associated with reduced glycolysis. Panel E lacks statistics.

Author's Response: We thank the Reviewer for the thoughtful comments.

- We acknowledge that certain genes such as *PFKFB4* and *PGK1* did not meet statistical significance in the IMvigor210[19] dataset (n=275), however, other critical genes in the glycolytic pathway such as *LDHA*, *ENO1*, *BPGM*, *HK2*, *PKM* and *PGM1* expression were significantly attenuated in patients harboring *KDM6A* mutation (Fig. **4A** in the revised manuscript). To address the Reviewer's concern, we extended our analysis to the TCGA-BLCA dataset (n=293)[1], and consistent to our previous analysis we saw significant attenuation in *LDHA* and *ENO1* in KDM6A mutant patients (Figure **15a** in the point-by-point response letter and Extended data Fig. **6A** in revised manuscript).

  Additionally, to address the Reviewer's concern regarding the RNA seq data, we have revised our manuscript describing the RNA seq analysis. We have reanalyzed our RNA seq data applying Benjamini–Hochberg FDR correction for multiple testing. To increase the robustness of the data, we have performed RNA seq analysis in another independent sgKdm6a clone (sgKdm6a C2). We observed a consistent decrease in glycolytic genes in both the sgKdm6a clones C1 and C2 as compared to sgScramble showing downregulation in glycolytic pathway in absence of KDM6A (Figure **15b** in the point-by-point response letter and Fig.**4D** and Extended data Fig. **6H** in revised manuscript).

  Further, to validate these findings in human bladder cancer cells with KDM6A knockout, we performed qPCR and ChIP-qPCR. Reduced glycolytic gene expression was observed in K2 and B7 with KDM6A deletion (Figure **16a, b** in the point-by-point response letter and Fig. **4E** and Extended data Fig. **6J** in revised manuscript). We also observed a decreased KDM6A occupancy and H3K4me3 enrichment at glycolytic promoters in the K2 cells as compared to RT4 cells from our ChIP-qPCR data (Figure **16c, d** in the point-by-point response letter and Extended data Fig. **6K, L** in revised manuscript).

  Together, these results demonstrate that KDM6A directly regulates glycolytic pathways and that its loss drives metabolic reprogramming.

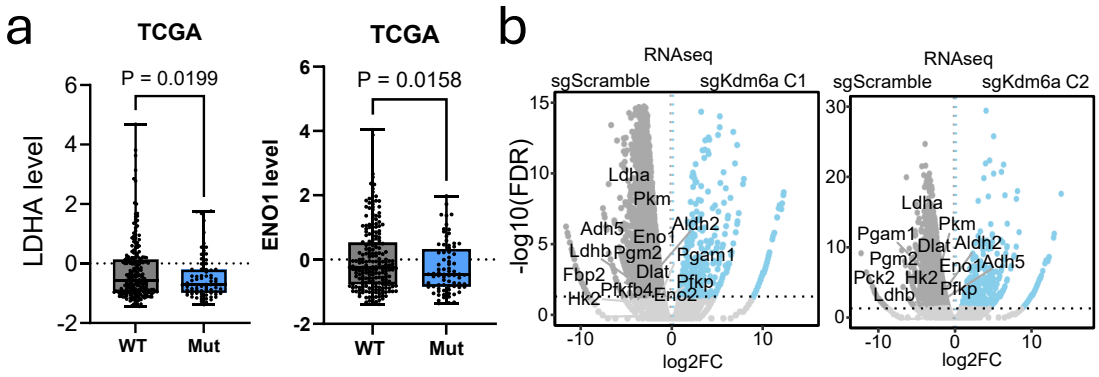

Figure 15: a: Box-and-whisker plots depicting the expression of the indicated genes involved in glycolysis and lactate production in KDM6A-WT and KDM6A-Mut patients, from the TCGA dataset. (n=295 patients). One-tailed Student's t-test was performed. **b:** Volcano plots representing differential expression of the indicated genes involved in glycolysis pathway between sgScramble and sgKdm6a C1(Left) and sgScramble and sgKdm6a C2 (Right) cell lines from RNA-seq. Volcano plots show the log2 ratio of fold change (log2FC) plotted against the Absolute Confidence, -log10 adjusted p-value (-log10(FDR)). The p-values were calculated with two tailed exact test under a negative binomial distribution using EdgeR and adjusted with Benjamini–Hochberg method. For all the box-and-whisker plots, the center line marks the median, the edges of the box represent the interquartile (25th–75th) percentile and the whiskers represent minimum-maximum values.

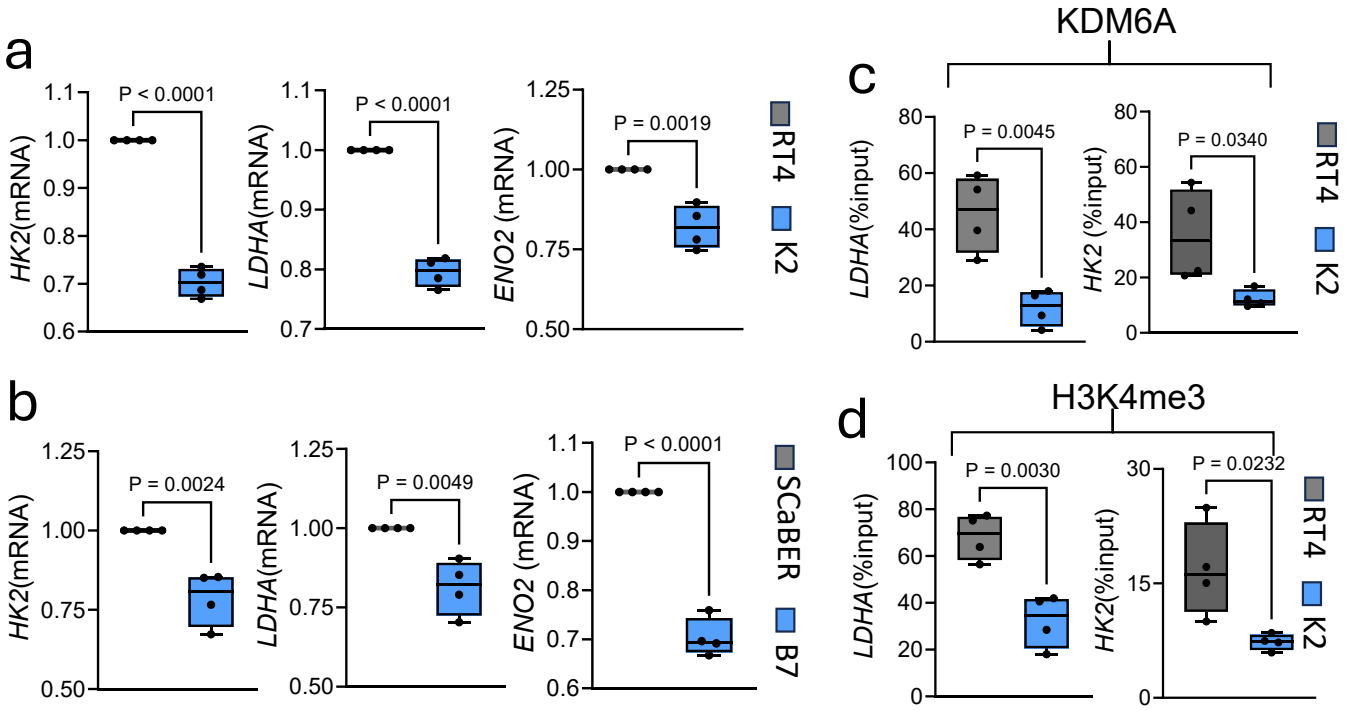

Figure 16: a-b: Box-and-whisker plots demonstrating relative expression of *HK2, LDHA* and *ENO2* genes in RT4 and K2 cell lines(**a**) and ScaBER and B7 cells (**b**) (n=4 biologically independent samples per group). Two-tailed Student's t-test was performed. **c-d:** Box and whisker plots showing the ChIP-qPCR analysis of KDM6A (**c**) and H3K4ME3 (**d**) enrichment at the *LDHA* and *HK2* gene promoters in RT4 and K2 cell lines. (n=4 biologically independent samples per group). Two-tailed Student's t-test was performed. For all the box-and-whisker plots, the center line marks the median, the edges of the box represent the interquartile (25th–75th) percentile and the whiskers represent minimum-maximum values.

- We acknowledge the Reviewer's comment regarding glycolysis and cell proliferation. In both murine and human cell lines, glycolytic ATP production was significantly reduced, accompanied by a compensatory metabolic shift toward oxidative phosphorylation (OXPHOS) following KDM6A loss (Figure **17a, b** in the point-by-point response letter and Fig. **4F-I** in revised manuscript).This is consistent with prior reports showing that cancer cells adapt to glycolysis inhibition by upregulating mitochondrial respiration[26] and activating the TCA cycle[27].

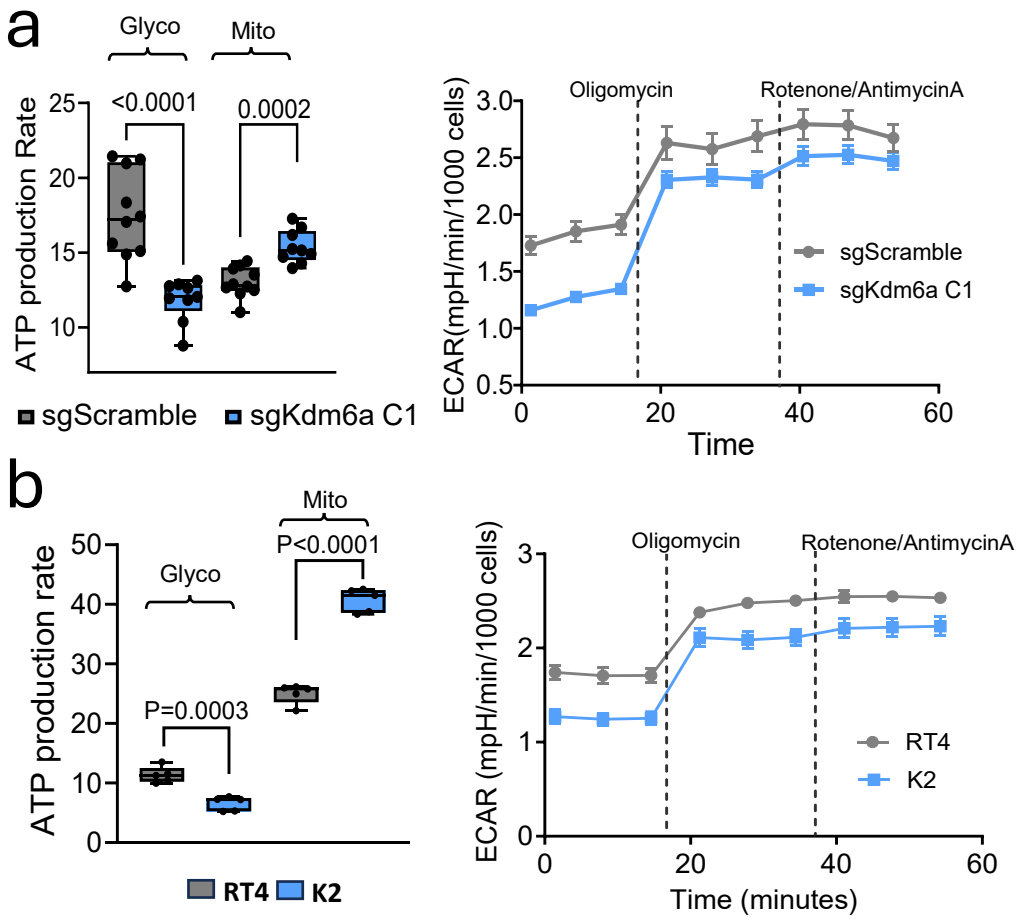

Figure 17: a-b: Box-and-whisker plots (Left) representing glycolytic and mitochondrial ATP production rate in sgScramble and sgKdm6a C1 (**a**) as well as in RT4 and K2 (**b**) cell lines measured by the Seahorse XF analyzer-based ATP Rate Determination Assay (n=9-10 (**a**) and n=5 (**b**) biologically independent samples per group). Two-tailed Student's t test was performed. Line plot (Right) comparing Extracellular acidification rate (ECAR) between sgScramble and sgKdm6a C1 (**a**) as well as in RT4 and K2 (**b**) cell lines as determined by the Seahorse assay. Data represented as mean +/- Standard error of mean (SEM). (n=11(**a**) and n=5(**b**) biologically independent samples per group). For all the box-and-whisker plots, the center line marks the median, the edges of the box represent the interquartile (25th–75th) percentile and the whiskers represent minimum-maximum values.

- To address the Reviewer's concern regarding Extended data Fig. **6E** in the revised manuscript, we would like to clarify that the profile plots represent chromatin signals at gene loci (e.g., *Ldha, Hk2, Eno2*), whereas the accompanying bar plots show RNA expression levels (counts per million) for genes identified in the differential ChIP-seq and RNA-seq analyses. For the profile plots, we extracted peak regions from the differential ChIP-seq analysis of the respective genes and calculated binding scores, which were visualized over a ±1 kb region surrounding the TSS to compare signal intensity between groups. We have revised the Methods section to include necessary details for ChIP-seq analysis.

5. The concentrations of lactate used are very high compared to physiological levels and the effects in Figure 5-6 are often quite small. The genomic analysis is not properly controlled, nor does it have sufficient explanation about replicates, statistics, etc.

Author's Response: We thank the Reviewer for this important comment. For our experiments, we used lactate concentrations that have been widely used in prior studies to assess functional effects on immune subsets[28, 29, 30, 31]. While physiological lactate levels in immune cells typically range from 1–2 mM, pathological states such as chronic inflammation and cancer create a microenvironment where lactate concentrations rise substantially due to rapid glycolysis and the "Warburg effect".

- To address the Reviewer's concern, we tested the impact of exogenous lactate on T regulatory (Treg) cell function using sodium lactate at 5, 10, 15, and 25 mM. We observed a dose-dependent increase in H3K18la and H3K9la histone lactylation, along with elevated PD-1 expression in Tregs even at lower concentrations. (Figure **18a, b** and **19** in the point-by-point response letter and Extended data Fig. **7C** and **8E, F** in revised manuscript).

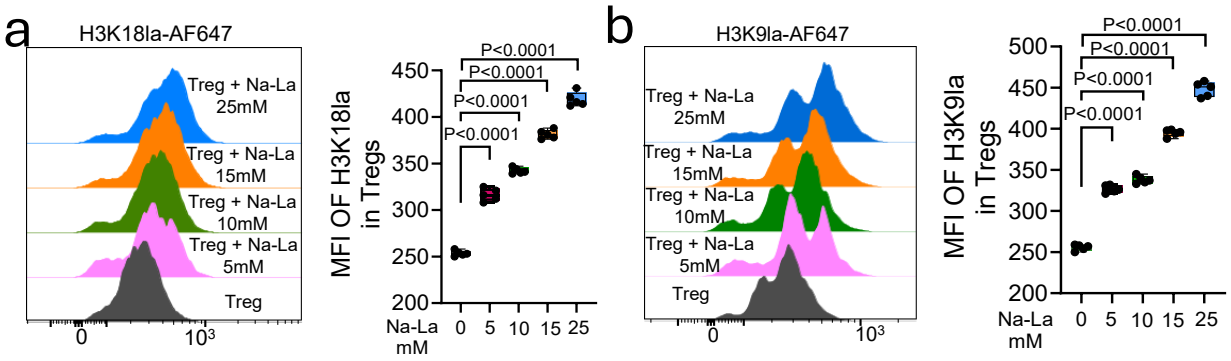

Figure 18: a: Representative Histograms (Left) and Box-and-whisker plots (Right) demonstrating the MFI for H3K18la(**a**) and H3K9la (**b**) in *in-vitro* generated Tregs treated with and without Na-La for 48 hours at the indicated doses. (n=5 biologically independent samples per group). Data representative of two independent experiments. Two-tailed Student's t test was performed. For all the box-and-whisker plots, the center line marks the median, the edges of the box represent the interquartile (25th–75th) percentile and the whiskers represent minimum-maximum values.

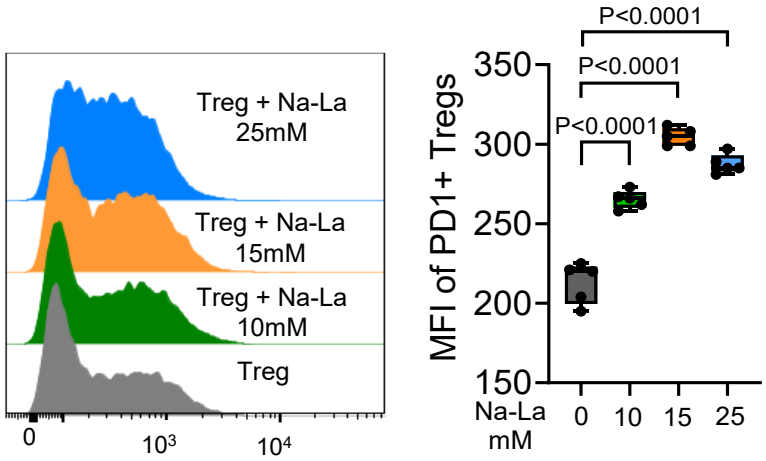

Figure 19: Representative Histogram (Left) and Box-and-whisker plot (Right) demonstrating the MFI for PD-1 in *in-vitro* generated Tregs treated with and without Na-La for 48 hours at the indicated doses. (n=5 biologically independent samples per group). Data representative of two independent experiments. Two-tailed Student's t test was performed. For the box-and-whisker plot, the center line marks the median, the edges of the box represent the interquartile (25th–75th) percentile and the whiskers represent minimum-maximum values.

- The details regarding replicates, controls, and statistical analyses for the genomic data presented in Fig. **6B**, Fig. **6C** and Extended data Fig. **8G** in the revised manuscript, have now been clarified in both the Methods and figure legends. Briefly, quality control, read mapping, and downstream processing of ChIP-seq data were performed using standard tools and approaches. In addition, matched "Input controls" were included to ensure accurate identification of significant ChIP-seq signal enrichment peaks.

We compared genomic occupancy and differential enrichment of histone PTMs (H3K9la, H3K18la, H3K4me3, and H3K27ac) in Tregs treated with sodium lactate (Treg + Na-La) versus untreated controls (Tregs). Notably, Na-La–treated Tregs exhibited higher enrichment of H3K9la and H3K18la, accompanied by increased expression of key genes regulating Treg identity and function, including *Foxp3, Pdcd1, and Tgfβ1* (Fig. **6C, D** and Extended data Fig. **8l** in revised manuscript). These findings support a role for exogenous lactate–derived H3K9la and H3K18la in modulating gene expression in Tregs. The Methods section of the revised manuscript has been updated to provide critical details of the genomic analyses.

Reviewer #2 (Remarks to the Author): with expertise in cancer, immunology

This study aims to elucidate an innovative model in which loss of KDM6A regulates therapeutic response in bladder cancer through two distinct mechanisms: accumulation of extrachromosomal circular DNA (eccDNA), contributing to platinum resistance, and lactate-mediated histone lactylation, which modulates Treg function and enhances immunotherapy sensitivity. The authors integrate multi-omics analyses with comprehensive in vitro and in vivo functional assays, and the conceptual framework holds promising translational potential. However, several important issues remain to be addressed:

We sincerely thank the Reviewer for the assessment of our manuscript and for recognizing the translational potential of our conceptual framework.

Major Comments

1.In Figure 1D, the figure legend states that the wound-healing assays under cisplatin treatment were performed with n = 9 biologically independent samples per group; however, the box-and-whisker plot shows approximately 12 data points for the sgScramble group and 15 for the sgKdm6a group, which is inconsistent with the stated sample size. A similar discrepancy appears in Figure 1C ("sgScramble + cisplatin" legend: n = 3 per group, yet only 2 data points are shown) and in Figure 3E, where the MFI of γ-H2AX shows 3 points for sgScramble but the percentage of γ-H2AX shows 6 points, while sgKdm6a shows 5 versus 6 points—contradicting the figure legend's claim of n = 3 for the left panel and n = 5 for the right. Such inconsistencies between declared and plotted sample sizes undermine confidence in the statistical analyses and, by extension, the study's mechanistic conclusions.

Author's Response: We thank the Reviewer for this important comment. We would like to emphasize that the sample sizes presented are not inconsistencies. Rather, they reflect the reporting format we were instructed to follow during a prior rebuttal for *Nature Immunology* (Raychaudhuri, Singh et al. [28]), where we were advised to report the lowest **n** within the total sample group rather than providing a range. In preparing this manuscript for *Nature Communications*, we adhered to the same formatting approach. Importantly, all plotted data points correspond to biological replicates, no data has been excluded, and all statistical analyses were performed on the complete dataset.

However, we are happy to revise the figure legends to explicitly indicate the full range of sample sizes if preferred by the Reviewer and the editorial team**.**

2.On line 89, the authors state, "we uncovered a previously uncharacterized role for KDM6A in tumor metabolic reprogramming. Loss of KDM6A suppressed glycolytic flux and decreased intratumoral lactate accumulation." However, Yang et al. (PMID: 36215227) have already reported that KDM6A regulates tumor glycolysis. The authors should temper their language, cite Yang et al., and discuss how their findings extend or differ from that prior work.

Author's Response: We thank the Reviewer for drawing our attention to the study by Yang et al.[32] which demonstrated that in glioblastoma HOXA3 activates KDM6A to remove the repressive H3K27me3 mark at glycolytic gene loci, thereby promoting glycolysis and tumor progression. We modified the sentence and acknowledged this study in our discussion section of the revised manuscript.

Our findings extend this concept by showing that KDM6A loss suppresses glycolysis and reduces intratumoral lactate production, thereby reshaping the tumor immune microenvironment in bladder cancer. Additionally, CRISPR-mediated KDM6A deletion attenuated H3K4me3 enrichment at glycolytic promoters linking the loss of a permissive histone mark to impaired glycolytic gene expression. This metabolic reprogramming shifted cells toward OXPHOS, lowered lactate levels, and reduced lactate-driven histone lactylation in Tregs, ultimately improving the CD8 T cells:Treg ratio and enhancing responsiveness to anti-PD-1 therapy.

Thus, while Yang et al. established a HOXA3–KDM6A–H3K27me3 axis in glioblastoma, our work demonstrates that KDM6A loss disrupts both H3K27me3 and H3K4me3 regulation, thereby linking metabolic reprogramming with immune modulation and therapeutic response in bladder cancer.

3.While the wound-healing assay in Figure 1 is informative, it assesses only two-dimensional migration and can be confounded by proliferation and scratch width variability. Incorporating Transwell migration and invasion assays would provide more quantitative and mechanistic insight into how KDM6A loss affects bladder cancer cell motility and invasiveness.

Author's Response: We thank the Reviewer for this insightful comment. Based on the Reviewer's suggestions, we measured cell proliferation and performed transwell invasion assays in both control and KDM6A knockout cells. We performed CRISPR-Cas9 mediated knockout of KDM6A in two human bladder cancer cell lines, RT4 and ScaBER and used multiple sgRNAs to generate independent Kdm6a knockout clones (sgKdm6a C1-C3) in murine MB49 cells. K2 and B7 are the respective KDM6A knockout cells of RT4 and ScaBER[2]. Western blot analysis was used to validate successful deletion of KDM6A in human as well as the murine cell lines (Figure **20a, b** in the point-by-point response letter and Extended data Fig.**1A, B** in revised manuscript).

We performed cell proliferation assay for the treatment period of 48 hours. Proliferation rates were comparable between the control and KDM6A knockout groups across the cell lines, ruling out proliferation as a confounder (Figure **20c** in the point-by-point response letter and Extended data Fig.**1L** in revised manuscript).

Additionally, KDM6A knockout cells (K2 and B7) from both the human cell lines and the murine sgKdm6a clones exhibited higher transwell invasion under cisplatin treatment compared to controls (Figure **20d-f** in the point-by-point response letter and Fig. **1D, E** and Extended data Fig.**1F, G** in revised manuscript).

To further validate our observations, we repeated wound-healing, spheroid formation and cisplatin cytotoxicity assays in additional murine and human KDM6A knockout cell lines, all of which confirmed that KDM6A loss is associated with enhanced cell motility and cisplatin resistance (Figure **21a-h** in the point-by-point response letter and Fig.**1C, F, G** and Extended data Fig.**1D, E, H-K** in revised manuscript).

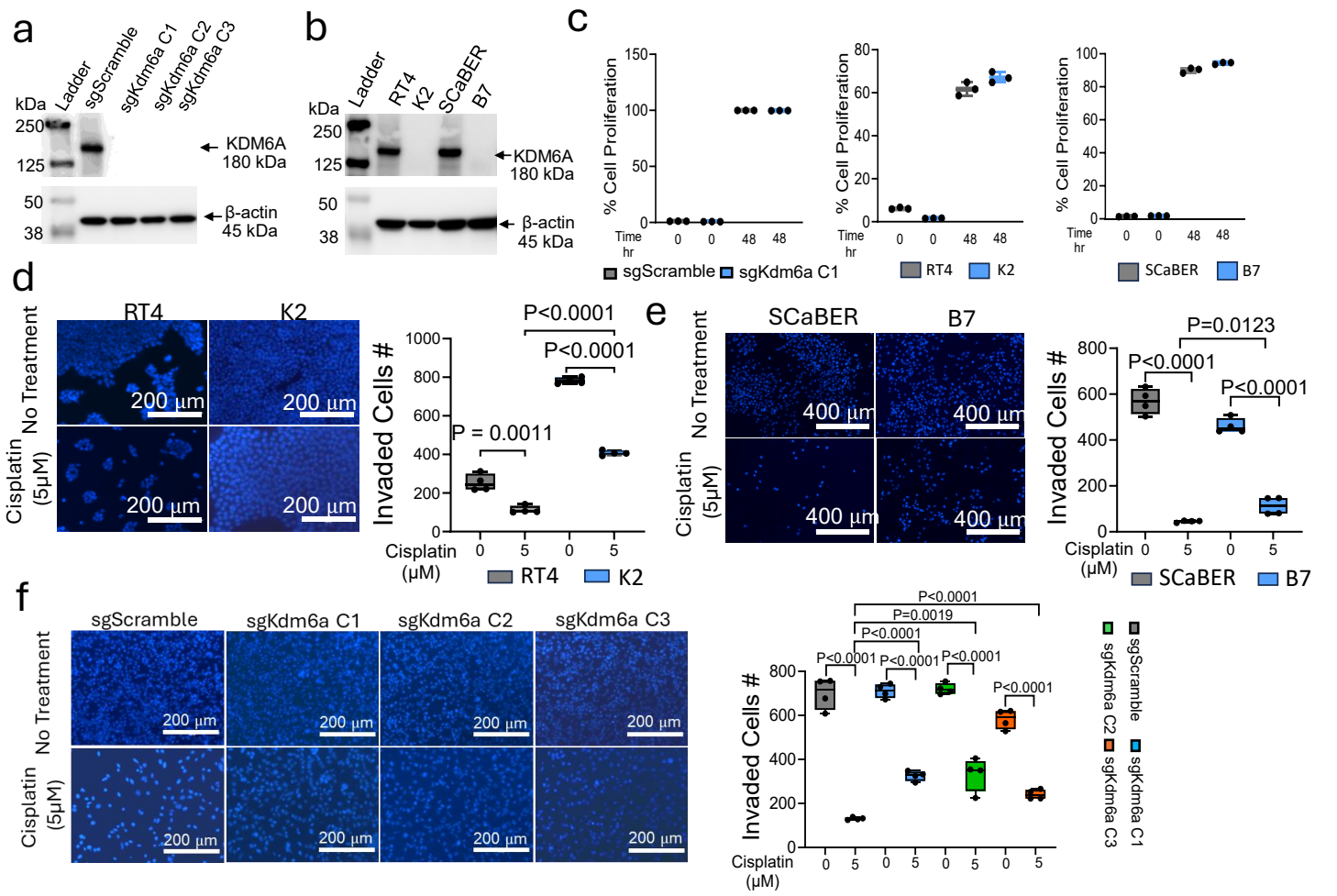

Figure 20: **a-b**: Representative western blot image indicating the expression of KDM6A (180 kDa) and β-ACTIN (45 kDa) in sgScramble and sgKdm6a clones (**a**) and RT4, K2, ScaBER and B7 cell lines (**b**). Data is representative of two independent experiments**. c:** Box-and-whisker plots demonstrating the percentage of cell proliferation in indicated cell lines at 0 and 48 hour timepoints (n=3 biologically independent samples per group). Data is indicative of two independent experiments. **d-f**: Representative images (Left) and box-and-whisker plots (Right) demonstrating the invaded cell number in Transwell assay for RT4 and K2 cells (**d**), ScaBER and B7 cells (**e**) and sgScramble and sgKdm6a clones cells (**f**) treated with or without 5 μM cisplatin for 48 hours (n=4 independent visual fields). Two-tailed Student's t-test was performed. For the representative images, data is indicative of two independent experiments. Scale bar is included. For all the box-and-whisker plots, the center line marks the median, the edges of the box represent the interquartile (25th–75th) percentile and the whiskers represent minimum-maximum values.

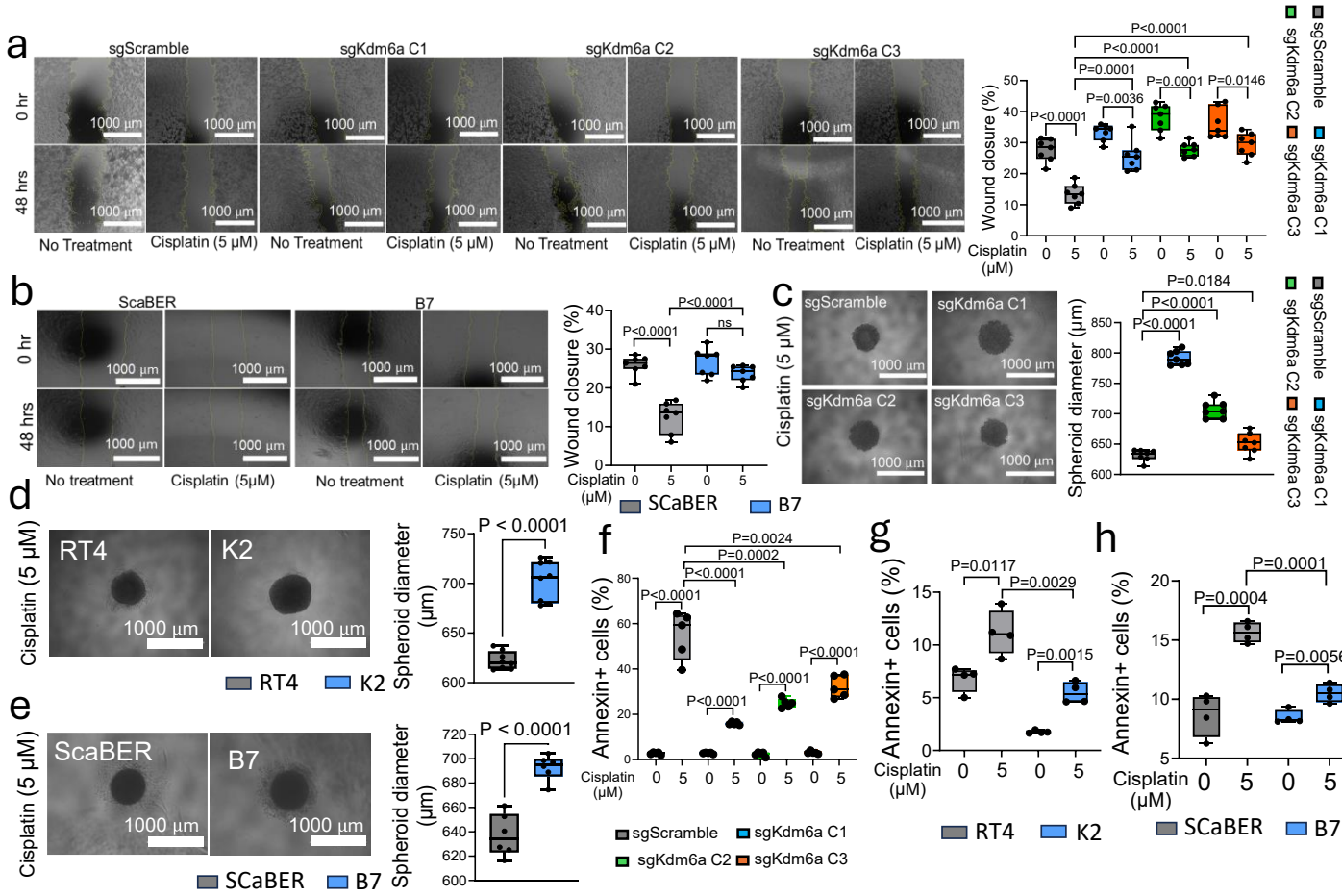

Figure 21: a-b: Representative images (Left) and box-and-whisker plots (Right) depicting the percentage of wound closure of sgScramble and sgKdm6a clones (**a**) and ScaBER and B7 (**b**) cells treated with or without 5 µM cisplatin for 48 hours. (n=7 biologically independent samples per group). Two-tailed Student's t-test was performed. For the representative images, data is indicative of two independent experiments. Scale bar is included. **c-e**: Representative images (Left) and box-and-whisker plots (Right) showing the diameter of sgScramble and sgKdm6a (**c**), RT4 and K2 (**d**) and ScaBER and B7 (**e**) spheroids treated with 5 µM cisplatin for 48 hours. (n=7 (**c**), n=8 (**d**) and n=6 (**e**) biologically independent samples per group). Two-tailed Student's t-test was performed. For the representative images, data is indicative of two independent experiments. Scale bar is included. **f-h:** Box-and-whisker plots demonstrating percentage of Annexin positive sgScramble and sgKdm6a (**f**) cells, RT4 and K2(**g**) cells and ScaBER and B7(**h**) cells treated with or without 5 µM cisplatin for 48 hours. (n=5 (**f**) and n=4(**g, h**) biologically independent samples per group) Two-tailed Student's t-test was performed. For all the box-and-whisker plots,the centre line marks the median, the edges of the box represent the interquartile (25th–75th) percentile and the whiskers represent minimum-maximum values.

4.Comparing J82 (KDM6A-mutant) and RT4 (KDM6A-wildtype) cell lines offers supportive evidence, but differences in their genetic backgrounds, signaling pathways, and chromosomal alterations may also influence cisplatin sensitivity. To attribute the phenotype specifically to KDM6A, the authors should perform isogenic manipulations—for example, re-expressing KDM6A in J82 and knocking out KDM6A in RT4—and assess cisplatin response in these matched backgrounds.

Author's Response: We thank the Reviewer for the comment regarding the potential impact of genetic background of J82 (KDM6A-mutant) and RT4 (KDM6A-wildtype) cell lines on cisplatin sensitivity. We acknowledge that differences in their genetic makeup, alongside other associated factors, could impact the observed results. To address this concern, we performed CRISPR-Cas9 mediated KDM6A knockout in two distinct human bladder cancer cell lines: RT4 and ScaBER. The knockout cell lines for RT4 and ScaBER are designated as K2 and B7, respectively. KDM6A knockout in the K2 and B7 cell lines was confirmed using western blot (Figure **22a** in the point-by-point response letter and Extended data Fig.**1B** in revised manuscript).

We repeated all the previous experiments, including transwell invasion, spheroid formation, wound healing assay and cisplatin-mediated cytotoxicity assays, to assess the impact of cisplatin treatment. Consistent with our original findings, the KDM6A knockout human bladder cancer cells exhibited increased invasion, migration and spheroid formation, as well as reduced cisplatin-mediated cytotoxicity compared to their respective control cells (Figure **22b-h** in the point-by-point response letter, Fig. **1C, E, G** and Extended data Fig.**1E, G, I, K** in revised manuscript). These results, obtained in multiple isogenic systems, confirm that the loss of KDM6A contributes to cisplatin resistance in bladder cancer cells, independent of broader genetic background differences.

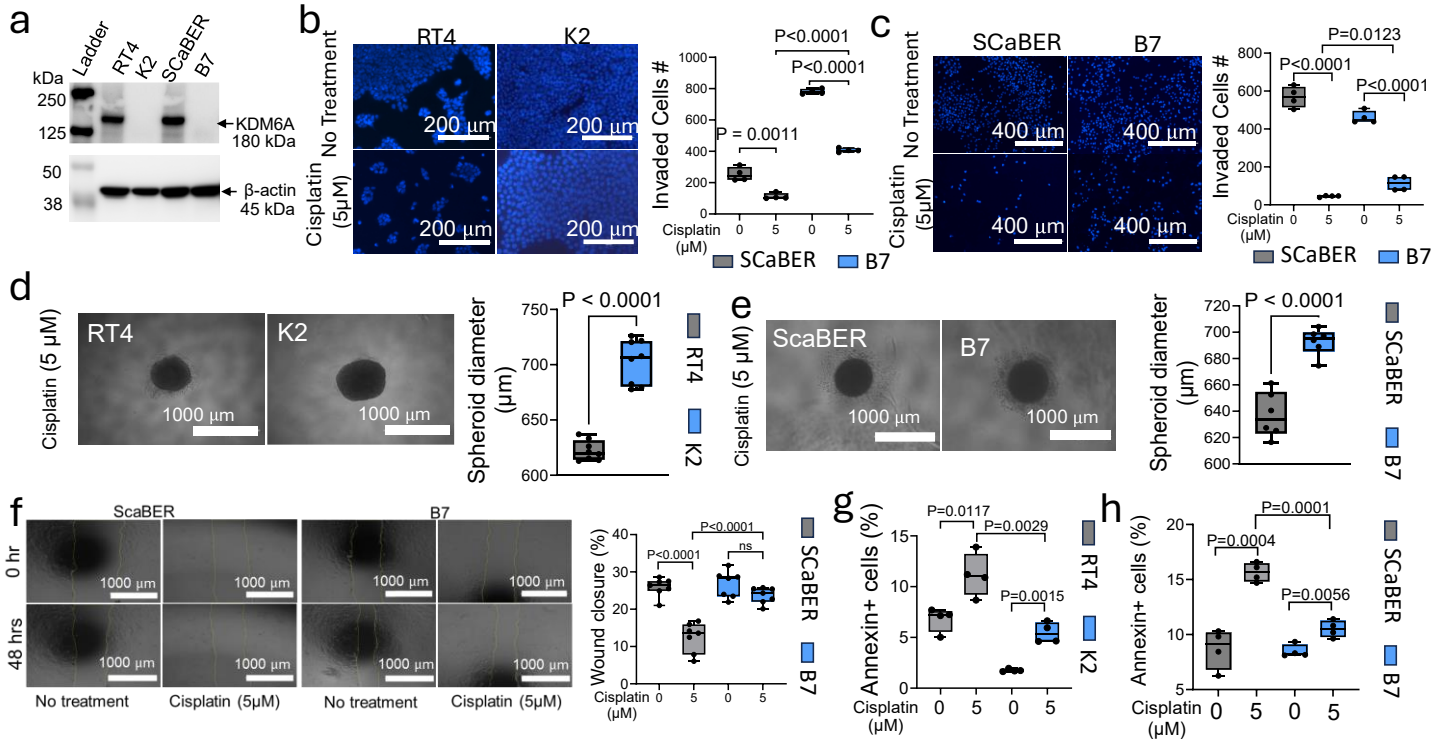

Figure 22: a: Representative western blot image indicating the expression of KDM6A (180 kDa) and β-ACTIN (45 kDa) in RT4, K2, ScaBER and B7 cell lines. Data is representative of two independent experiments. **b-c:** Representative images (Left) and box-and-whisker plots (Right) showing the number of invaded cells in Transwell assay in RT4 and K2 cells (**b**) and ScaBER and B7 cells (**c**) treated with or without 5 μM cisplatin for 48 hours (n=4 independent visual fields). Two-tailed Student's t-test was performed. For the representative images, data is indicative of two independent experiments. Scale bar is included. **d-e:** Representative images (Left) and box-and-whisker plots (Right) showing the diameter of RT4 and K2 (**d**) and ScaBER and B7 spheroids (**e**) treated with 5 μM cisplatin for 48 hours. (n=8(**d**) and n=6(**e**) biologically independent samples per group). Two-tailed Student's t-test was performed. For the representative images, data is indicative of two independent experiments. Scale bar is included. **f:** Representative images (left) and box-and-whisker plot (right) depicting the percentage of wound closure of ScaBER and B7 cells treated with or without 5 μM cisplatin for 48 hours. (n=7 biologically independent samples per group). Two-tailed Student's t-test was performed. **g-h:** Box-and-whisker plots demonstrating percentage of Annexin positive RT4 and K2 cells (**g**) and ScaBER and B7 cells (**h**) treated with or without 5 μM cisplatin for 48 hours. (n=4 biologically independent samples per group) Two-tailed Student's t-test was performed. For all the box-and-whisker plots, the center line marks the median, the edges of the box represent the interquartile (25th–75th) percentile and the whiskers represent minimum-maximum values.

Minor Comments

1.Lines 252–253: In "in J82 cells compared to RT4 cells" (Figure 4C), should this reference be to Extended Data Figure 4C?

Author's Response: We thank the Reviewer for the comment. To eliminate the potential confounding effect of genetic background between distinct cell lines, we have performed CRISPR-Cas9 mediated knockout in two human bladder cancer cell lines RT4 and ScaBER. The knockout cell lines for RT4 and ScaBER are designated as K2 and B7, respectively. We have updated the manuscript to incorporate all experimental data generated using these cell lines. Importantly, consistent to our data from murine KDM6A knockout cells, human cell lines with KDM6A loss

also demonstrated significantly increased cisplatin resistance, which was mediated by the amplification of circular eccDNA amplicons carrying genes associated with cisplatin resistance along with an impairment in MMR, DSBR, and Glycolysis pathways.

2.All histological images lack scale bars; in Figure 3D, the white arrows are unexplained—please add scale bars and clarify the meaning of these arrows.

Author's Response: We thank the Reviewer for their careful review. We apologize for the oversight. The white arrows were mistakenly duplicated from another image and incorrectly placed in Figure 3D. We have rectified this mistake and uploaded the corrected figure in the revised manuscript (Fig **3D** in the revised manuscript). We have also added scale bars to all relevant microscopy images throughout the manuscript.

3.In Figure 4B, correct "Chip-seq" to "ChIP-seq."

Author's Response: We have made the necessary corrections in the updated manuscript.

4.The figure legend numbering for Figures 3E and 3F does not match the order shown in the panels.

Author's Response: We have made the necessary corrections in the updated manuscript.

5.In Figure 4F, the right-hand ECAR y-axis is labeled "mpH/min/Norm. Unit." Please clarify whether "Norm. Unit" refers to normalization by cell number or by protein content. Additionally, the points at which oligomycin and rotenone/antimycin A were added should be indicated on the graph.

Author's Response: We thank the Reviewer for the comment. We had used "cell number" as the Normalization unit. We have updated the y-axis label in the figure. Additionally, we have added the points at which oligomycin and rotenone/antimycin A were added on the graph (Fig **4G, I** in the revised manuscript).

Reviewer #3 (Remarks to the Author): with expertise in bladder cancer, epigenetics

In this manuscript, Singh et al report that KDM6A loss in bladder cancer is associated with altered response to chemotherapy and immune checkpoint blockade treatments, by performing retrospective analysis in published data from advanced bladder cancer patients. They utilize murine cell lines and allograft tumors, as well as human cell lines, and report that KDM6A regulates key genes in several molecular pathways, including genome integrity and metabolism. The authors link the presence of oncogene copies in extrachromosomal DNA to chemotherapy resistance, and metabolic rewiring to improved immune checkpoint blockade (ICB) efficacy. Additionally KDM6A is shown to dysregulate DNA repair pathways that could also contribute to altered therapy response.
Overall, there is considerable novelty in their findings, but several mechanistic connections lack sufficient evidence. To address this issue, the authors should perform functional experiments and change the language in text so that in the revised manuscript it is clear which transcriptional effects of KDM6A loss contribute to altered therapy response and to what degree.

We sincerely thank the Reviewer for the thoughtful assessment of our work and for recognizing the novelty and translational relevance of our findings.

Major comments:
1. Overall the evidence that implicate eccDNA as a cause of chemotherapy resistance is weak (Figures 1G-J,

Lines 386-387). The authors should provide experiments that show presence of oncogenes and/or chemoresistance-associated genes in eccDNA of KDM6A KO/MUT cells (e.g. by FISH). In addition, the authors should provide evidence of specific eccDNA involvement in chemoristance, e.g. by ablation of candidate genes in KDM6A MUT cells to restore chemotherapy sensitivity.

Author's Response:

- We thank the Reviewer for this important comment. In our prior analysis of chromosomal structural variants in the TCGA-BLCA cohort[33], we showed that patients harboring *KDM6A* mutation exhibited more circular amplicons (eccDNA) along with elevated *POLQ* expression, consistent with a role for KDM6A in regulating eccDNA formation (Figure **23a, b** in the point-by-point response letter and Extended Data Fig. **2B, C** in the revised manuscript). To build on these findings and to directly examine the presence of oncogenes and cisplatin resistance–associated genes within eccDNA, we first generated a KDM6A-knockout of the human RT4[2] bladder cancer cell line (designated K2) using CRISPR-Cas9 gene editing. Western blot analysis confirmed successful deletion of KDM6A in K2 cells (Figure **23c** in the point-by-point response letter and Extended Data Fig. **1B** in the revised manuscript). We then performed whole-genome sequencing (WGS) on RT4 and K2 cell lines, which enabled us to characterize eccDNA content and identify oncogene and resistance-associated loci enriched upon KDM6A loss.

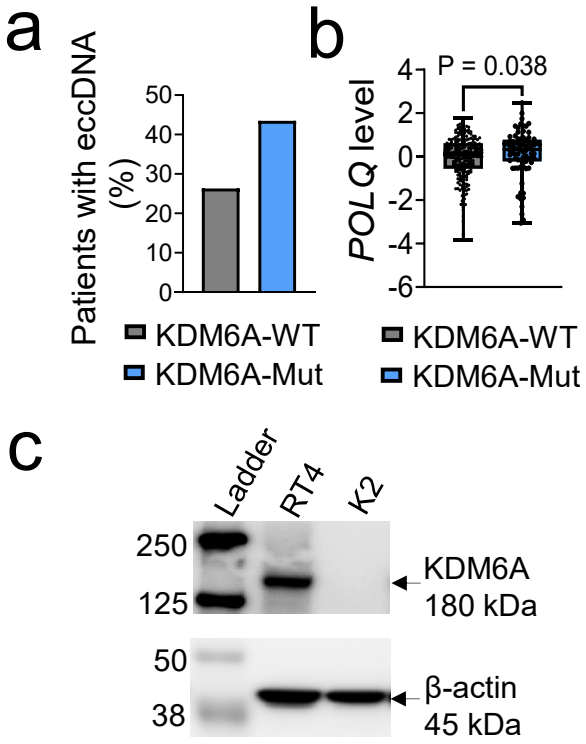

Figure 23: a: Bar graph showing the percentage of KDM6A-WT and KDM6A-Mut patients harboring eccDNA of the TCGA dataset (BLCA cohort). **b**: Box-and-whisker plots depicting the expression of *POLQ*, in KDM6A-WT and KDM6A-Mut patients from the TCGA-BLCA cohort (n=296 patients). Exact Mann-Whitney test was performed. **c:** Representative western blot images depicting KDM6A (180 kDa) and β-ACTIN (45 kDa) expression in RT4 with its KDM6A KO Clone K2. Data is representative of two independent experiments. For the box-and-whisker plot, the center line marks the median, the edges of the box represent the interquartile (25th–75th) percentile and the whiskers represent minimum-maximum values.

- The genome-wide copy number analysis showed increased copy number gains in various genomic regions specifically in chromosomes 2, 3, and 7 in K2 cells, indicating increased amplifications in these regions upon KDM6A loss (Figure **24** in the point-by-point response letter and Fig.**1H** in revised manuscript).

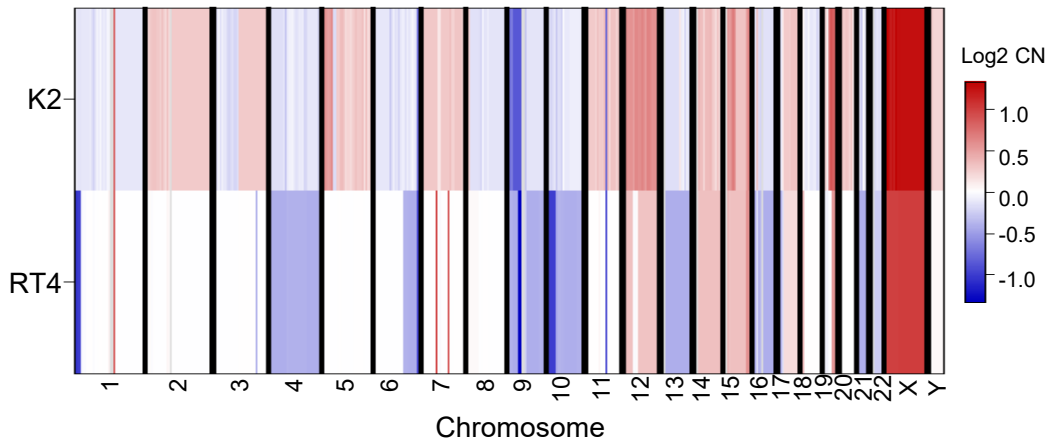

Figure 24: The heatmap showing genome-wide copy-number changes in K2 and RT4 bladder cancer cell lines. The red tones denote copy number gains or amplifications, and blue tones represent copy number losses or deletions.

- Analysis of the circular-amplicons using Circle-map showed multiple circular amplicons carrying critical genes implicated in promoting cisplatin resistance including *TP63*[3, 4, 5], , *CLDN4*[6, 7], *GLI2*[8, 9, 10, 11], *LUC7L3*[12, 13], *ERCC4*[14, 15]and *SHCBP1*[16, 17, 18] in KDM6A KO cells (K2 cells) (Figure **25** in the point-by-point response letter and Fig **1I** and Extended data Fig. **2E** in revised manuscript). We used the standard thresholds of split reads greater than 2 and circle score higher than 50 to ensure the reliability of observations.

  As the genome wide copy number heatmap showed increased amplifications in chromosomes 2, 3, and 7, we evaluated copy numbers for the eccDNA gene loci. Coverage plot of the genes showed increased copy numbers in K2 cells than RT4 cells. (Figure **26** in the point-by-point response letter and Fig **1I** and Extended data Fig. **2F** in revised manuscript).

  To summarize, these results show KDM6A loss mediated formation of eccDNA as a vehicle for multiple critical genes that drive in cisplatin resistance in bladder cancer cells.

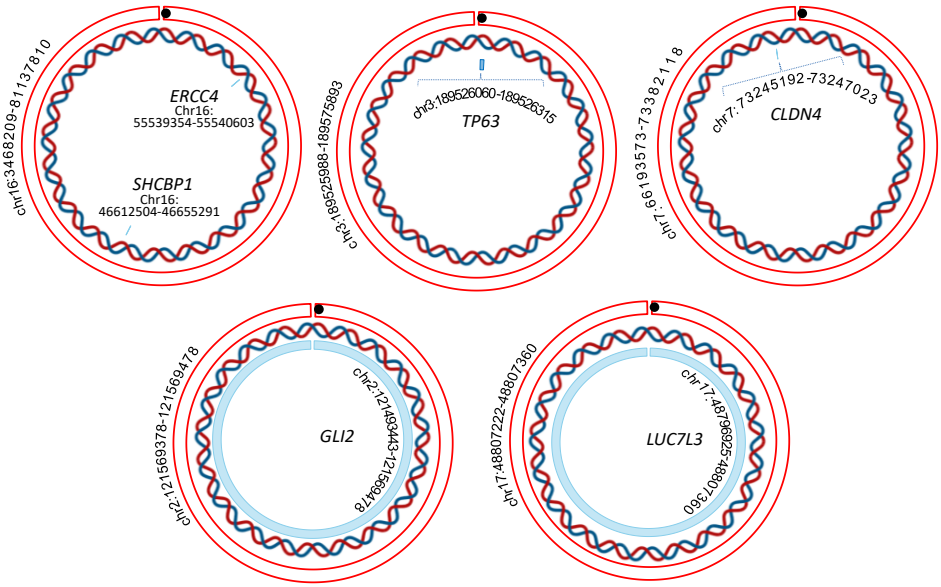

Figure 25: Circos plots displaying indicated eccDNA amplicons identified in K2 cells. The outer red ring represents whole amplicon, the black dot marks the start coordinate of indicated amplicon, and the inner blue region denotes the regions mapped to indicated genes within the respective amplicon.

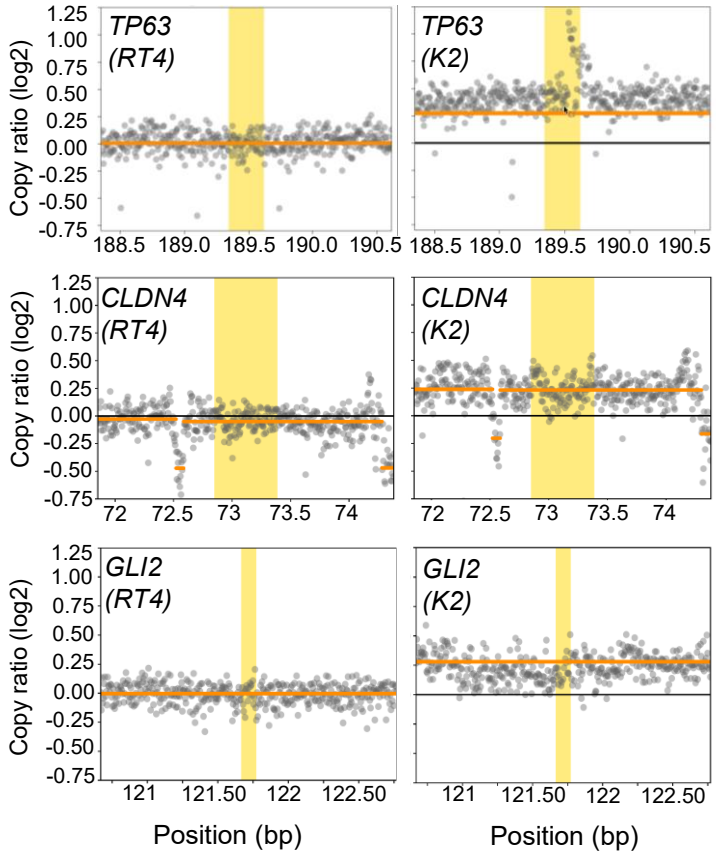

Figure 26: The scatter plots showing the copy number amplifications for indicated genes at their eccDNA loci in RT4 and K2 cells. The gray dots represent probes across the region labeled on x-axis, while y-axis represents the copy ratio (log2) at that genomic position for the gray dots. The orange horizontal line is the segmentation line indicating true copy number state for the segment, and the yellow vertical bars mark the indicated regions for *TP63, CLDN4* and *GLI2* within the amplicon.

Regarding functional validation, we carefully considered the Reviewer's suggestion to ablate individual candidates. However, because multiple resistance genes co-occur on the same eccDNA amplicons, targeting a single locus would not recapitulate the collective oncogenic pressure mediated by eccDNA amplification. Our data instead support a model in which the cumulative amplification of several resistance-associated genes within eccDNA underlies the cisplatin-resistant phenotype of KDM6A-deficient tumors.

2. Comparison of only two human cell lines is not sufficient to draw conclusions about conservation of findings in human cells (Figures 1F, 2H, 3G, Extended Data Figure 4C). The authors should either use more KDM6A WT and KDM6A MUT cells (at least 3 per condition) or perform KO/KD experiments in KDM6A WT cells and/or KDM6A rescue experiments, e.g. by OE, in KDM6A MUT cells.

Author's Response: We thank the Reviewer for this important comment. To directly address the concern, we expanded our analyses beyond the initial comparison of two human bladder cancer cell lines. Specifically, we generated CRISPR-Cas9–mediated KDM6A knockout in RT4 and ScaBER[2] cells, hereafter referred to as K2 and B7, respectively. Western blot analysis verified the successful knockout of KDM6A in K2 and B7.(Figure **27a** in the point-by-point response letter and Extended data Fig. **1B** in revised manuscript).In addition, we validated our results using multiple independent murine Kdm6a-knockout clones.

- To corroborate our previous findings of cisplatin resistance in murine *Kdm6a* knockout MB49 cell lines, we performed similar series of experiments on the human cell lines. We conducted transwell invasion, spheroid formation, cisplatin-mediated cell cytotoxicity and wound healing assays. Consistent with our murine cell line data, the human KDM6A knockout cells showed a significant increase in migration and spheroid formation (Figure **27b-f** in the point-by-point response letter and Fig.**1E, 1G** and Extended data Fig. **1G, I, K** in revised manuscript). We also observed a notable reduction in cisplatin-mediated cell death in the cells with KDM6A ablation (Figure **27g, h** in the point-by-point response letter and Fig.**1C** and Extended data Fig.**1E** in revised manuscript).

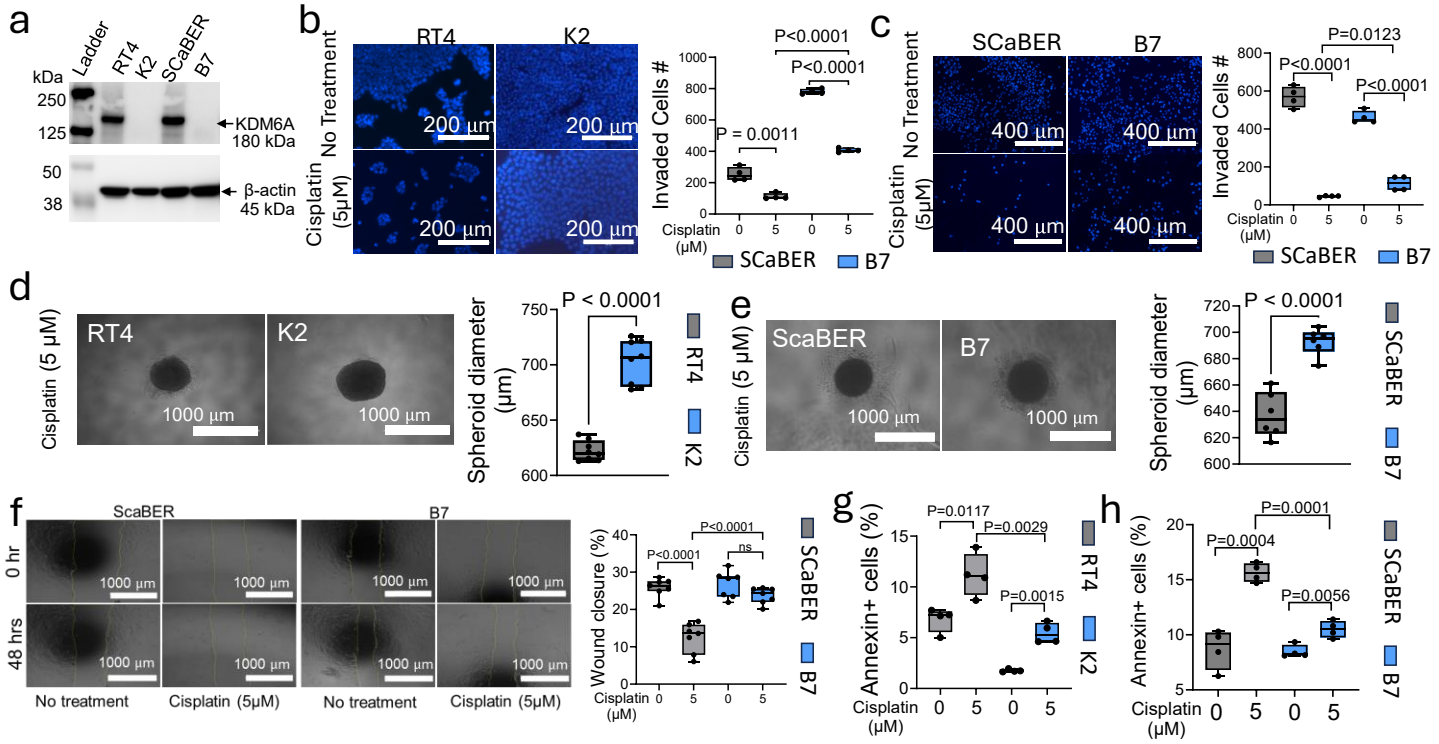

Figure 27: a: Representative western blot image indicating the expression of KDM6A (180 kDa) and β-ACTIN (45 kDa) in RT4, K2, ScaBER and B7 cell lines. Data is representative of two independent experiments. **b-c:** Representative images (Left) and box-and-whisker plots (Right) showing the number of invaded cells in transwells in RT4 and K2 cells (**b**) and ScaBER and B7 cells (**c**) treated with or without 5 μM cisplatin for 48 hours (n=4 independent visual fields). Two-tailed Student's t-test was performed. For the representative images, data is indicative of two independent experiments. Scale bar is included. **d-e:** Representative images (Left) and box-and-whisker plots (Right) showing the diameter of RT4 and K2 (**d**) and ScaBER and B7 spheroids (**e**) treated with 5 μM cisplatin for 48 hours. (n=8(**d**) and n=6(**e**) biologically independent samples per group). Two-tailed Student's t-test was performed. For the representative images, data is indicative of two independent experiments. Scale bar is included. **f:** Representative images (Left) and box-and-whisker plot (Right) depicting the percentage of wound closure of ScaBER and B7 cells treated with or without 5 μM cisplatin for 48 hours. (n=7 biologically independent samples per group). Two-tailed Student's t-test was performed. **g-h:** Box-and-whisker plots demonstrating percentage of Annexin positive RT4 and K2 cells (**g**) and ScaBER and B7 cells (**h**) treated with or without 5 μM cisplatin for 48 hours. (n=4 biologically independent samples per group) Two-tailed Student's t-test was performed. For all the box-and-whisker plots, the center line marks the median, the edges of the box represent the interquartile (25th–75th) percentile and the whiskers represent minimum-maximum values.

- Additionally, we observed a significant decrease in the expression of genes associated with the MMR pathway KDM6A knockout human bladder cancer cells, which is in line with our findings in murine cells lacking KDM6A. Quantitative RT-PCR and Flow cytometry were used to confirm the reduction in expression of MSH2 and MSH6 in the human KDM6A knockout cells K2 and B7(Figure **28a-d** in the point-by-point response letter and Fig.**2I** and Extended data Fig.**4A-C** in revised manuscript).

- To further investigate whether KDM6A directly regulates MMR pathway genes, we performed ChIP-qPCR in RT4 and K2 cells. Our results were consistent with our murine ChIP-seq data, showing reduced KDM6A binding at these MMR-associated genes (Figure **28e** in the point-by-point response letter and Extended data Fig.**4D** in revised manuscript). Additionally, we found a corresponding decrease in the enrichment of H3K4me3, a histone mark associated with active gene transcription, at these same genes in the K2 cells with KDM6A knockout (Figure **28f** in the point-by-point response letter and Extended data Fig. **4E** in revised manuscript).

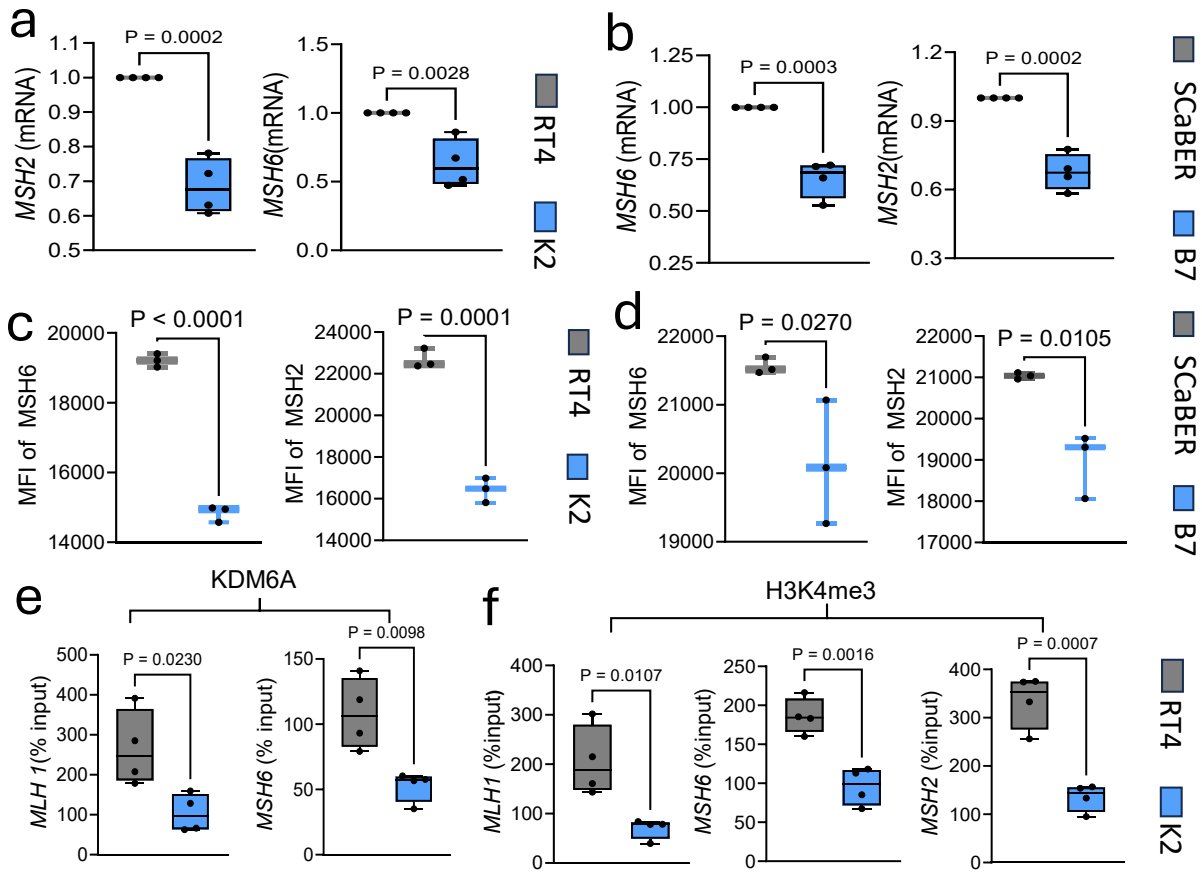

Figure 28: a-b: Box-and-whisker plots demonstrating relative expression of *MSH6* and *MSH2* genes in RT4 and K2 cell lines(**a**) and ScaBER and B7 (**b**) cell lines (n=4 biologically independent samples per group). Two-tailed Student's t-test was performed. **c-d:** Box-and-whisker plots demonstrating the MFI of MSH6 and MSH2 in RT4 and K2 cell lines (**c**) and ScaBER and B7 cell lines (**d**). (n=3 biologically independent samples per group). Two-tailed Student's t-test was performed. **e-f:** Box and whisker plots showing the ChIP-qPCR analysis of KDM6A (**e**) and H3K4me3 (**f**) enrichment at the indicated gene promoters in RT4 and K2 cell lines. (n=4 biologically independent samples per group). Two-tailed Student's t-test was performed. For all the box-and-whisker plots, the center line marks the median, the edges of the box represent the interquartile (25th–75th) percentile and the whiskers represent minimum-maximum values.

- Next, we assessed the impact of loss of KDM6A in human bladder cancer cell lines on the expression of genes associated with DSBR pathway. Consistent with our mouse data, we observed decreased expression of specific genes, such as *BAZ1B*, *EXO1* and *Lig3*, in the human cells K2 and B7 with KDM6A knockout (Figure **29a, b** in the point-by-point response letter and Extended data Fig.**5I, J** in revised manuscript). Our ChIP-seq data further validated these findings, showing reduced binding of KDM6A and a decrease in the enrichment of the H3K4me3 histone mark at these same genes in K2 cells with KDM6A downregulation (Figure **29c, d** in the point-by-point response letter and Extended data Fig. **5K, L** in revised manuscript).

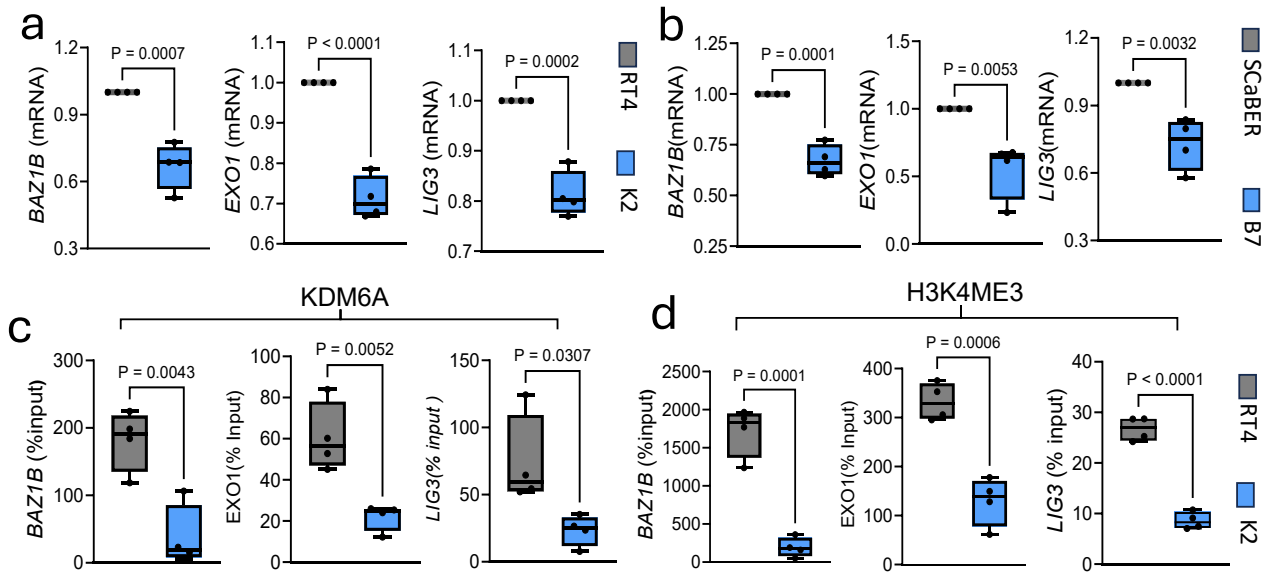

Figure 29: a-b: Box-and-whisker plots demonstrating relative expression of *BAZ1B, EXO1* and *LIG3* genes in RT4 and K2 cell lines (**a**) and ScaBER and B7 cell lines (**b**) (n=4 biologically independent samples per group). Two-tailed Student's t-test was performed. **c-d:** Box and whisker plots showing the ChIP-qPCR analysis of KDM6A (**c**) and H3K4me3 (**d**) enrichment at the *BAZ1B, EXO1* and *LIG3* gene promoters in RT4 and K2 cell lines (n=4 biologically independent samples per group). Two-tailed Student's t-test was performed. For all the box-and-whisker plots, the center line marks the median, the edges of the box represent the interquartile (25th–75th) percentile and the whiskers represent minimum-maximum values.

- We also observed a reduction in the expression of glycolytic genes like *HK2*, *LDHA* and *ENO2* in the human KDM6A knockout cell lines, which we had previously demonstrated in our murine cell lines in absence of KDM6A (Figure **30a, b** in the point-by-point response letter and Fig. **4E** and Extended data Fig **6J** in revised manuscript). Our ChIP qPCR results in the human cell lines also demonstrated decreased KDM6A binding and reduced enrichment of the H3K4me3 histone mark at glycolysis-associated genes like *HK2* and *LDHA*. (Figure **30c, d** in the point-by-point response letter and Extended data Fig.**6K, L** in revised manuscript). Furthermore, these transcriptional changes correlated with a shift in cellular metabolism. Consistent with our murine data, the human KDM6A knockout cells showed reduced glycolytic ATP production and a compensatory increase in mitochondrial ATP production. (Figure **30e** in the point-by-point response letter and Fig.**4H, I** in revised manuscript).

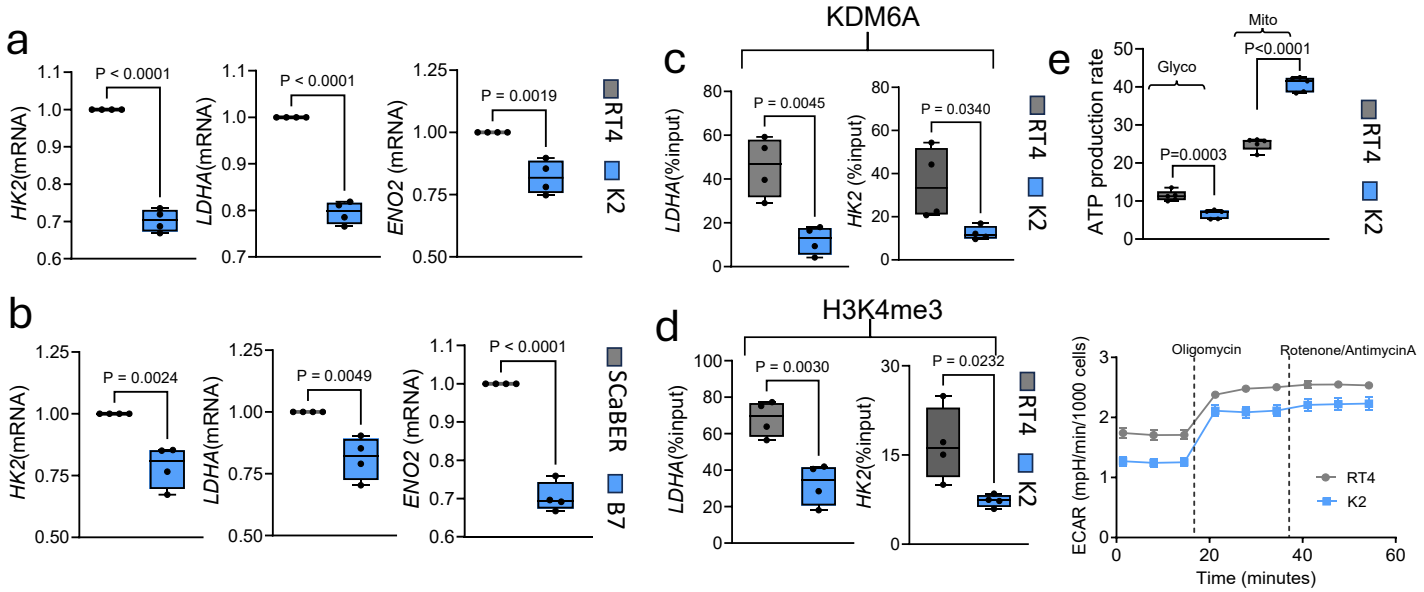

Figure 30: a-b: Box-and-whisker plots demonstrating relative expression of *HK2, LDHA* and *ENO2* genes in RT4 and K2 (**a**) and ScaBER and B7 cell lines cell lines(**b**) (n=4 biologically independent samples per group). Two-tailed Student's t-test was performed. **c-d:** Box-and-whisker plots showing the ChIP-qPCR analysis of KDM6A (**c**) and H3K4me3 (**d**) enrichment at the indicated gene promoters in RT4 and K2 cell lines(n=4 biologically independent samples per group). Two-tailed Student's t-test was performed. **e:** Box-and-whisker plot (Top) representing glycolytic and mitochondrial ATP production rate in RT4 and K2 cell lines measured by the Seahorse XF analyzer-based ATP Rate Determination Assay (n=5 biologically independent samples per group). Two-tailed Student's t test was performed. Line plot (Bottom) comparing Extracellular acidification rate (ECAR) between RT4 and K2 cell lines as determined by the Seahorse assay Data represented as mean +/- Standard error of mean (SEM). (n=5 biologically independent samples per group). For all the box-and-whisker plots, the center line marks the median, the edges of the box represent the interquartile (25th–75th) percentile and the whiskers represent minimum-maximum values.

3. Related to Lines 171-175, Figures 2E,G and Extended Data Figures 2C-D, and Lines 212-215 3A,C, Extended Data Figures 3C-D, and Figures 4B-C and Extended Data Figure 6E: The authors should provide IGV track images (or similar) for visualization of KDM6A and H3K4me3 peaks. Also to strengthen causal relationship of KDM6A binding and Msh2 Msh6 downregulation they could show H3K27me3 ChIP-seq at these loci. Similarly, for Figure 6C, the enrichment of H3K9la and H3K18la at specific genes should be vizualized in IGV.

Author's Response: We thank the Reviewer for this constructive comment. Based on the Reviewer's recommendations,

- The IGV track images for visualization of KDM6A and H3K4me3 differential peaks for critical genes involved in MMR, DSBR and glycolysis are included in the manuscript (Figure **31a-c** in the point-by-point response letter and Fig. **2F, 3B, 4C** in revised manuscript). Consistent with our findings, sgKdm6a cells showed a decreased enrichment of both KDM6A and H3K4me3 at the promoter regions of key genes involved in MMR, DSBR and glycolysis.

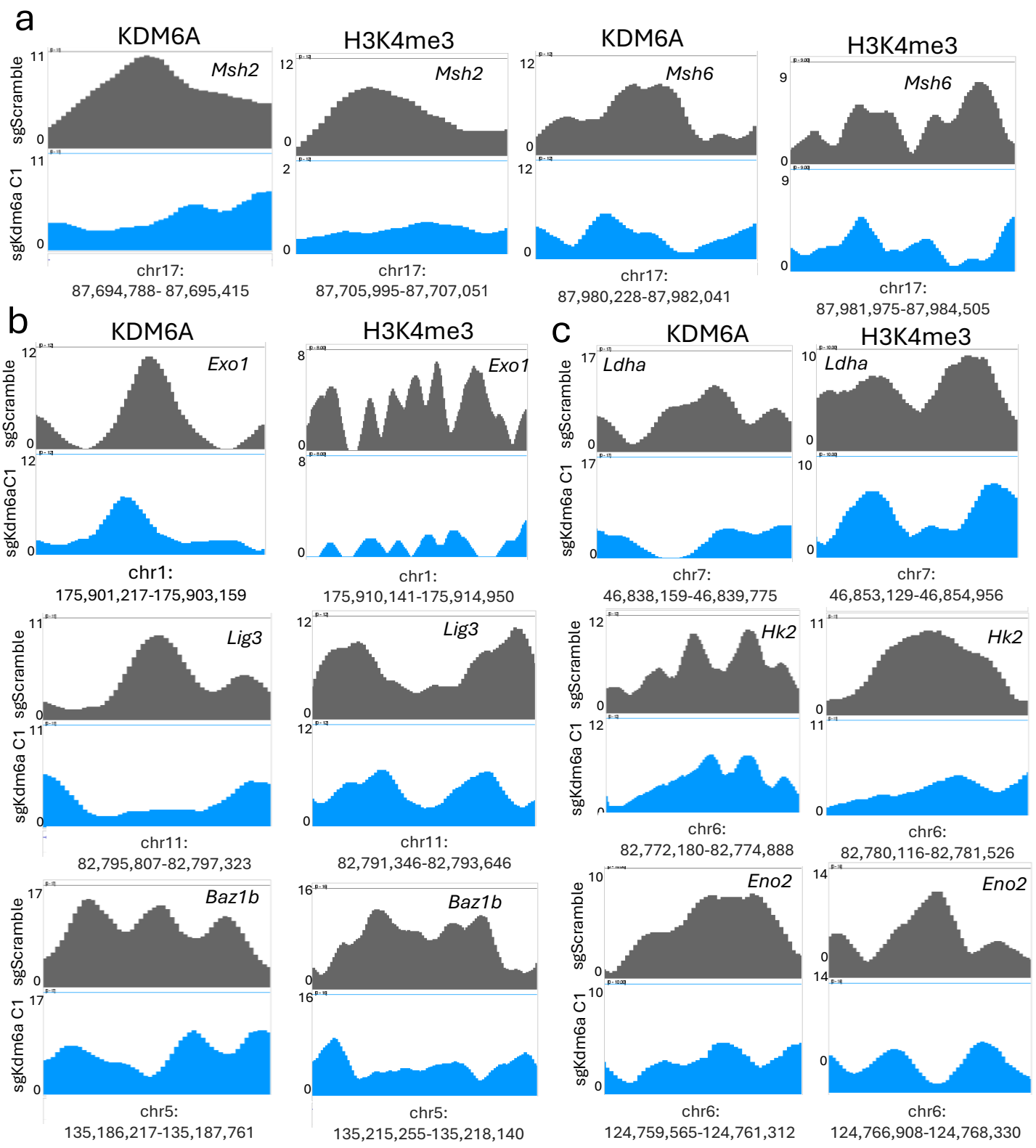

Figure 31: a-c: Genome browser plots demonstrating KDM6A (Left) and H3K4me3 (Right) peaks for *Msh2 and Msh6* (**a**), *Exo1, Lig3* and *Baz1b* (**b**) and *Ldha, Hk2* and *Eno2* (**c**) gene loci in sgKdm6a C1 and sgScramble cells.

- Additionally, to address the Reviewer's comment regarding the causal relationship of KDM6A binding and MMR pathway gene downregulation, we have analyzed and provided the IGV plots for H3K27me3 enrichment of in the revised manuscript. The differential ChIP-seq analysis between sgKdm6a and sgScramble showed increased enrichment of H3K27me3 within +/- 5kb TSS regions of Msh2 and Msh6 genes. Additionally, we observed similar trends of increased H3K27me3 enrichment in genomic regions of *Baz1b*, *Ldha* and *Eno2* (Figure **32** in the point-by-point response letter and Extended data Fig. **3G, 5E, 6D** in revised manuscript).

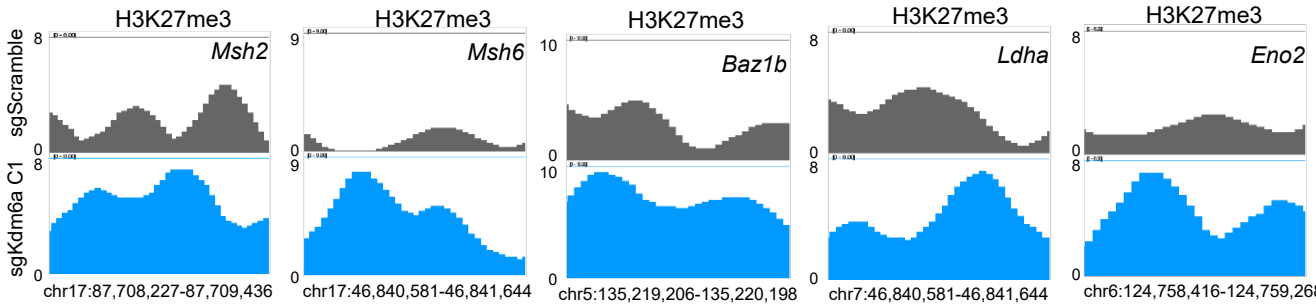

Figure 32: Genome browser plots demonstrating H3K27me3 enrichment at genomic regions of *Msh2, Msh6, Baz1b, Ldha* and *Eno2* in sgKdm6a C1 and sgScramble cells**.**

Overall, these data demonstrated that loss of KDM6A results in reduced H3K4me3 at the gene loci with concurrent enrichment of H3K27me3 resulting in the attenuation of the expression of key genes associated with the MMR, DSRB and glycolysis pathways.

- The IGV browser plots for Figure **6C**, showing enrichment of H3K9la and H3K18la at *Pdcd1* and *Tgfb1* are also included in the revised manuscript (Figure **33** in the point-by-point response letter and Extended data Fig. **8H** in revised manuscript). Consistent with genomic data reported in the browser plots demonstrated that Na-La–treated Tregs exhibited higher enrichment of H3K9la and H3K18la, accompanied by increased expression of key genes regulating Treg identity and function, including *Foxp3, Pdcd1,* and *Tgfβ1*. These findings support a role for exogenous lactate–derived H3K9la and H3K18la in modulating gene expression in Tregs.

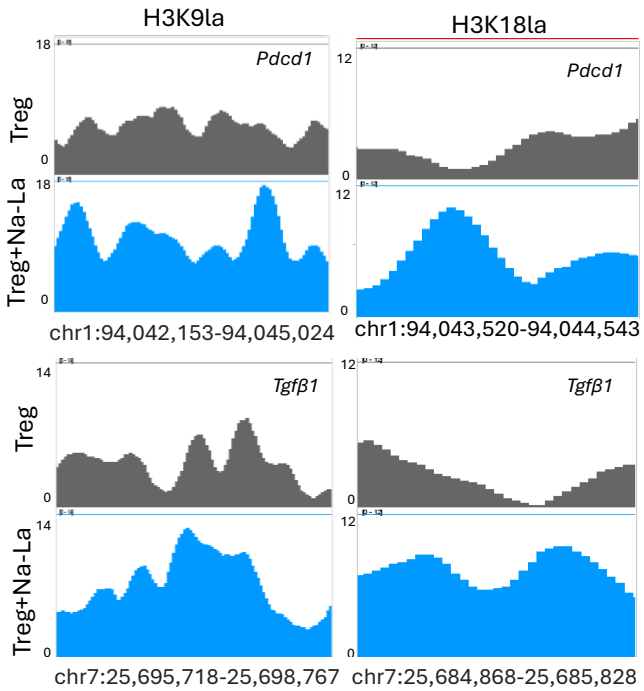

Figure 33: Genome browser plots demonstrating H3K9la and H3K18la peaks for *Pdcd1 and Tgfβ1* gene loci in Tregs treated with and without Na-La (25mM).

4. The authors provide evidence for multiple pathways that could contribute to improved ICB efficacy (Figures 2-5), yet they do not provide mechanistic evidence to assess the degree of contribution for each one. For example, overexpression of Mlh1/Msh2, Exo1/Lig3, and Ldha/HK2/Eno2 in KDM6A KO cells could lead to ICB resistance.

Author's Response: We thank the Reviewer for this thoughtful comment. Prior studies have shown that defective DNA repair pathways, including MMR and DSBR, promote the accumulation of mutations and neoantigens, rendering tumors more sensitive to immune checkpoint therapy (ICT), while hyperactive glycolysis creates an immunosuppressive environment through lactate accumulation.

In our study, we demonstrate that KDM6A loss functions as an upstream regulator of these pathways. Loss of KDM6A impaired MMR and DSBR gene expression and reduced glycolytic activity, collectively reshaping the tumor microenvironment. To further address the Reviewer's concern, we performed multivariable Cox regression incorporating TMB and KDM6A status. This analysis showed that the survival advantage conferred by KDM6A mutations persisted even after adjusting for TMB (Figure **34a** in the point-by-point response letter). Moreover, within the subgroup of patients with low MMR signatures in the IMvigor210[19] , KDM6A-mutant tumors exhibited improved survival compared with KDM6A-WT tumors (Figure **34b** in the point-by-point response letter). These findings suggest that additional mechanisms beyond MMR loss contribute to ICT sensitivity, likely through the combined effects of increased tumor immunogenicity and a more favorable immune microenvironment driven by reduced lactate production. These data were generated for the Reviewer's perusal and have not been included in the revised manuscript.

We also emphasize that dissecting each pathway in isolation would not accurately reflect KDM6A's role as an upstream regulator. For example, knocking down LDHA to study glycolysis alone would impair anti-tumor immunity, as we and others have previously shown (Raychaudhuri, Singh et al. [28]). Similarly, selective perturbation of MMR or DSBR genes alters genomic stability in ways that do not capture the integrated regulatory role of KDM6A. Thus, isolating these pathways risks oversimplifying the biology. Our study instead highlights the convergent and cumulative effects of KDM6A loss, which more faithfully represent its impact on tumor–immune interactions.

Together, these findings establish KDM6A as an upstream regulator that coordinates DNA repair and metabolic pathways to reshape the tumor immune landscape and enhance ICT sensitivity. Importantly, they also underscore the potential of KDM6A as a biomarker to stratify bladder cancer patients for therapeutic interventions, particularly in guiding the use of chemotherapy and ICT.

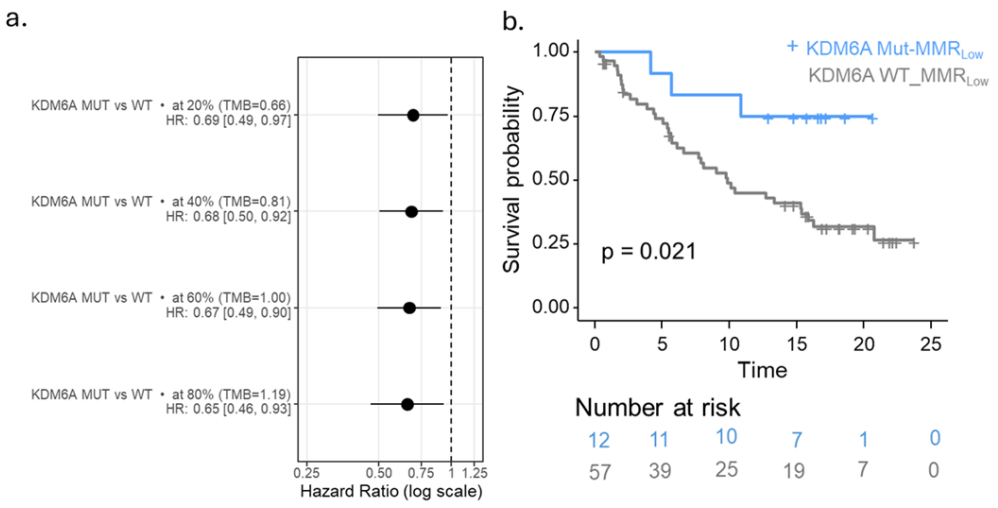

Figure 34: a: Hazard ratio estimates for overall survival comparing KDM6A-Mut and KDM6A-Mut status at different TMB levels. **b:** Kaplan-Meier plot demonstrating OS of KDM6A-Mut patients and KDM6A-WT patients with low MMR signature from IMvigor210 (n=69 patients). To define MMR signature groups, mean of normalized expression values for *MSH2, MSH6, MSH3, MLH1, MLH3, PMS2* and *PMS1* was ranked. Samples in the bottom 25 % (≤ 25th percentile) were classified as MMR-Low.

5. For Figures 1B and 2B, tumor growth curves should be provided.

Author's Response: We thank the reviewer for the comment. We have added the tumor growth curves in the revised manuscript. (Figure **35a-d** in the point-by-point response letter and Fig **1B, 2B** and Extended data Fig. **1C, 3B** in revised manuscript).

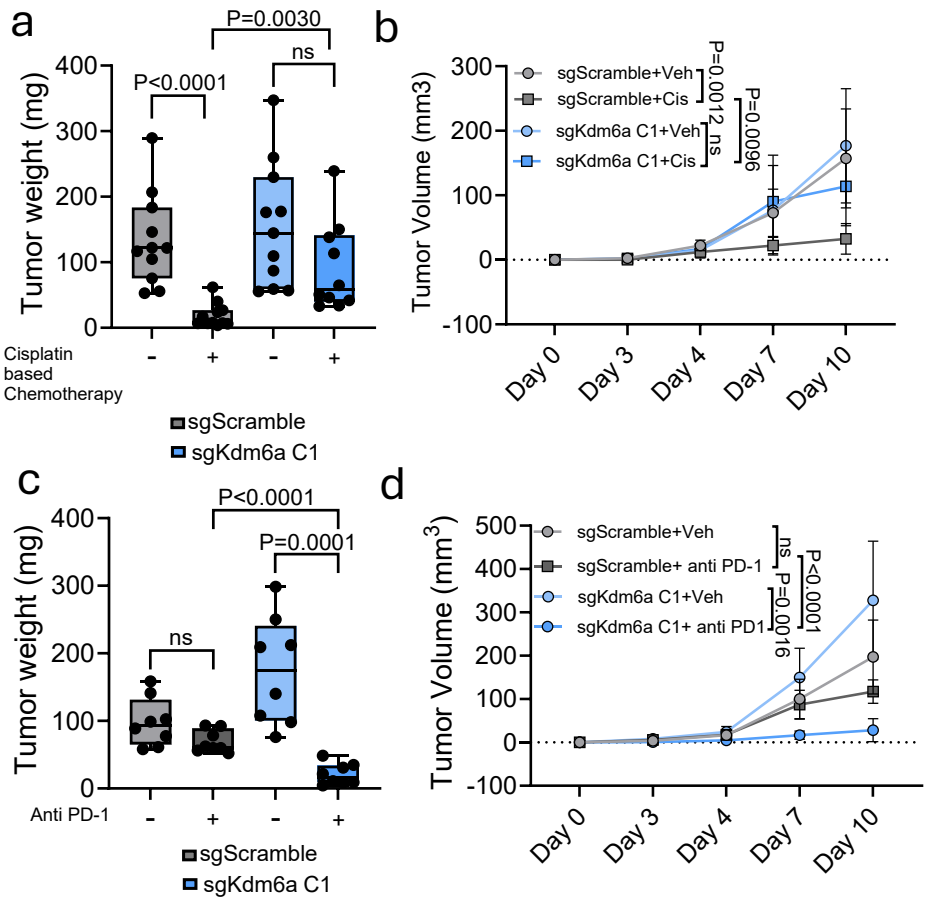

Figure 35: a-b: Box-and-whisker plot illustrating the final tumor weights (**a**) and Tumor growth curves (**b**) of sgScramble and sgKdm6a C1 tumors in mice treated with and without cisplatin-based chemotherapy (n=10-11 mice per group). Two-tailed Student's t-test (**a**) and Two-way ANOVA (**b**) was performed. **c-d:** Box-and-whisker plot illustrating the final tumor weights(**c**) and Tumor growth curves (**d**) of sgScramble and sgKdm6a C1 tumors in mice treated with anti-PD-1. (n= 8 mice per group). Two-tailed Student's t-test (**c**) and Two-way ANOVA (**d**) was performed. For all the box-and-whisker plots, the center line marks the median, the edges of the box represent the interquartile (25th–75th) percentile and the whiskers represent minimum-maximum values.

Minor:

6. Lines 138-139 and Extended Data Figure 1B: The eccDNA study in KMD6A WT and MUT patients is incompletely described in the text, methods and the related figure. Are the levels and heterogeneity of eccDNA different between WT and MUT patients?

Authors' response: Thank you for the comment. We apologize for the lack of clarity in the text and other sections. We have revised the manuscript to include the methods used for eccDNA analysis in the patient cohort. We observed eccDNA amplicons for *SHCBP1, SPP1* and *EGFR* were only present in patients harboring *KDM6A* mutation (Extended data Fig. **2D** in revised manuscript). Further, our WGS studies in human cell lines showed multiple eccDNA amplicons mapping critical cisplatin resistant genes including *SHCBP1, TP63* and *CLDN4.*

Additionally, our results show elevated levels of copy number amplification in K2 (KDM6A knocked out) than parental RT4 cells (Figure **25, 26** in the point-by-point response letter and Fig. **1I** and Extended data Fig. **2E, F** in revised manuscript).

7. Figure 2B description is incorrect, wrong treatment is mentioned.

Authors' response: We apologize for the oversight. We have included the corrected treatment regimen in the revised manuscript.

8. Figure 3D: how many tumors analyzed? Provide quantitation

Authors' response: Thank you for the comment. We have quantified Exo1 expression in n=5 tumors. We have included the quantification data in the manuscript (Figure **36a, b** in the point-by-point response letter and Fig. **3D** in the revised manuscript).

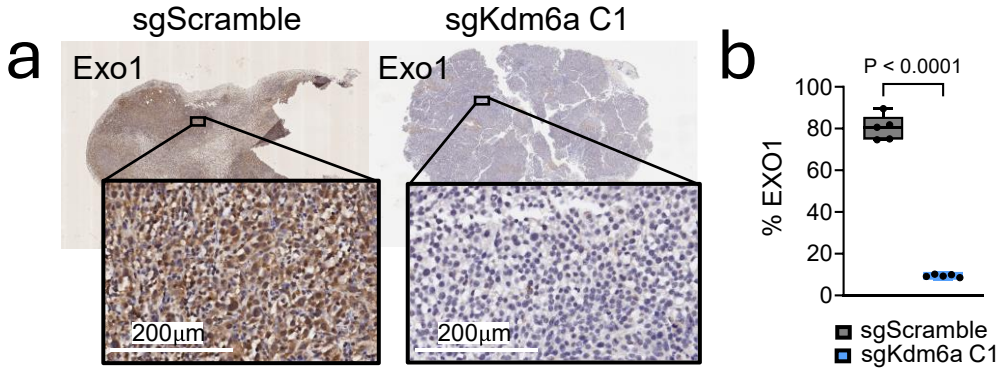

Figure 36: a: Representative images of IHC staining for EXO1 expression (Brown) in tissue sections obtained from sgScramble and sgKdm6a C1 tumors. **b.** Box-and-whisker plot showing percentage of EXO1 expression in sgScramble and sgKdm6a C1 tumors (n=5 tumors per group). Two-tailed Student's t-test was performed. For the representative images, data is indicative of two independent experiments. Scale bar is included.

9. Lines 230 S3E reference irrelevant

Authors' response: We thank the Reviewer for pointing this out. We have corrected this in the revised manuscript.

10. Lines 228-230 3E: please also provide representative images of gH2AX staining'

Authors' response: We thank the Reviewer for this comment. We have added all the representative images of gamma-H2AX confocal microscopy in the updated manuscript.

11. Lines 252-253 fix reference to Extended Data Figure 4C

Authors' response: We thank the Reviewer for bringing it to our attention. We have modified it in our revised manuscript.

12. Cell line supernatant experiments in human cell lines

Authors' response: We thank the Reviewer for this comment. We have performed cell supernatant experiments with RT4 and K2 (KDM6A-KO) human bladder cancer cell lines. We have noted that following KDM6A loss, the glycolytic ATP production was significantly reduced, accompanied by a compensatory metabolic shift toward oxidative phosphorylation (OXPHOS) and reduced lactate production. We have added the results and figures in the updated manuscript (Figure **37a, b** in the point-by-point response letter and Fig. **4H, I, K** in revised manuscript).

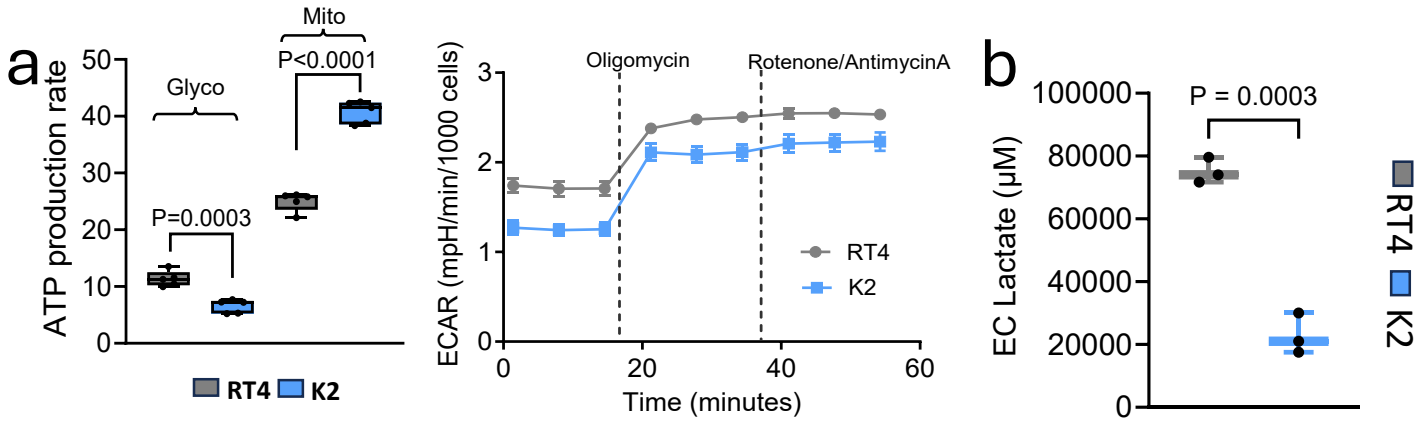

Figure 37: a: Box-and-whisker plot (Left) representing glycolytic and mitochondrial ATP production rate in RT4 and K2 cell lines measured by the Seahorse XF analyzer-based ATP Rate Determination Assay. Two-tailed Student's t-test was performed. Line plot (Right) comparing Extracellular acidification rate (ECAR) between RT4 and K2 cell lines as determined by the Seahorse assay Data represented as mean +/- Standard error of mean (SEM). (n=5 biologically independent samples per group). **b.** Box-and-whiskers plot showing EC lactate concentration in supernatant of RT4 and K2 cell lines. (n=3 biologically independent samples per group). Two-tailed Student's t-test was performed.

13. Lines 266-269: please reference the studies mentioned.

Authors' response: We thank the Reviewer for bringing it to our attention. We have added the reference in our revised manuscript.

Reviewer #4 (Remarks to the Author): with expertise in cancer epigenetics

This study describes a mechanistic framework by which loss-of-function mutations in the histone demethylase KDM6A modulate therapeutic responses in bladder cancer. The authors present analyses of numerous clinical cohorts and data from model systems indicating that KDM6A deficiency is associated with worse overall survival following cisplatin-based chemotherapy, but improved outcomes with immune checkpoint blockade (ICB); a noteworthy and potentially important result. Mechanistically, the authors show data that KDM6A loss promotes the accumulation of extrachromosomal circular DNA (eccDNA), contributing to cisplatin resistance. The authors show that KDM6A directly regulates DNA mismatch repair (MMR) and double-strand break repair (DSBR) genes, and that its loss impairs these pathways, resulting in genomic instability, elevated tumor mutational burden, and enhanced immunogenicity. In parallel, KDM6A deficiency suppresses intratumoral lactate production, which leads to diminished histone lactylation (H3K9la, H3K18la) in regulatory T cells (Tregs). This epigenetic alteration attenuates the expression of immunosuppressive genes, thereby enhancing effector T cell activity in the tumor microenvironment. Collectively, the authors conclude that the findings position KDM6A mutation status as a potential predictive biomarker for therapeutic stratification in bladder cancer.
Overall this paper combines epigenetic, metabolic, and immune experiments to create a mechanistically rich study linking KDM6A loss to divergent therapeutic responses in bladder cancer. However, the limited validation of some key claims needs to be addressed to solidify its mechanistic and clinical impact. I recommend the following points be addressed prior to acceptance.

We are grateful to the Reviewer for the thorough and insightful evaluation of our work, and for recognizing the integrative framework that connects epigenetic, metabolic, and immune mechanisms to therapeutic response in bladder cancer.

1. The association between KDM6A inactivating mutations and eccDNA is very intriguing but the mechanistic experiments rely heavily on a single murine bladder cancer cell line (MB49)+/- CRISPR-Cas9 knockout and a limited number of human cell lines. In particular the authors attempted to validate the cisplatin-resistant phenotype of KDM6A-mutant murine bladder cancer cells with the human cell lines RT4 and J82 (Fig 1F). Comparing two different human cell lines, even from the same tumor type, is prone to confounding as cell specific copy number alterations or epigenetic differences may strongly influence therapeutic response. (References "Oncogene volume 36, pages35–46 (2017); Scientific Reports volume 6, Article number: 38531 (2016)" show some of the known cell line differences.) The authors need to provide cisplatin resistance data from either a larger panel of bladder cancer cell lines with known KDM6A status or knockdown KDM6A in the T24 line to show validation in a human system comparable to the murine sgScramble and sgKdm6a cells.

Author's Response: We thank the Reviewer for this thoughtful comment. We agree that comparing two distinct human bladder cancer cell lines, RT4 (KDM6A-WT) and J82 (KDM6A-Mut), could be confounded by differences in their genetic backgrounds. To address this concern, we performed CRISPR-Cas9 mediated knockout of KDM6A in two human bladder cancer cell lines, RT4 and ScaBER[2]. K2 and B7 are the respective KDM6A knockout cells of RT4 and ScaBER. Western blot was used to verify KDM6A deletion in both K2 and B7 cells (Figure **38a** in the point-by-point response letter and Extended data Fig. **1B** in revised manuscript). Subsequently, we repeated key functional assays, including cisplatin-mediated cytotoxicity, spheroid formation, transwell invasion and wound healing assays (Figure **38b-f** in the point-by-point response letter and Fig **1C, E, G** and Extended data Fig. **1E, G, I, K** in revised manuscript). Consistent with our original findings, KDM6A knockout human bladder cancer cells demonstrated increased migration, enhanced spheroid formation, and reduced sensitivity to cisplatin.

To further strengthen these results, we also generated independent sgKdm6a clones in murine MB49 cells using alternative sgRNAs. Western blot confirmed Kdm6a deletion in the sgKdm6a cell clones (sgKdm6a C1-C3) (Figure **39a** in the point-by-point response letter and Extended data Fig. **1A** in revised manuscript). These clones exhibited enhanced migration, spheroid formation, and cisplatin resistance, reinforcing the reproducibility of our findings (Figure **39b-e** in the point-by-point response letter and Fig.**1C, D, F** and Extended data Fig.**1D, F, H, J** in revised manuscript). Together, these additional experiments in both murine and human systems confirm that KDM6A loss contributes to cisplatin resistance in bladder cancer cells.

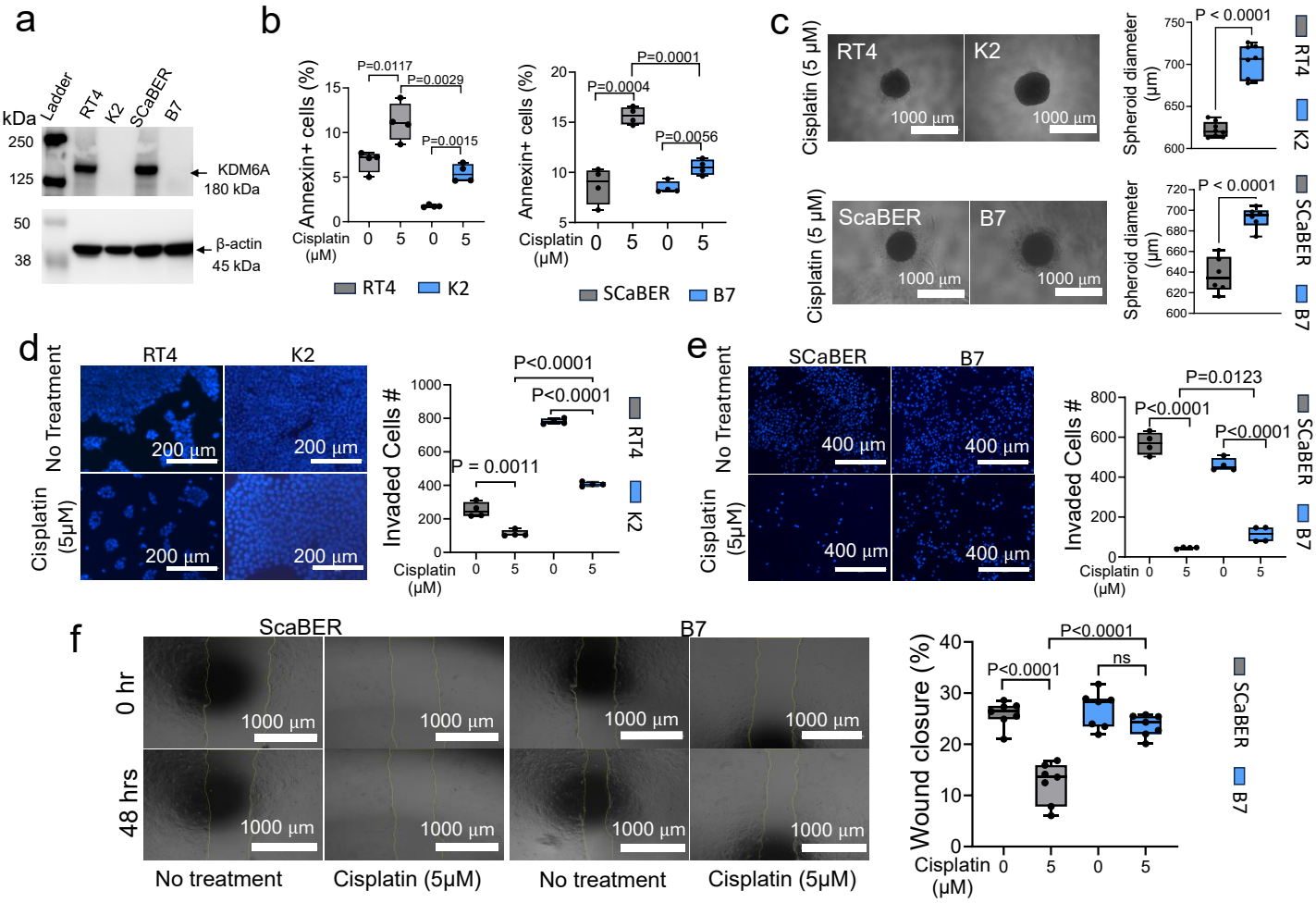

Figure 38: a: Representative western blot image indicating the expression of KDM6A (180 kDa) and β-ACTIN (45 kDa) in RT4, K2, ScaBER and B7 cell lines. Data is representative of two independent experiments. **b:** Box-and-whisker plots demonstrating percentage of Annexin positive cells of RT4 and K2 (Left) and ScaBER and B7 (Right) cell lines treated with or without 5 μM cisplatin for 48 hours. (n=4 biologically independent samples per group). Two-tailed Student's t-test was performed. **c:** Representative images (Left) and box-and-whisker plot (Right) comparing the diameter of RT4 and K2 (Top) and ScaBER and B7 (Bottom) spheroids treated with 5 μM cisplatin for 48 hours. (n=8 (Top) and n=6 (Bottom) biologically independent samples per group). Two-tailed Student's t-test was performed. For the representative images, data is indicative of two independent experiments. Scale bar is included. **d-e:** Representative images (Left) and box-and-whisker plot (Right) showing the number of invaded cells in Transwell assay for RT4 and K2 (**d**) and ScaBER and B7 (**e**) cell lines treated with or without 5 μM cisplatin for 48 hours (n=4 independent visual fields). Two-tailed Student's t-test was performed. For the representative images, data is indicative of two independent experiments. Scale bar is included. **f:** Representative images (Left) and box-and-whisker plot (Right) depicting the percentage of wound closure of ScaBER and B7 cells treated with or without 5 μM cisplatin for 48 hours (n=7 biologically independent samples per group). Two-tailed Student's t-test was performed. For the representative images, data is indicative of two independent experiments. Scale bar is included. For all the box-and-whisker plots, the centre line marks the median, the edges of the box represent the interquartile (25th–75th) percentile and the whiskers represent minimum-maximum values.

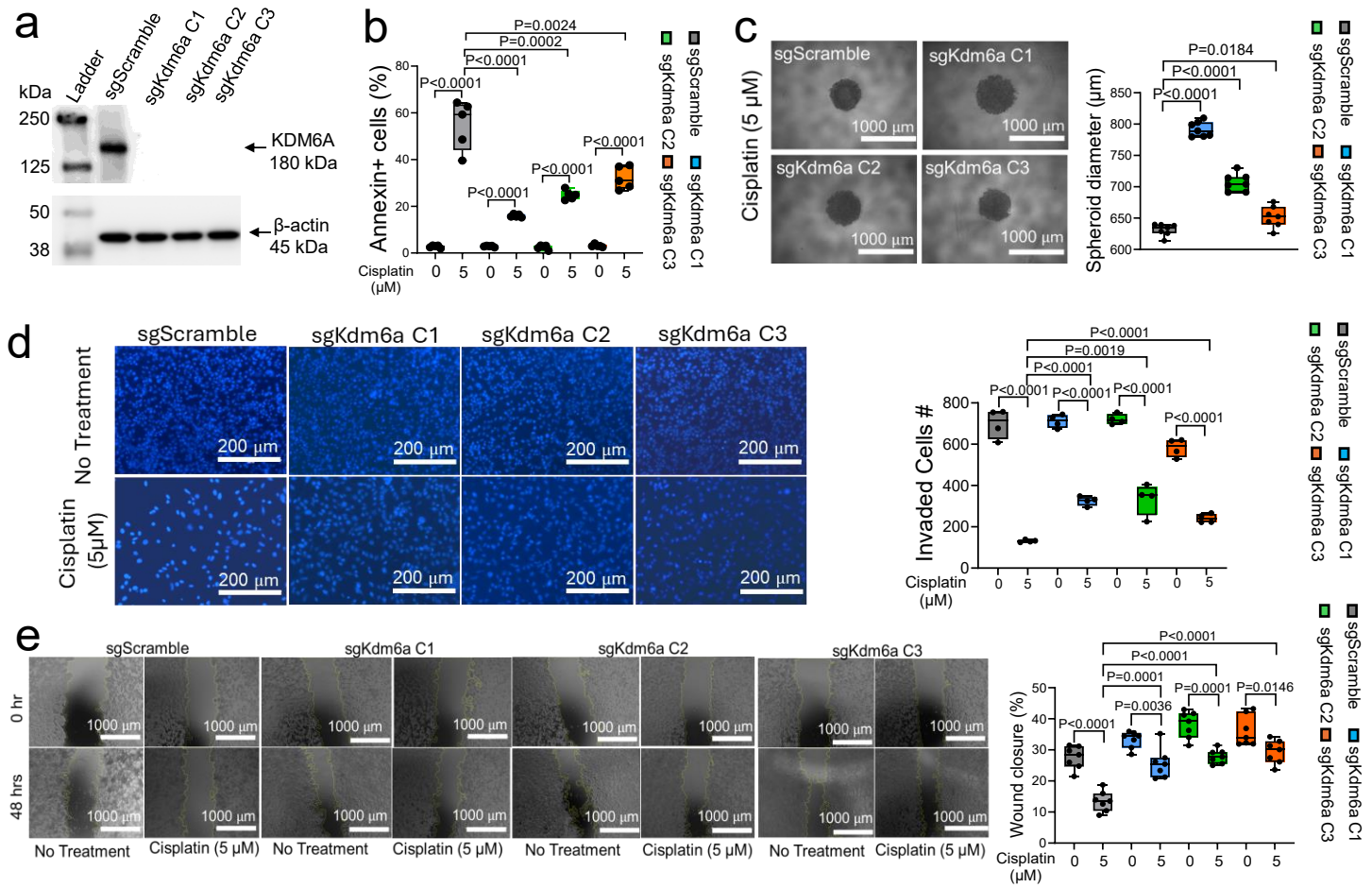

Figure 39: a: Representative western blot image indicating the expression of KDM6A (180 kDa) and β-ACTIN (45 kDa) in sgScramble and sgKdm6a Clones C1, C2 and C3 cell lines. Data is representative of two independent experiments. **b:** Box-and-whisker plot demonstrating percentage of Annexin positive cells of sgScramble and sgKdm6a cell lines treated with or without 5 μM cisplatin for 48 hours. (n=5 biologically independent samples per group). Two-tailed Student's t-test was performed. **c:** Representative images (Left) and box-and-whisker plot (Right) showing the diameter of sgScramble and sgKdm6a spheroids treated with 5 μM cisplatin for 48 hours. (n=7 biologically independent samples per group). Two-tailed Student's t-test was performed. For the representative images, data is indicative of two independent experiments. Scale bar is included. **d:** Representative images (Left) and box-and-whisker plot (Right) demonstrating the invaded cell number in Transwell assay for sgScamble and sgKdm6a clones treated with or without 5 μM cisplatin for 48 hours. (n=4 independent visual fields). Two-tailed Student's t-test was performed. For the representative images, data is indicative of two independent experiments. Scale bar is included. **e:** Representative images (Left) and box-and-whisker plot (Right) depicting the percentage of wound closure of sgScramble and sgKdm6a clones treated with or without 5 μM cisplatin for 48 hours. (n=7 biologically independent samples per group). Two-tailed Student's t-test was performed. For the representative images, data is indicative of two independent experiments. Scale bar is included. For all the box-and-whisker plots,the centre line marks the median, the edges of the box represent the interquartile (25th–75th) percentile and the whiskers represent minimum-maximum values.

2. While the study clearly demonstrates increased eccDNA in the murine sgKdm6a cells compared with sgScramble (Fig 1G), a more detailed characterization of these amplifications is needed. At the very least genome wide copy number plots of the sgScramble and sgKdm6a cells should be generated and presented. This along with sequencing the eccDNA will enable eccDNA differences to be clearly observed and specific genetic loci identified. It will significantly strengthen the association the authors are trying to show if any of the eccDNA loci correspond to some of the key oncogenes already associated with cisplatin resistance or identify new resistance genes.

Author Response: We thank the Reviewer for this important comment. In our prior chromosomal structural variants analysis of the TCGA-BLCA cohort[1] , we showed that *KDM6A*-mutant bladder cancer patients exhibited more circular amplicons (eccDNA) along with elevated *POLQ*[34] expression which is implicated in eccDNA formation (Extended data Fig. **2B, C** in revised manuscript). Building on these results and to address the Reviewer's comment regarding the presence of oncogenes and/or cisplatin resistance associated genes in eccDNA of KDM6A KO cells, we performed whole genome sequencing (WGS) on human bladder cancer cell line, RT4 and K2 (KDM6A-KO RT4 cells). WGS analysis demonstrated the following:

- The genome-wide copy number analysis showed increased copy number gains in various genomic regions specifically in chromosomes 2, 3, and 7 in K2 cells, indicating increased amplifications in these regions upon KDM6A loss (Figure **40** in the point-by-point response letter and Fig. **1H** in revised manuscript).

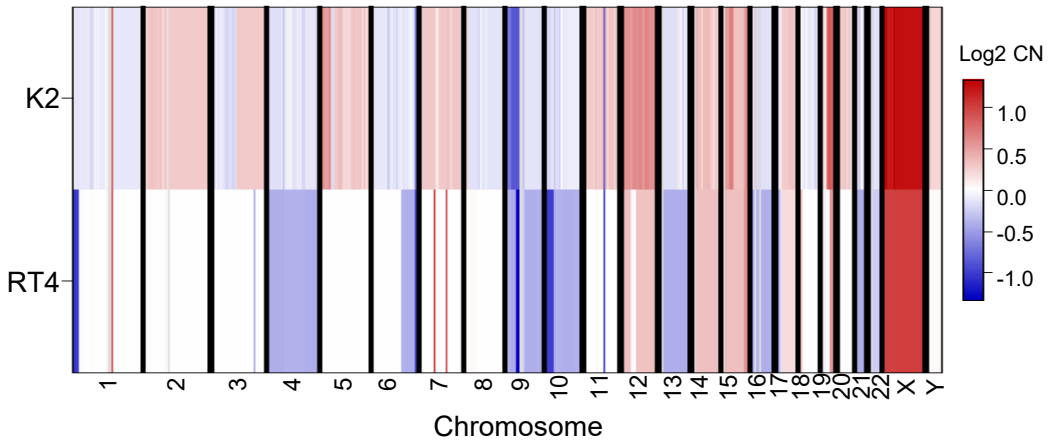

Figure 40: The heatmap showing genome-wide copy-number changes in K2 and RT4 bladder cancer cell lines. The red tones denote copy number gains or amplifications, and blue tones denote copy number losses or deletions.

- Analysis of the circular-amplicons using Circle-map showed multiple circular amplicons carrying critical genes implicated in promoting cisplatin resistance including *TP63*[3, 4, 5], , *CLDN4*[6, 7], *GLI2*[8, 9, 10, 11], *LUC7L3*[12, 13], *ERCC4*[14, 15]and *SHCBP1*[16, 17, 18] in KDM6A KO cells (K2 cells) (Figure **41** in the point-by-point response letter and Fig **1I** and Extended data Fig. **2E** in revised manuscript). We used the standard thresholds of split reads greater than 2 and circle score higher than 50 to ensure the reliability of observations.

- As the genome wide copy number heatmap showed increased amplifications in chromosomes 2, 3, and 7, we evaluated copy numbers for the eccDNA gene loci. Coverage plot of the genes showed increased copy numbers in K2 cells than RT4 cells. (Figure **42** in the point-by-point response letter and Fig **1I** and Extended data Fig. **2F** in revised manuscript).

  To summarize, these results show KDM6A loss mediated formation of eccDNA as a vehicle for multiple critical genes that drive in cisplatin resistance in bladder cancer cells.

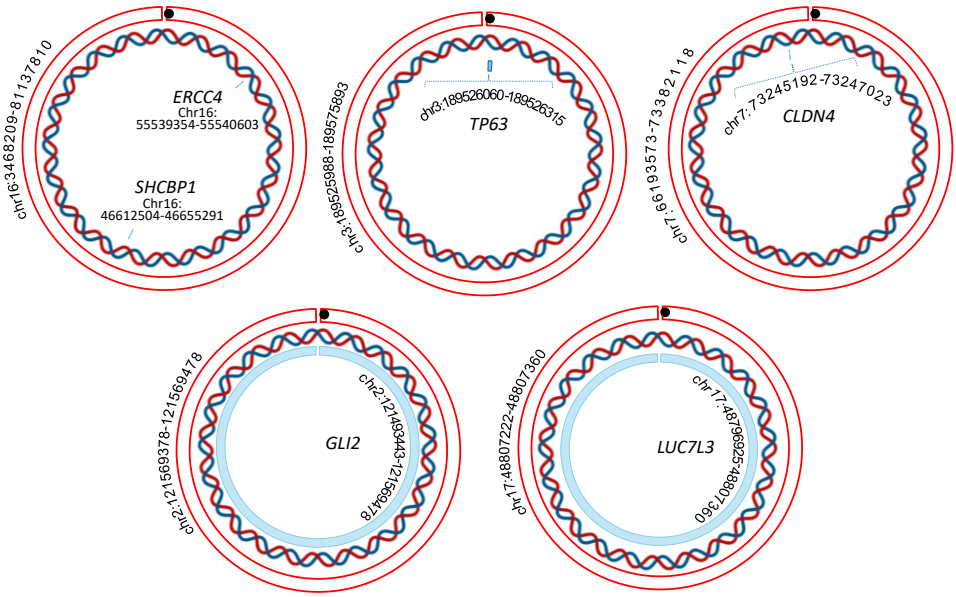

Figure 41: Circos plots showing eccDNA amplicons identified in K2 Cells. The out red ring represents the whole amplicon, while the black dot represents the start coordinate of indicated amplicon. The inner blue region represents the regions mapped to indicated genes within the respective amplicon.

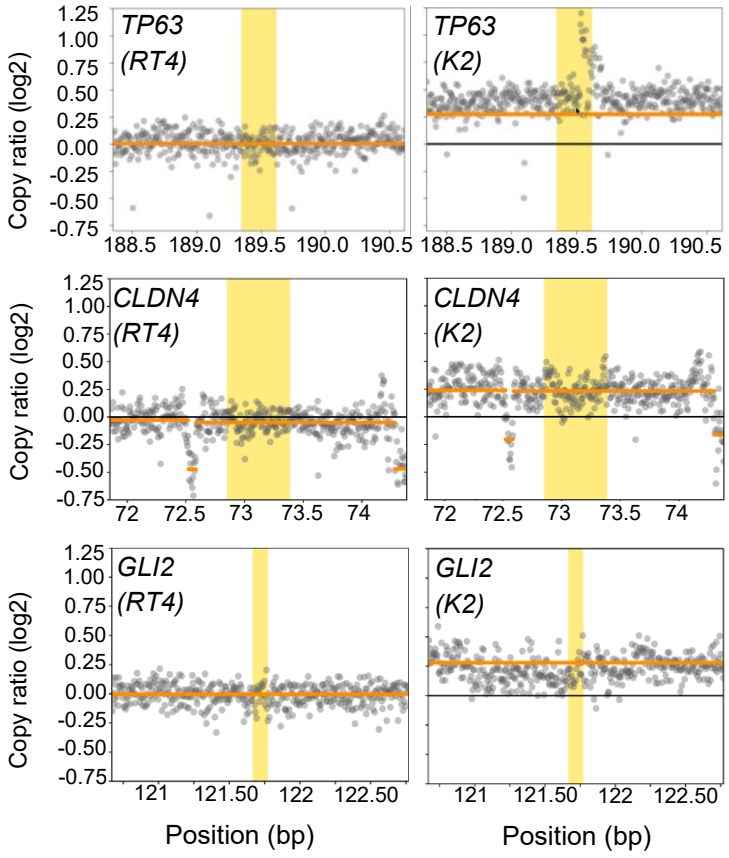

Figure 42: The scatter plots showing the copy number amplifications for indicated genes at their eccDNA loci in RT4 and K2 cells. The gray dots represent probes across the region labeled on x-axis, while y-axis represents the copy ratio (log2) at that genomic position for the gray dots. The orange horizontal line is the segmentation line indicating true copy number state for the segment, and the yellow vertical bars mark the indicated regions for *TP63, CLDN4* and *GLI2* within the amplicon.

3. The Chip-seq results need to be clarified. The authors present numerous “Profile Plots” of their ChIP-seq data. I cannot find an explanation in the Methods, but it seems to be a plot of the Chip-seq signal averaged across samples (e.g. Fig. 3C) and/or gene sets (e.g. Fig. 4C). This needs to be clarified for each plot; exactly what genes or gene sets and how many samples were averaged in the plot needs to be stated. Also, all the replicates for the individual gene Profile plots need to be shown in supplementary to evaluate the variability in the raw data.

Author’s Response: We thank the Reviewer for the comment. We have revised the Methods section to include the details of downstream analysis to ensure clarity.

- For the profile plots of individual genes shown in Extended data Fig.**3H**, **5F**, **6E** in revised manuscript, we extracted peak regions from the differential ChIP-seq analysis for the respective genes and calculated binding scores. These scores were visualized as profile plots over a ±1 kb region surrounding the TSS to compare signal intensity between sgKdm6a and sgScramble. We consistently observed reduced enrichment of KDM6A and H3K4me3 in sgKdm6a cells at critical loci involved in MMR, DSBR, and glycolysis, concordant with the decreased expression of these genes detected in our RNA-seq analysis (Fig. **2E, 2G, 3A**, **3C**, **4B**, **4D** in revised manuscript).

- For the profile plots of the MMR pathway, DSBR pathway and glycolytic pathway, we extracted differential peak regions for the corresponding gene sets from the ChIP-seq analysis comparing sgKdm6a C1 and sgScramble cells for KDM6A and H3K4me3 (Extended Data Fig. **3D**, **3E, 5C, 6B** in the revised manuscript). For each pathway, signal intensities across these regions were consolidated, quantified, and visualized to compare enrichment. Consistent with the individual gene plots, we observed reduced enrichment of both KDM6A and H3K4me3 in sgKdm6a cells, highlighting a consolidated effect of KDM6A loss on MMR, DSBR, and glycolytic pathways.

- Previously, we reported that KDM6A regulates the expression of genes involved in the MMR, DSBR, and glycolysis pathways in bladder cancer by performing ChIP-seq on CRISPR-Cas9–deleted Kdm6a murine MB49 bladder cancer cells (sgKdm6a C1) and control cells (sgScramble) (Fig. **2E, 3A**, **4B**, in revised manuscript). In response to the Reviewer’s suggestion and to provide an additional biological replicate, we extended ChIP-seq on an additional clone of CRISPR-Cas9–excised Kdm6a cells (sgKdm6a C2). We extracted peaks associated with key genes in MMR, DSBR, and glycolysis from the differential comparison between sgKdm6a C2 and sgScramble, and calculated binding scores. These were visualized as profile plots across a ±1 kb region surrounding the TSS to compare signal intensity between groups (Figure **43** in the point-by-point response letter and Extended data Fig. **3I**, **5G, 6F** in revised manuscript). As observed previously, sgKdm6a C2 cells displayed reduced enrichment of KDM6A and H3K4me3 at gene loci, in line with decreased expression of these genes in sgKdm6a C2 cells.

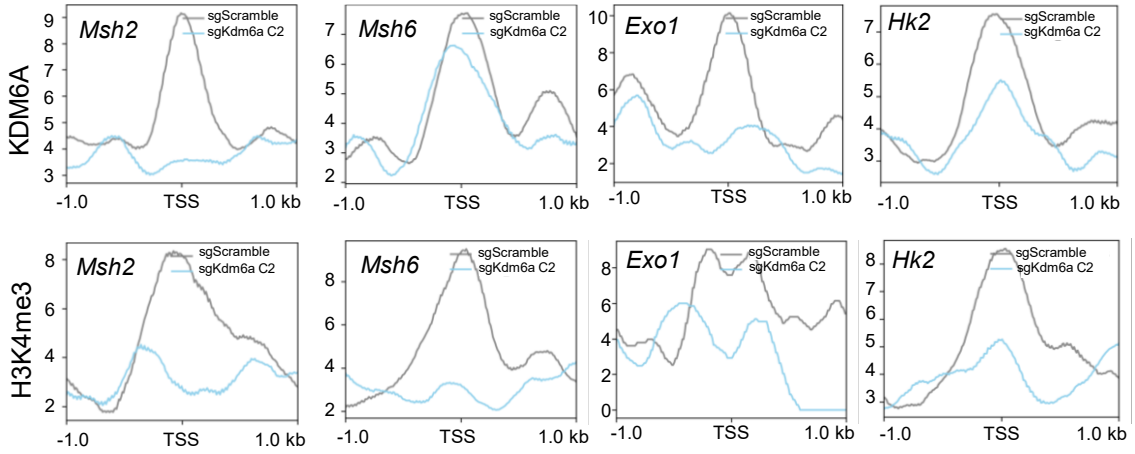

Figure 43: Profile plots representing the probability scores of KDM6A and H3K4me3 binding at ±1 kb regions from TSS and TES for genes involved in MMR, DSBR and glycolytic pathway in sgScramble and sgKdm6a C2 cells.

1. Robertson AG*, et al*. Comprehensive Molecular Characterization of Muscle-Invasive Bladder Cancer. *Cell* **171**, 540-556 e525 (2017).

2. Qiu H*, et al*. KDM6A Loss Triggers an Epigenetic Switch That Disrupts Urothelial Differentiation and Drives Cell Proliferation in Bladder Cancer. *Cancer Res* **83**, 814-829 (2023).

3. Prieto-Garcia C*, et al*. Inhibition of USP28 overcomes Cisplatin-resistance of squamous tumors by suppression of the Fanconi anemia pathway. *Cell Death Differ* **29**, 568-584 (2022).

4. Hira A, Zhang J, Kadakia MP. TIP60 enhances cisplatin resistance via regulating DeltaNp63alpha acetylation in SCC. *Cell Death Dis* **15**, 877 (2024).

5. Mendoza-Rodriguez MG, Ayala-Sumuano JT, Garcia-Morales L, Zamudio-Meza H, Perez-Yepez EA, Meza I. IL-1beta Inflammatory Cytokine-Induced TP63 Isoform ΔNP63alpha Signaling Cascade Contributes to Cisplatin Resistance in Human Breast Cancer Cells. *Int J Mol Sci* **20**, (2019).

6. Breed C*, et al*. Ovarian Tumor Cell Expression of Claudin-4 Reduces Apoptotic Response to Paclitaxel. *Mol Cancer Res* **17**, 741-750 (2019).

7. Stewart JJ*, et al*. Proteins associated with Cisplatin resistance in ovarian cancer cells identified by quantitative proteomic technology and integrated with mRNA expression levels. *Mol Cell Proteomics* **5**, 433-443 (2006).

8. Zhu W*, et al*. GLI2 inhibits cisplatin sensitivity in gastric cancer through DEC1/ZEB1 mediated EMT. *Cell Death Dis* **16**, 204 (2025).

9. Wang Q, Wei X, Hu L, Zhuang L, Zhang H, Chen Q. Hedgehog-Gli2 Signaling Promotes Chemoresistance in Ovarian Cancer Cells by Regulating MDR1. *Front Oncol* **11**, 794959 (2021).

10. Tang YA*, et al*. Hypoxic tumor microenvironment activates GLI2 via HIF-1alpha and TGF-beta2 to promote chemoresistance in colorectal cancer. *Proc Natl Acad Sci U S A* **115**, E5990-E5999 (2018).

11. Jia Y*, et al*. The role of GLI-SOX2 signaling axis for gemcitabine resistance in pancreatic cancer. *Oncogene* **38**, 1764-1777 (2019).

12. Hou Y*, et al*. Proteomics Identifies LUC7L3 as a Prognostic Biomarker for Hepatocellular Carcinoma. *Curr Issues Mol Biol* **46**, 4004-4020 (2024).

13. Nishii Y*, et al*. CROP/Luc7A, a novel serine/arginine-rich nuclear protein, isolated from cisplatin-resistant cell line. *FEBS Lett* **465**, 153-156 (2000).

14. Borcsok J*, et al*. Identification of a Synthetic Lethal Relationship between Nucleotide Excision Repair Deficiency and Irofulven Sensitivity in Urothelial Cancer. *Clin Cancer Res* **27**, 2011-2022 (2021).

15. Huang D*, et al*. A highly annotated database of genes associated with platinum resistance in cancer. *Oncogene* **40**, 6395-6405 (2021).

16. Qi G*, et al*. SHCBP1 promotes cisplatin resistance of ovarian cancer through AKT/mTOR/Autophagy pathway. *Apoptosis* **30**, 83-98 (2025).

17. Sun Y, Pan H, He Y, Hu C, Gu Y. Functional roles of the SHCBP1 and KIF23 interaction in modulating the cell-cycle and cisplatin resistance of head and neck squamous cell carcinoma. *Head Neck* **44**, 591-605 (2022).

18. Zou A, Wu A, Luo M, Zhou C, Lu Y, Yu X. SHCBP1 promotes cisplatin induced apoptosis resistance, migration and invasion through activating Wnt pathway. *Life Sci* **235**, 116798 (2019).

19. Mariathasan S*, et al*. TGFbeta attenuates tumour response to PD-L1 blockade by contributing to exclusion of T cells. *Nature* **554**, 544-548 (2018).

20. Robinson MD, McCarthy DJ, Smyth GK. edgeR: a Bioconductor package for differential expression analysis of digital gene expression data. *Bioinformatics* **26**, 139-140 (2010).

21. Bolderson E*, et al*. Phosphorylation of Exo1 modulates homologous recombination repair of DNA double-strand breaks. *Nucleic Acids Res* **38**, 1821-1831 (2010).

22. Yan S*, et al*. ZGRF1 promotes end resection of DNA homologous recombination via forming complex with BRCA1/EXO1. *Cell Death Discov* **7**, 260 (2021).

23. Goellner EM, Putnam CD, Graham WJt, Rahal CM, Li BZ, Kolodner RD. Identification of Exo1-Msh2 interaction motifs in DNA mismatch repair and new Msh2-binding partners. *Nat Struct Mol Biol* **25**, 650-659 (2018).

24. Roy M*, et al*. EXO1 promotes the meiotic MLH1-MLH3 endonuclease through conserved interactions with MLH1, MSH4 and DNA. *Nat Commun* **16**, 4141 (2025).

25. Lu G*, et al*. Ligase I and ligase III mediate the DNA double-strand break ligation in alternative end-joining. *Proc Natl Acad Sci U S A* **113**, 1256-1260 (2016).

26. Bonnet S*, et al*. A mitochondria-K+ channel axis is suppressed in cancer and its normalization promotes apoptosis and inhibits cancer growth. *Cancer Cell* **11**, 37-51 (2007).

27. Shiratori R, *et al*. Glycolytic suppression dramatically changes the intracellular metabolic profile of multiple cancer cell lines in a mitochondrial metabolism-dependent manner. *Sci Rep* **9**, 18699 (2019).

28. Raychaudhuri D, *et al*. Histone lactylation drives CD8(+) T cell metabolism and function. *Nat Immunol* **25**, 2140-2151 (2024).

29. Zhang D, *et al*. Metabolic regulation of gene expression by histone lactylation. *Nature* **574**, 575-580 (2019).

30. Lopez Krol A, *et al*. Lactate induces metabolic and epigenetic reprogramming of pro-inflammatory Th17 cells. *EMBO Rep* **23**, e54685 (2022).

31. Angelin A, *et al*. Foxp3 Reprograms T Cell Metabolism to Function in Low-Glucose, High-Lactate Environments. *Cell Metab* **25**, 1282-1293 e1287 (2017).

32. Yang R, *et al*. Homeobox A3 and KDM6A cooperate in transcriptional control of aerobic glycolysis and glioblastoma progression. *Neuro Oncol* **25**, 635-647 (2023).

33. Kim H, *et al*. Extrachromosomal DNA is associated with oncogene amplification and poor outcome across multiple cancers. *Nat Genet* **52**, 891-897 (2020).

34. Paulsen T, *et al*. MicroDNA levels are dependent on MMEJ, repressed by c-NHEJ pathway, and stimulated by DNA damage. *Nucleic Acids Res* **49**, 11787-11799 (2021).

Reviewer #2 (Remarks to the Author):

Thank you for the careful and thorough revision. Your changes address my previous concerns and the manuscript is now acceptable for publication.

We thank the Reviewer for the thoughtful review of the manuscript.

Reviewer #3 (Remarks to the Author):

The authors addressed the majority of my comments adequately. The only exception is major comment 3: the authors presented genome viewer plots that are (a) low quality since the range is too small to be discerned, and (b) too zoomed in, meaning they show a very narrow view of the gene locus that does not allow proper evaluation of peak signal compared to background.

We appreciate the Reviewer's comment regarding the genome viewer plots. In response, we have prepared "zoomed-out" browser plots for each representative gene, allowing for a more comprehensive visualization of peak distribution and background signal intensity across the full gene locus (Figure **1a-f** in the point-by-point response letter and Fig. **2F**, **3B**, **4C** and Extended Data Fig. **3H**, **6D** in revised manuscript). This adjustment ensures clearer evaluation of peak enrichment patterns relative to baseline. Because the full-locus browser tracks and associated data figures are large, therefore we could include few representative plots in an already dense main and supplementary figures. The sequencing data files have already been uploaded to the SRA database, enabling independent examination of the ChIP-seq signal tracks, if needed.

Of note, our initial browser plots included the FDR-corrected differential peak regions identified between sgScramble and sgKdm6a samples. We have used similar analytical approaches and browser plots in our previous publications as well[1, 2]. Importantly, we have validated the differential expression of these genes through multiple orthogonal approaches, including RNA-seq, ChIP-qPCR, flow cytometry, and immunohistochemistry across both murine and human cell lines. These complementary assays further substantiate the observations derived from our ChIP-seq analyses.

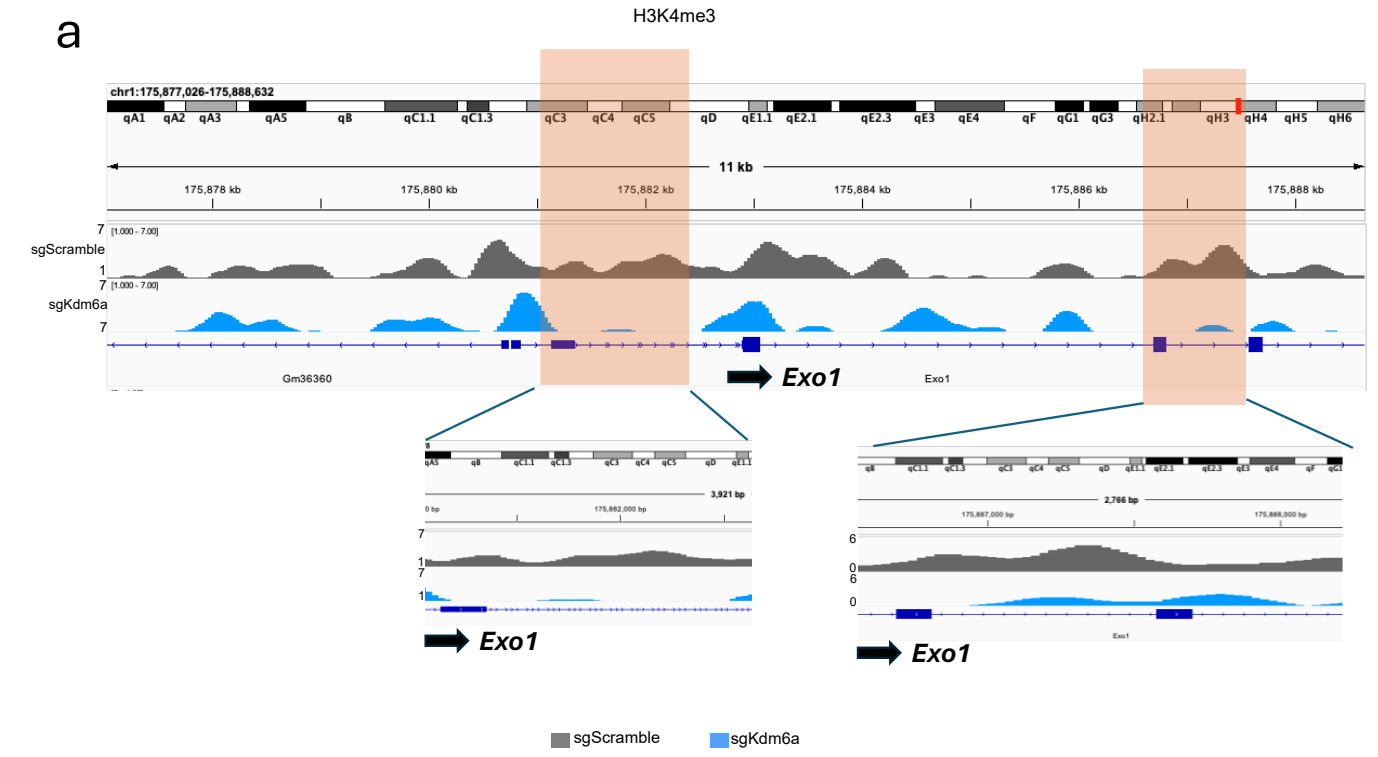
a
H3K4me3
chr1:175,877,026-175,888,632
11 kb
sgScramble
sgKdm6a
Gm36360
Exo1
Exo1
Exo1
sgScramble
sgKdm6a

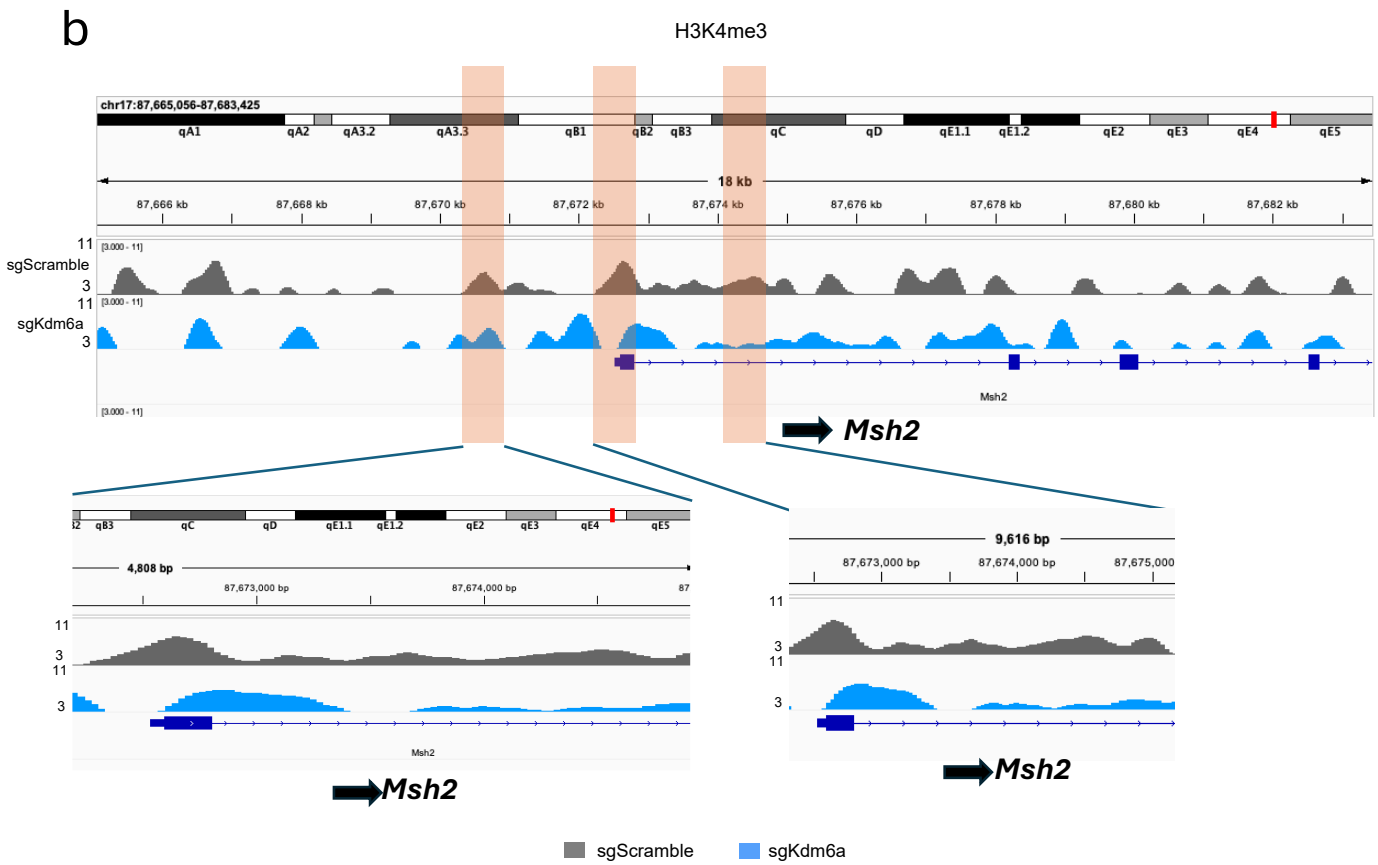
b
H3K4me3
chr17:87,665,056-87,683,425
18 kb
sgScramble
sgKdm6a
Msh2
Msh2
Msh2
sgScramble
sgKdm6a

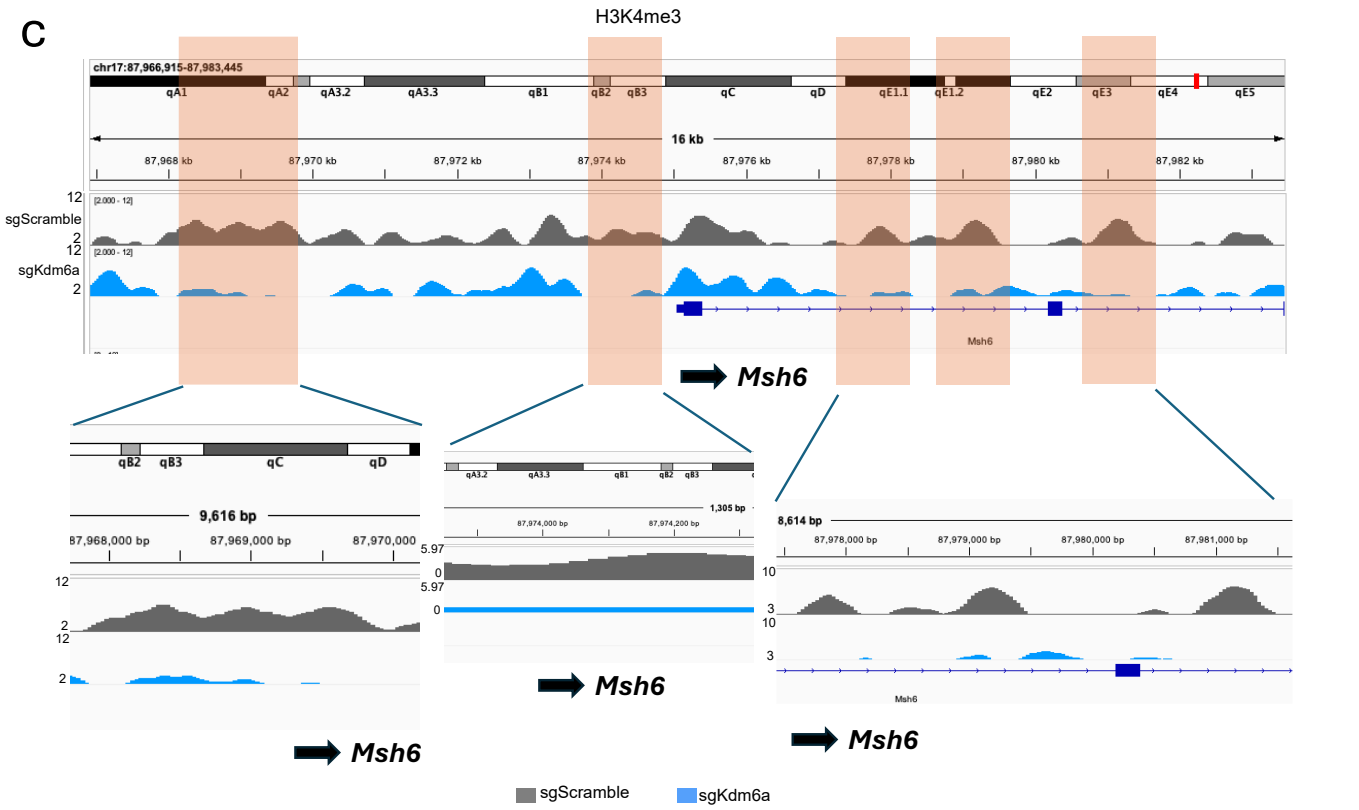
c
H3K4me3
chr17:87,966,915-87,983,445
16 kb
sgScramble
sgKdm6a
Msh6
9,616 bp
1,305 bp
8,614 bp
sgScramble
sgKdm6a

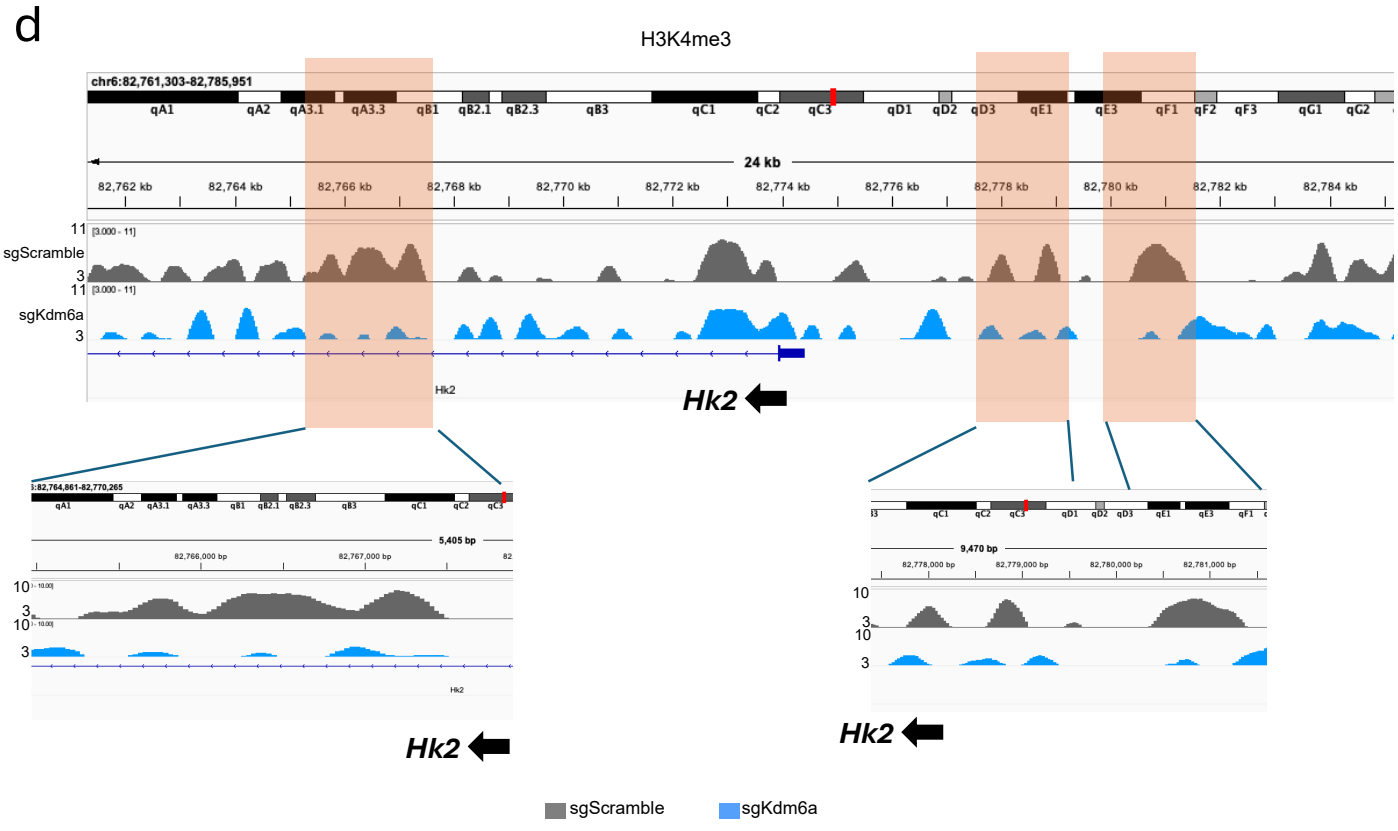
d
H3K4me3
chr6:82,761,303-82,785,951
24 kb
sgScramble
sgKdm6a
Hk2
5,405 bp
9,470 bp
sgScramble
sgKdm6a

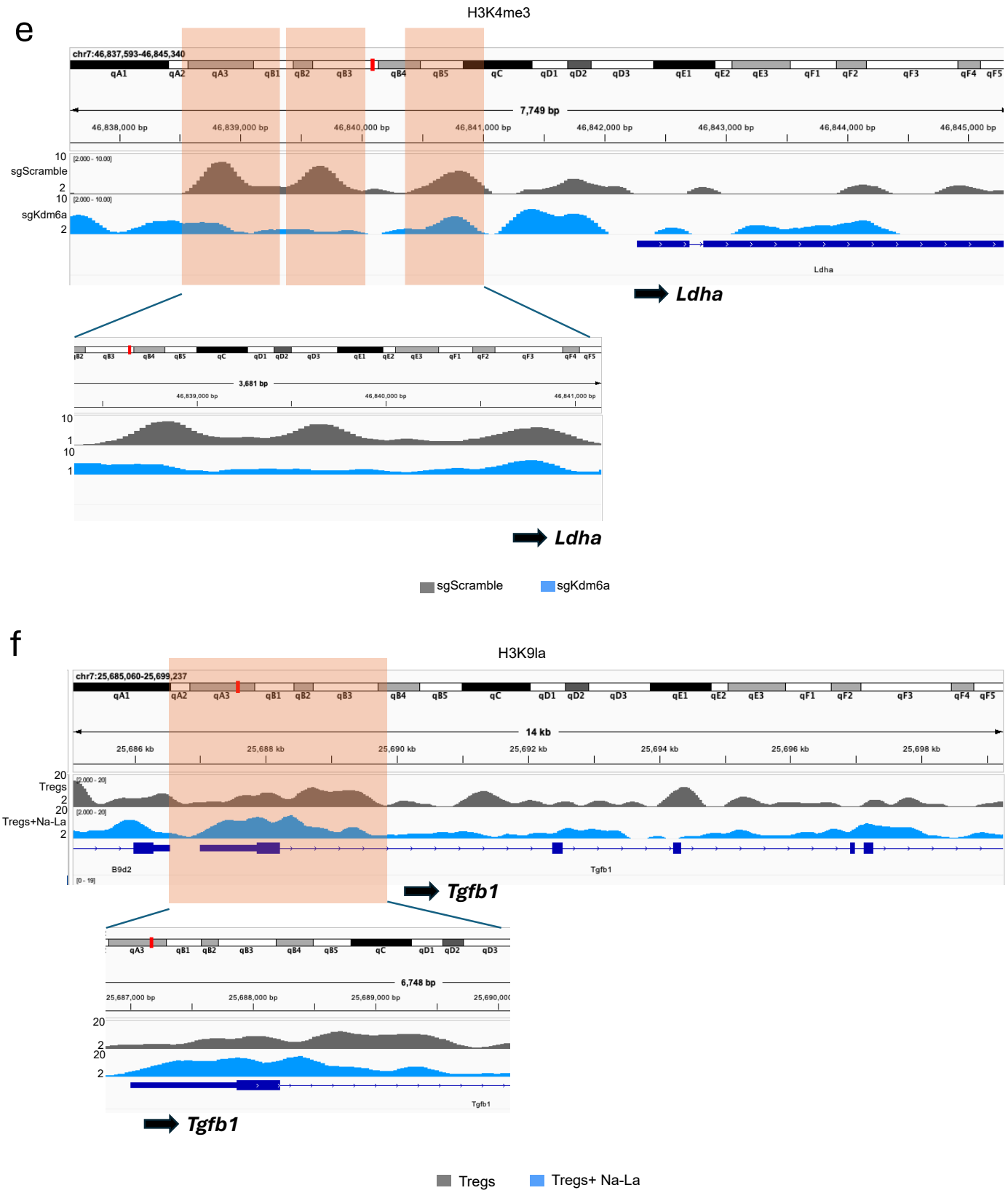

Figure 1: a-e: Genome browser plots demonstrating H3K4me3 peaks for *Exo1* (**a**), *Msh2* (**b**), *Msh6* (**c**), *Hk2* (**d**) and *Ldha* (**e**) gene loci in sgScramble and sgKdm6a cells**. f:** Genome browser plots demonstrating H3k9la peaks for *Tgfb1* gene loci in Tregs and Tregs treated with Na-La.

Editorial note: please note that Reviewer #3 has also commented on your responses to the concerns originally raised by Reviewers #1 and #4. In their view, the majority of the comments have been satisfactorily addressed. In response to comment 3 of Reviewer #4, they would still suggest to include all replicates/samples in a single plot (to allow evaluation of consistency between replicates).

We thank the Reviewer for the thoughtful review of the manuscript and appreciate the suggestion to include all replicates/samples in a single plot to allow evaluation of consistency between replicates. We have updated the relevant figure to include all samples in a single plot (Figure **2a** from point-by-point response letter and Extended Data Fig. **3I**, **5G**, **6F** in revised manuscript). We would like to add here that ChIP sequencing was performed using pooled samples from sgScramble and two biological replicates of sgKdm6a murine cell lines (sgKdm6a C1 and C2). Additionally, we used CRISPR-Cas9 mediated KDM6A knockout in human bladder cancer cell line RT4 and performed ChIP qPCR to validate our findings. The data showing all the replicates are presented in Figure **2b** of the point-by-point response letter and Extended Data Fig. **4D**, **4E**, **5K**, **5L**, **6K**, **6L** in revised manuscript.

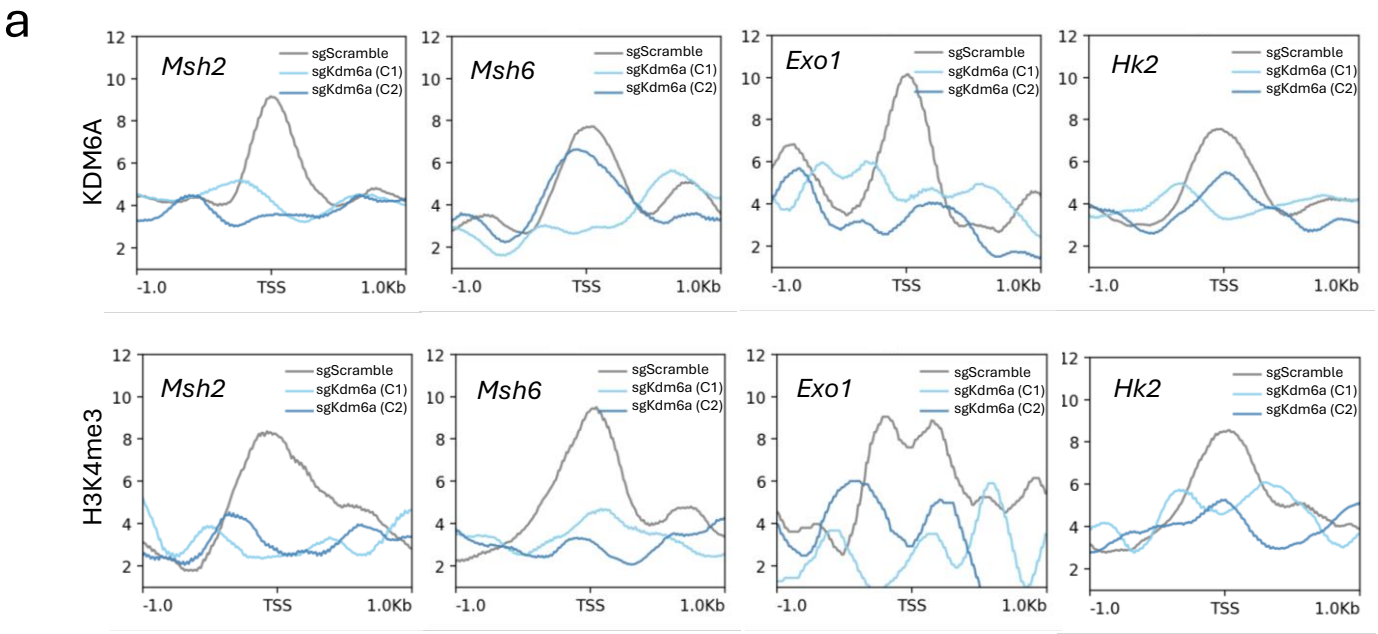

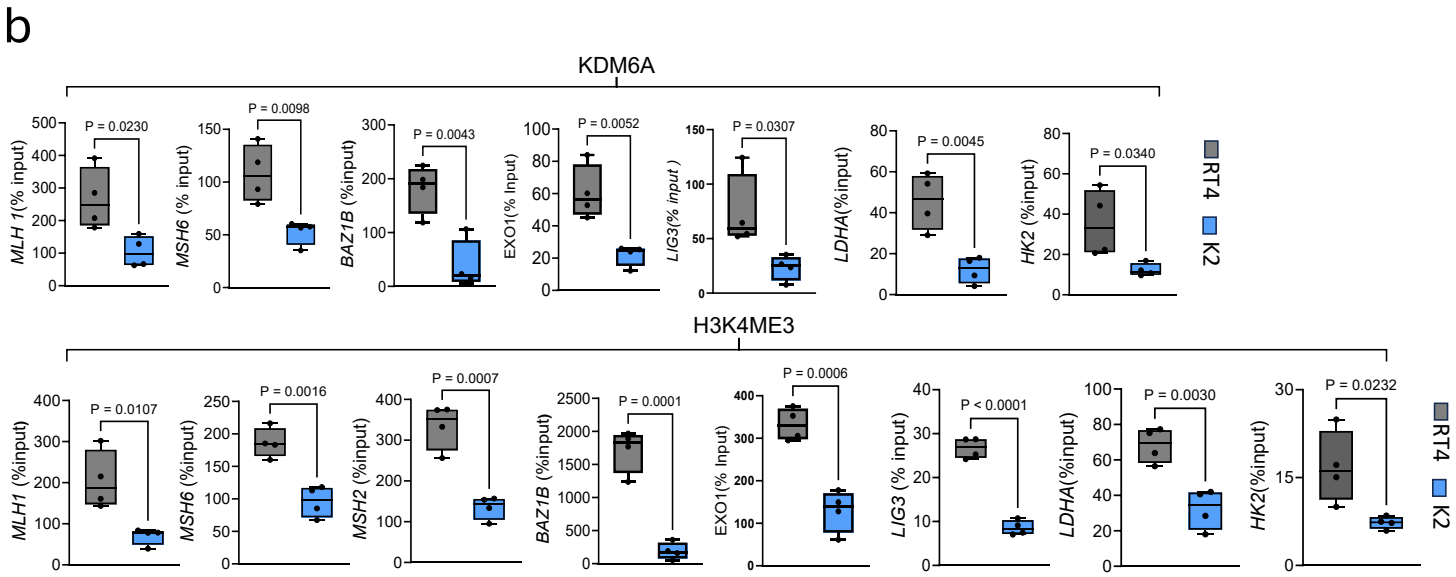

Figure 2: a: Profile plots representing the probability scores of KDM6A and H3K4me3 binding at ±1 kb regions from TSS and TES for genes involved in MMR, DSBR and glycolytic pathway in sgScramble, sgKdm6a C1 and C2 cells. **b:** Box-and-whisker plots showing the ChIP-qPCR analysis of KDM6A (Top panel) and H3K4me3 (Bottom panel) gene enrichment at the indicated gene promoters in RT4 and K2 cell lines. K2 is the KDM6A knockout cell line for RT4 (n=4 biologically independent samples per group). Two-tailed Student's t-test was performed. For all the box-and-whisker plots, the center line marks the median, the edges of the box represent the interquartile (25th–75th) percentile and the whiskers represent minimum-maximum values.

References:

1. Raychaudhuri D*, et al*. Histone lactylation drives CD8(+) T cell metabolism and function. *Nat Immunol* **25**, 2140-2151 (2024).

2. Goswami S*, et al*. Myeloid-specific KDM6B inhibition sensitizes glioblastoma to PD1 blockade. *Nat Cancer* **4**, 1455-1473 (2023).

Reviewer #3 (Remarks to the Author):

The authors addressed the requests properly. I would note that the zoomed out genomic visualization of ChIP-seq reveals that the peaks evaluated are quite small and their significance is questionable. Since this is clearly shown in the main figure, the manuscript is acceptable for publication. The authors might want to be more reserved in their claims concerning changes in H3K4me3.

We appreciate the Reviewer for careful evaluation of the manuscript and for acknowledging that the revisions adequately address the prior concerns. As per the Reviewer's recommendation, we have now refined the wordings concerning the changes in H3K4me3 marks in the manuscript (Discussion section) to present a more measured interpretation of the data.